University of Reading

Self-assembling peptide and protein amyloids: from structure to tailored function in nanotechnology

Article

Accepted Version

Wei, G., Su, Z., Reynolds, N. P., Arosio, P., Hamley, I. W. ORCID: https://orcid.org/0000-0002-4549-0926, Gazit, E. and Mezzenga, R. (2017) Self-assembling peptide and protein amyloids: from structure to tailored function in nanotechnology. Chemical Society Reviews, 46 (15). pp. 4661-4708. ISSN 0306-0012 doi: 10.1039/C6CS00542J Available at https://centaur.reading.ac.uk/71120/

It is advisable to refer to the publisher's version if you intend to cite from the work. See Guidance on citing.

To link to this article DOI: http://dx.doi.org/10.1039/C6CS00542J

Publisher: Royal Society of Chemistry

All outputs in CentAUR are protected by Intellectual Property Rights law, including copyright law. Copyright and IPR is retained by the creators or other copyright holders. Terms and conditions for use of this material are defined in the End User Agreement.

www.reading.ac.uk/centaur

University of Reading

CentAUR

Central Archive at the University of Reading

Reading's research outputs online

Journal Name

Review

Self-assembling peptide and protein amyloids: from structure to tailored function in nanotechnology

Received 00th January 20xx,
Accepted 00th January 20xx

DOI: 10.1039/x0xx00000x

www.rsc.org/

Gang Wei,[a†] Zhiqiang Su,[b†] Nicholas P. Reynolds,[c] Paolo Arosio,[d] Ian W. Hamley,[e] Ehud Gazit[f] and Raffaele Mezzenga[g,*]

Self-assembled peptide and protein amyloid nanostructures have traditionally been considered only as pathological aggregates implicated in human neurodegenerative diseases. In more recent times these nanostructures have found interesting applications as advanced materials in biomedicine, tissue engineering, renewable energy, environmental science, nanotechnology and material science, to name only a few fields. In all these applications, the final function depends on: i) the specific mechanisms of protein aggregation, ii) the hierarchical structure of the protein and peptide amyloids from atomistic to mesoscopic length scales, and iii) the physical properties of the amyloids in the context of their surrounding environment (biological or artificial). In this review we will discuss recent progress made in the field of functional and artificial amyloids and highlight connections between protein/peptide folding, unfolding, and aggregation mechanisms, with resulting amyloid structure and functionality. We also highlight current advances in the design and synthesis of amyloid-based biological and functional materials and identify new potential fields in which amyloid-based structures promise new breakthroughs.

Table of Contents

1. Introduction

2. Self-assembly and aggregation mechanisms of amyloids
- 2.1 Amyloidogenic proteins and peptides
  - 2.1.1 Protein folding and unfolding
  - 2.1.2 Unfolded proteins
  - 2.1.3 Misfolded proteins
  - 2.1.4 Peptide-based amyloids
  - 2.1.5 Peptide nanostructures and non-protein amyloids
- 2.2 Factors controlling amyloid growth and kinetics
  - 2.2.1 Solution property-mediated formation
    - 2.2.1.1 PH-mediated amyloids
    - 2.2.1.2 Ionic strength-mediated amyloids
  - 2.2.2 Temperature-mediated fibrillation
  - 2.2.3 Organic reagent-induced fibrillation
  - 2.2.4 Metal ion-induced fibrillation
  - 2.2.5 Biopolymer-induced formation
  - 2.2.6 Nanoparticle induced/inhibited amyloid fibrillation
  - 2.2.7 Interface- and mechanical force-mediated amyloid formation
- 2.3 Aggregation mechanisms and kinetics of proteins and peptides
  - 2.3.1 Aggregation mechanisms of unfolded and folded proteins
  - 2.3.2 Identifying aggregation mechanisms from kinetic studies
  - 2.3.3 Aggregation mechanisms and fibril length distribution

3. Atomic to mesoscopic structure of protein and peptide amyloids
- 3.1 Amyloid oligomers
- 3.2 0D amyloid aggregates
  - 3.2.1 Nanoparticles and nanospheres
  - 3.2.2 Annular oligomers: Loops, triangles, squares and rings
- 3.3 1D amyloid superstructures
  - 3.3.1 Amyloid protofilaments, protofibrils and nanofibrils
  - 3.3.2 Twisted ribbons and helical ribbons
  - 3.3.3 Amyloid nanotubes
- 3.4 2D amyloid (sheets, films, and membranes)
  - 3.4.1 2D protein amyloids
  - 3.4.2 2D peptide amyloids
- 3.5 3D amyloid plaques and scaffolds
- 3.6 Summary on the characteristic length scale of various amyloid structures

4. Manifold functionality of biological and artificial protein/peptide amyloid materials
- 4.1 Fabrication and functions of biological amyloids
  - 4.1.1 Amyloid-based biofilms
  - 4.1.2 Amyloid hydrogels and aerogels
- 4.2 Fabrication and functions of artificial amyloid-based hybrid materials

This journal is © The Royal Society of Chemistry 20xx

4.2.1 1D amyloid-based hybrid materials
4.2.1.1 Amyloid-nanoparticle
4.2.1.2 Amyloid-quantum dots
4.2.1.3 Amyloid-hydroxyapatite
4.2.1.4 Amyloid-carbon materials
4.2.1.5 Amyloid-biomacromolecules
4.2.2 2D amyloid-based hybrid materials
4.2.3 3D amyloid-based hybrid materials

5. Various applications of amyloid-based hybrid nanomaterials
5.1 Biomedical engineering
5.2 Tissue engineering
5.3 Energy materials
5.4 Environmental science and technology
5.5 Electronic nanodevices
5.6 Biosensor architectures
5.7 Other functional nanomaterials

6. Conclusions and outlook

Acknowledgements

Main abbreviations

Notes and references

1. Introduction

The self-assembly and aggregation of peptides and proteins play crucial roles in many of the human's body functions.[1] For instance, networks of collagen fibrils provide a biochemical scaffold with many functions governing the morphology and mechanical properties of biological tissue.[2, 3] Self-assembled actin fibrils are essential elements for many key functions in eukaryotic cells, such as motility, morphology, maintenance of cell polarity and the regulation of transcription.[4] In blood coagulation, wound healing proceeds through aggregation of fibrin into sealing clots, allowing tissue repair. In addition, there are a number of diseases associated with errant protein aggregation. The misfolding of proteins and their subsequent assembly into amyloid fibrils are pathological hallmarks of a number of devastating degenerative diseases, including Parkinson's, Alzheimer's, type II diabetes, and others.[5]

Historically, due to the discovery of their association with disease states, the study of amyloid fibrils has been largely centred on those associated with neurodegenerative disorders. A great deal of research has been performed to elucidate formation mechanisms and to understand mechanisms of toxicity arising from various amyloid species ranging from oligomers to mature amyloid nanofibrils.[6] Consequently, a large number of biomedical studies have been devoted to uncovering how to inhibit amyloid formation, and a multitude of biomedical, biochemical, biophysical, and nanotechnological processes have been investigated in an attempt to design therapies that can slow down the progress of amyloid-related diseases.[7-10]

The discovery that functional amyloid fibrils in living organisms also play vital physiological roles within and on the surface of living cells has introduced a new paradigm for the study of amyloid fibrils. Examples of the physiological roles of functional amyloids include, curli fibrils,[11] associated with the adhesive properties of E. Coli biofilms, catalysis of melanin synthesis in mammalian melanosomes,[12] and human peptide hormone storage.[13]

In addition to toxic and functional amyloids, in recent years there has been a growing interest in the applications of amyloid fibrils as templates or building blocks in ordered nanomaterials for biomedical, biomaterial, and nanotechnological applications.[14] Amyloid nanofibrils have been successfully employed as a fundamental component in biomembranes,[15] functional nanodevices,[16, 17] hydrogels for cell culture and drug delivery,[18, 19] biosensors,[20] functional materials with high biocompatibility and unique bio-recognition ability,[21, 22] and energy conversion materials.[23] All the above functions and applications of amyloid fibrils arise due to their unique structural features, enabling them to serve in an extremely vast context of fundamental and applied sciences, spanning from biology to materials science and nanotechnology.

At the atomistic length-scale the structural features of amyloid fibrils are remarkably similar,[24, 25] with amino acids arranged into β-strands (separated by ~ 4 Å) running orthogonal to the fibril axis and closely packed into β-sheets running parallel to the fibril axis (typical intersheet distance ~ 10-12 Å). In sharp contrast, the mesoscopic structure of amyloid fibrils shows a remarkable diversity, with a multitude of shapes and topologies, depending on the specific aggregation pathways followed.[26, 27] To date, nanoparticles, nanofibrils, nanotubes, ribbons, nanosheets, and 3D scaffolds or multilayers represent just some of the amyloid morphologies observed.[28-31] A wide spectrum of available morphologies and free energies, high surface-to-volume ratio, high density of hydrogen bonds and the presence of biocompatible amino acids on their surfaces gives amyloid fibrils a remarkable range of nanomechanical properties and applications across many scientific fields.[32,33]

In this review, we will comprehensively analyse the relationship between the molecular mechanisms of assembly into amyloid fibrils, the resulting amyloid structure and polymorphism, and the ensuing physical properties. We will then discuss how the structure and physical properties of amyloids can be harnessed to provide applications as advanced materials and in nanotechnology. In Part 2 we discuss the self-assembly and aggregation mechanisms of amyloids from unfolded proteins (e.g. α-synuclein), folded globular proteins (e.g. β-lactoglobulin) and peptides (e.g. Amyloid β, Aβ). In Part 3 we review the main structural traits of amyloids from the atomic to mesoscopic length scale. In parts 4 and 5 we discuss the functionality of natural and artificial amyloid materials, and present

[a] *Faculty of Production Engineering, University of Bremen, Bremen, Germany.*
[b] *State Key Laboratory of Chemical Resource Engineering, Beijing University of Chemical Technology, China*
[c] *ARC Training Centre for Biodevices, Swinburne University of Technology, Melbourne, Australia*
[d] *Chemistry Department, University of Cambridge, UK and Chemical and Biotechnology Engineering, ETH-Zurich, Switzerland*
[e] *Chemistry Department, University of Reading, UK*
[f] *Faculty of Life Sciences, Tel Aviv University, Israel*
[g] *Department of Health Science and Technology, ETH-Zurich, Switzerland. E-mail: raffaele.mezzenga@hest.ethz.ch*
† Equal contributions to this work

This journal is © The Royal Society of Chemistry 20xx

current biomedical, material, and nanotechnological applications of amyloid-based hybrid materials. We conclude by highlighting the current challenges and future perspectives of amyloid based materials and discuss emerging fields in which amyloid fibrils are ideal candidates to contribute to their development. It is expected that this comprehensive review will forge new directions for the design, synthesis, and wider applications of protein and peptide amyloid-based biological and functional materials.

2. Self-assembly and aggregation mechanisms of amyloids

The formation of amyloids can be achieved with either native folded proteins, which often have to undergo activation reactions such as unfolding and hydrolysis before aggregating, or unfolded proteins and peptides, which under a broad range of conditions exhibit 1D growth after a fast nucleation step. In this part, we would like to introduce key information on the self-assembly and aggregation mechanisms of peptides and proteins, which include a series of microscopic events such as protein unfolding, hydrolysis and aggregation. We describe the application of chemical kinetic studies to identify different microscopic mechanisms and we will discuss the connections between aggregation mechanisms and the length distribution of the aggregate population, which is a key property defining the function of the final amyloid product.

2.1 Amyloidogenic proteins and peptides

2.1.1 Protein folding and unfolding

The formation of well-folded protein structures is central to the function of every living cell.[34] Based on the information coded by DNA molecules and transcribed into messenger RNA, the ribosome synthesizes polypeptide chains of specific amino acid sequence that undergo internal organization to form distinct conformational arrangements. The spontaneous arrangement of the amino acid chain based on the physicochemical properties of its constituents is denoted as "protein folding".[35] The correct organization of the polypeptide chain into well-folded three-dimensional arrangements allows the proper activity of proteins, including enzymatic activity, storage, transport, sensing, signalling and structural functions. The folding of proteins into the distinct thermodynamically favourable conformations is achieved through folding pathways that hierarchically direct the protein into the lowest energy thermodynamic state. Several canonical secondary structures, such as alpha-helix and beta-sheet, constitute the tertiary folding, a much more complex energy-minimized molecular organization. As will be further discussed, this dogma is currently challenged as the amyloid state of proteins and polypeptides may actually represent the true energetic minimum of protein assemblies.

Even though correct protein folding is required for their biological function, under certain conditions proteins can undergo an unfolding process losing their tertiary as well as secondary structure.[36] The unfolding can be induced physically, especially by temperature changes (mostly heating and in some cases cooling), as well as by hydrostatic pressure, or chemically, by the addition of chaotropic agents (such as urea, guanidinium chloride, magnesium chloride, alcohols and detergents) that are able to disrupt the hydrogen bonding network between water molecules.

Protein unfolding can be either reversible or irreversible, depending on potential irregular interactions of the unfolded protein either within the same polypeptide chain (intramolecular interactions) or with neighbouring molecules (intermolecular interactions). The association of exposed hydrophobic surfaces is the main driving force of intermolecular interactions. Instead of a normal folding process in which the hydrophobic parts of a protein are buried in its core, many of these parts are held together by non-covalent interactions. In the case of intermolecular interactions, the molecular assemblies can form ordered assemblies such as crystals or amyloid fibrils.[37]

2.1.2 Unfolded proteins

Unlike the more common case of folded proteins, many intrinsically unfolded proteins exist in a natively unfolded state, either for the entire molecule or at specific regions of the peptide chain.[38-40] In such a case, hydrophobic parts of the proteins are exposed without any external unfolding reaction. Solution methods including nuclear magnetic resonance (NMR) and circular dichroism (CD) have allowed the determination of the unfolded state of proteins. The use of temperature-controlled experiments allows the melting temperature to be determined. Indeed, in some cases proteins were found to be unfolded at physiological temperature (37 ^{o}C) but completely folded at a low temperature (e.g., 4 ^{o}C).[41, 42]

The basis for the existence of proteins in an unfolded state might have a clear physiological significance. One of the roles of protein unfolding is to control the physiological stability of such proteins. The fact that unfolded proteins expose hydrophobic patches, that are otherwise buried within the core of the protein, results in their identification as damaged proteins, leading to their degradation by the protein quality control machinery.[43] The existence of proteins in this state allows the modulation of their half-life. In extreme cases, some proteins molecules could be degraded in a few minutes. This property is useful for two-component systems, such as bacterial toxin-antitoxin systems, in which the instability of one component is critical for the physiological control of the system.[44]

Protein unfolding plays a critical role in at least three biological processes such as protein translocation, protein degradation, and passive elasticity of striated muscle,[45] in which the unfolding is thought to be induced by the cellular machinery pulling the polypeptide chain to better disentangle the native domains. For the amyloid fibrils formed by globular proteins, the unfolding is a necessary step to change the conformation of the protein from a minimum to another minimum in the protein folding energy landscape.[46]

2.1.3. Misfolded proteins

As mentioned above, proteins can exist in an aggregated amyloid organization which was first associated with human diseases, including Alzheimer's disease (AD), Parkinson's disease and Type II diabetes.[47] The intermolecular interaction between unfolded or partially unfolded proteins can lead to the formation of supramolecular β-sheet structures constituted of more than one protein molecule. This could be considered an abnormal organization in which a handful of protein or polypeptide molecules join together to form ordered assemblies.

Amyloids were already identified more than a century ago in association with disease. In 1901, Dr. Eugene L. Opie, an American physician, had identified the formation of deposits in the pancreas of Type II diabetes patients.[48] A few years later, in 1906, the deposition of biomaterial in the brain of a demented patient *post mortem* was found by Aloysius "Alois" Alzheimer in Germany.[49] The deposits were denoted amyloids (starch-like) due to their positive staining by iodine as carbohydrate deposits. Only decades later, these aggregative forms were found to be made of proteins. With the advancement of electron microscopy in the 1950s, it was discovered that these protein assemblies have a typical nanoscale order. This regularity at the nanoscale underlies some of the properties that were later utilized for various technological applications, as described in this review.

The structure of amyloids regardless of their source is a very typical one comprising elongated supramolecular structures with a diameter of 7-10 nm. Amyloids have a predominantly β-sheet secondary structure as determined by X-ray fiber diffraction (XRFD) and infrared or CD spectroscopy. Interestingly, both parallel and anti-parallel β-sheet structures were observed within amyloid fibrils of different sources in spite of the very uniform ultrastructure. Amyloid fibrils were also found to bind to specific dyes. Beyond their ability to be stained with iodine, later on other amyloid specific dyes were identified, including Thioflavin T (ThT) and Congo red.[50, 51] The use of Congo red is especially interesting due to the typical birefringence that is observed upon the staining of the amyloid fibrils when placed between cross-polarizers. It was suggested that proteins of unrelated origin could form remarkably similar structures in disease state. The hypothesis was that the formation of such structures plays a role in the damage to various organs and tissues observed in these diseases. Indeed this "amyloid hypothesis" was supported by the observation of notable toxicity of the amyloids or their earlier soluble intermediates.

A very important extension of the "amyloid hypothesis" was provided by Dobson and co-workers who realized that non-disease related proteins could also form typical amyloid fibrils with all the common structural and biophysical characteristics of disease-associated amyloid assemblies.[52] It was thus suggested that the amyloid structure may actually reflect a generic minimal energy organization of polypeptide chains and that the structure of folded proteins is essentially a meta-stable kinetically trapped state, suggesting that most or all proteins would reach the favorable amyloidal organization at infinite time.[53] This hypothetical notion was later supported empirically, as it was found that most cellular proteins are at the verge of aggregation ("life at the edge" phenomenon) and that the proteostasis of the biological system requires an advanced cellular machinery that can keep the proteins and polypeptides in a soluble state.[54]

2.1.4. Peptide-based amyloids

The formation of amyloid fibrils has also been identified in various functional peptides, including the islet amyloid polypeptide (37 amino acids), Amyloid β (40-42 amino acids), and human calcitonin (31 amino acids), all associated with human disease. The aggregated form of the islet amyloid peptide is found in the pancreas of Type II diabetes patients,[55] aggregated forms of Aβ are found in the brain of Alzheimer's disease patients and similar structures made of calcitonin are found in the thyroid of patients with thyroid carcinoma, all identified using electron microscopy (EM). Furthermore, the peptide amyloids were found to share all other biophysical properties of protein amyloids, including the spectroscopic features, XRFD patterns and the staining with specific dyes.

As noted above, the formation of amyloid fibrils was initially identified in naturally occurring proteins and polypeptides. A reductionist approach has since been applied to identify the minimal peptide fragments that can form amyloid fibrils. Tenidis and co-workers were able to identify hexapeptide fragments of the islet amyloid polypeptide that form amyloid fibrils.[56] Later studies identified the ability of a pentapeptide fragment of calcitonin, as well as heptapeptide fragments of Aβ, to form such ordered assemblies.[57]

2.1.5. Peptide nanostructures and non-protein amyloids

Further reductionist approaches were used in order to identify even shorter amyloid-forming peptide motifs. It was found that the dipeptides diphenylalanine (FF) can form amyloid-related assemblies. The diphenylalanine motif is at the center of the Aβ polypeptide associated with Alzheimer's disease. As noted above, it was demonstrated that a heptapeptide fragment of Aβ, KLVFFAE (Lys-Leu-Val-Phe-Phe-Ala-Glu) could form fibrillar assemblies, and two pentapeptide fragments, KLVFF and LVFFA, are inhibitors of amyloid formation by the full-length protein.[58] It was found that the nanostructures made by FF shares many functional properties with amyloid assemblies,[59, 60] including the intrinsic luminescence properties, binding of amyloid-specific dyes, mechanical rigidity and the production of reactive oxygen species. This suggests that the FF nanostructures indeed represent a highly simplified model that reflects the structural, biophysical and biochemical properties of amyloid structures.[28, 61]

Later studies identified the ability of various short peptides to form ordered assemblies. Frederix and co-workers screened over 8,000 naturally occurring tripeptides for the formation of supramolecular entities using molecular dynamics simulations.[62] The most aggregation prone peptide screened peptide was PFF (Pro-Phe-Phe), and many other highly aggregating peptides contained the FF motif, and to a lower extent other diaromatic motifs (including FW, WF, FY and

 This journal is © The Royal Society of Chemistry 20xx

WW). This comprehensive non-biased analysis of all peptides is consistent with the observation of the high occurrence of aromatic amino acids in short peptides that can form typical amyloid fibrils.

In order to identify the minimal requirement for amyloid formation, amino acids were also tested for their ability to self-associate. Very surprisingly, it was found that phenylalanine could form amyloid fibrils with all the characteristics of protein fibrils, including nanoscale fibrillar morphology, binding of ThT and Congo Red and notable cytotoxicity.[63] X-ray crystallography suggested the formation of β-sheet like structures by this amino acid. Similar to protein amyloids, the phenylalanine amyloids were also found to bind to phospholipid membranes. Later on, it was found that other amino acids (including Trp, Tyr, and Cys), as well as nucleotides and other metabolites, could also form typical amyloid-like structures.[64, 65] The formed assemblies reveal many ultrastructural similarities among themselves and to protein and peptide amyloids. It was therefore suggested that the amyloid hypothesis could be even further extended to include nonproteinaceous building blocks.

The simple synthesis, chemical diversity, small size and low cost make very short motifs, including tripeptides, dipeptides and single amino acids, ideal building blocks for various applications in nanoscience and nanotechnology.[66, 67] Moreover, the mechanical, optical, electric and piezoelectric properties of some self-assembled structures should allow their use as alternatives to inorganic components in electronic, electro-optic and electromechanical systems. The bottom-up assembly of complex nanostructures from these simple building blocks allows the utilization of fabrication techniques that were previously used in surface modification applications, including physical vapor deposition, printing using inkjet technology and unidirectional axial growth by controlled evaporation of volatile solvents.

2.2 Factors controlling amyloid growth and kinetics

2.2.1 Solution property-mediated amyloid formation

2.2.1.1 PH-mediated amyloids

The growth of amyloid fibrils is highly sensitive to solution conditions including pH, the presence of salts or denaturing agents etc. Very careful preparation protocols have to be followed in studying fibrillization of $A\beta_{42}$, for example starting from a well-defined state of unaggregated peptide (achieved by initial dissolution in a hydrophobic solvent) and then carefully controlling the addition of water or buffer to a dried film.[68]

Typically, amyloid fibril formation by proteins is induced by reduction of pH. The aggregation of short peptides will depend on the pI of the peptide or the pKa of its constituent residues and its relationship to the solution pH. It has been suggested that fibril formation is favoured when the net charge of the peptide is not too large (in the range -1 to +1).[69]

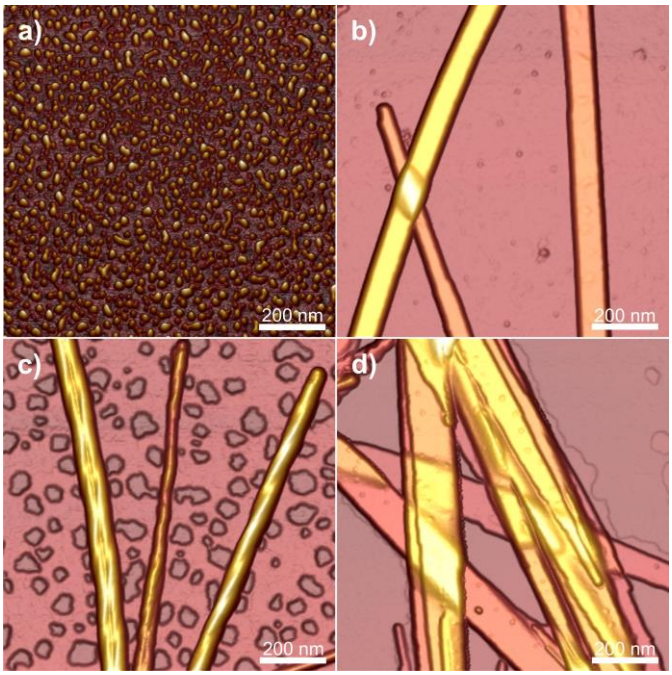

Fig. 1 Tapping mode AFM height images showing the morphology of C_{16}-KTTKS at pH values (a) pH 2, (b) pH 3, (c) pH 4, (d) pH 7. Reprinted with permission from Ref. 76. Copyright 2013, Royal Society of Chemistry.

A study of amylin peptide fibrillization indicates the presence of two ionisable residues – the α-amino group at the N terminus and His18.[70] The pKa values of the former unit in the amylin peptide is found to be similar to the random coil value (pKa = 8) however the His18 residue has pKa = 5.0, significantly lower than the random coil value pKa = 6.5. This is ascribed to the local influence of hydrophobic residues. His18 is found to act as an electrostatic switch hindering fibrillization in its charged state. An apparent pKa = 4.0 for an amylin fragment peptide, NAc-SNNFGAILSS-NH_2, which contains no titratable groups, is instead ascribed to the pH-induced ionization of the amyloid-sensitive dye, ThT.

In another example, the aggregation of the Amyloid β peptide $A\beta_{1-42}$ was studied as a function of pH.[71] This was investigated experimentally and the analysis was facilitated by molecular mechanics modelling of the fragment peptide $A\beta_{17-42}$ which revealed favourable electrostatic interactions between Asp23 and Lys28 (i.e. salt bridge formation) above the pI of the peptide. The aggregation of the $A\beta_{1-42}$ peptide itself was analysed at lower pH. At pH > 9.5, aggregation was not observed because Lys28 was uncharged.[71]

The self-assembly of another type of amyloid-forming building block, the so-called peptide amiphiphiles (PAs), can also be mediated by the solution property. PAs are designed amyloidogenic peptides modified by the attachment of hydrophobic lipid tails,[72] which then show combined surfactant-like properties and self-assembly ability.[73] The pH value has a pronounced effect on the self-assembly of PAs. For example, the Stupp group has demonstrated that the PAs containing acidic amino acids could be triggered to self-

assemble into nanofibrils at acidic pH[74] or with the use of divalent cations.[75]

In another case, Dehsorkhi et al. found that a PAs containing the pentapeptide KTTKS sequence, i.e. containing two cationic lysine residues, could be assisted to form adjustable nanostructures ranging from spherical micelles to tape-like and twisted structures by simply adjusting the pH of the solution at 2, 3, 4, and 7, respectively.[76] Atomic force microscopy (AFM) was used to image the morphology at selected pH values. It can be seen from Fig. 1 that fibrils, tapes or spherical micelles form depending on the pH (the net charge is approximately +1 at pH 7 and +2 at low pH). Small-angle x-ray scattering (SAXS) confirmed these morphology transitions and CD indicated a transition from β-sheet conformation in fibrils and tapes to disordered conformation at pH 2 for the spherical micelles.

2.2.1.2 Ionic strength-mediated amyloids

Along with the pH dependence of amyloid formation, we also highlight a few pertinent examples, in which the ionic strength of solution as well shows close effects on the formation of amyloids.

Hoyer et al. investigated, together with the effects of pH, the role of salt concentration on the in vitro aggregation of α-synuclein, and observed morphologies of different aggregates formed by α-synuclein at varying pH values and in the presence and absence of salts (NaCl and $MgCl_2$).[77] Their results indicated that the morphology of α-synuclein aggregates is highly sensitive to the solutions conditions (both pH value and ionic strength). In another case, Raman et al. investigated the effect of salts such as NaCl, NaI, $NaClO_4$, and Na_2SO_4 on the formation of β_2-microglobulin amyloid.[78] The presence of salts increased the hydrophobicity of proteins, and the anion interaction caused an interplay between electrostatic and hydrophobic interactions during amyloid formation. The particular role of SO_4^{2-} ions was identified, and this was suggested to be important in terms of the role of glycosaminoglycans and proteoglycans in amyloidogenesis. The critical aggregation concentration of β-lactoglobulin also depends on ionic strength, and below this concentration, mainly "dead-end" species are formed that consist of irreversibly denatured protein.[79] The morphology of the fibrils also changes and shorter and more flexible fibrils are formed at higher ionic strength.

The formation of peptide amyloids could also be affected by ionic strength. For example, Marek et al. investigated the ionic strength effects on the formation of islet amyloid polypeptide (IAPP) fibrils.[80] They suggested that the kinetics of IAPP amyloid formation is strongly dependent on the ionic strength in the range of 20-600 mM at pH 8.0. Recently, Abelein and co-workers characterized the explicit effect of ionic strength on the microscopic aggregation rates of $A\beta_{40}$,[81] and found that the physiological ionic strength could accelerate the aggregation kinetics of $A\beta_{40}$ by promoting the surface-catalyzed secondary nucleation reactions. Their results indicated the salts could decrease the free-energy barrier for $A\beta_{40}$ folding to a mature stable state, favoring the formation of mature fibrils.

A recent model, based on DLVO-type colloid theory, accounts for the stability of amyloid fibril dispersions and allows for the influence of ionic strength, salt concentration (as well as the presence of organic reagents).[82] The theory can be used to calculate quantities (fibril hydrodynamic radius and Fuchs stability ratio, which describes the energy barrier between two interacting fibrils) which were compared to experimental data for a model amphiphilic peptide (RADA 16-I).[82]

2.2.2 Temperature-mediated fibrillation

Heating (with or without pH adjustment to acidic conditions) is another common method of inducing amyloid formation with proteins and peptides.[25] Again, there are too many studies involving heat treatment to review them all and space permits only selected examples to be discussed herein. At sufficiently high concentration, the fibrillization of peptides is accompanied by gelation. For example, β-lactoglobulin forms fibrillar gels on heating at low pH values. Particulate gels are formed at higher pH values, close to the isoelectric point where the protein has a low net charge.[83, 84] Cold denaturation is generally a milder form than hot denaturation and leads only to partial unfolding of proteins[85] and so rarely, amyloid formation is reported under these conditions. However, cold can be used to dissociate amyloid fibrils, as discussed below.

Peptide amphiphiles (PAs) can show thermal transitions mediated by lipid chain melting behaviour as well as changes in the hydrogen bonding of amino acid residues, and temperature-dependent changes in solubility. In one example, conjugates of C_{23} or C_{25} alkyl chains (both containing one diacetylene unit) and the bio-derived GANPNAAG peptide sequence were shown to have very different disassembly transition temperatures on heating, and distinct thermosreversibility properties.[86] The longer chain PA reassembled on cooling, the shorter one did not.[86] The same PA C_{16}-KTTKS discussed in the previous section also exhibits interesting temperature-mediated fibrillization below 30 °C (depending on concentration), which may be associated with the palmitoyl chain melting temperature.[87] At low temperature, this compound (Tradename Matrixyl) forms extended tape-like fibrils, but at high temperature small spherical micelles are observed.[87] The thermoresponsiveness of other lipopeptides and peptides, for example elastin-like peptides which undergo LCST (lower critical solution temperature) behaviour, has been reviewed elsewhere.[88]

The formation of amyloid fibrils by the egg white protein ovalbumin occurs at high temperature (90 °C) and low pH, and the fibril morphology has been examined with or without NaCl.[89] Two types of aggregate were observed – thin flexible wormlike fibrils or thicker periodically twisted ribbons. Differences in β-sheet content between the two were studied by CD, WAXS and Fourier transform infrared spectroscopy (FTIR) (the latter aggregate lacks amyloid characteristics). The stiffness of the two types of fibril also differs, as quantified by peak force-quantitative nanomechanical AFM.[89]

In another example, the fibrillization and defibrillization ('depolymerization') of β_2-microglobulin was followed by detailed Thioflavin T fluorescence measurements.[90] Incubation at 99 °C for 10 min was found to lead to complete dissociation of fibrils into monomers. This occurred via both fibril breakage

This journal is © The Royal Society of Chemistry 20xx

and dissociation of monomers from fibril ends. Repolymerization experiments revealed that the number of extendable fibril ends increased significantly upon incubation at elevated temperatures. Stabilization of fibrils using a number of additives (salts or surfactant) was examined and it was found that the anionic surfactant SDS (sodium dodecyl sulfate) can prevent fibril dissociation up to 99 °C.[90]

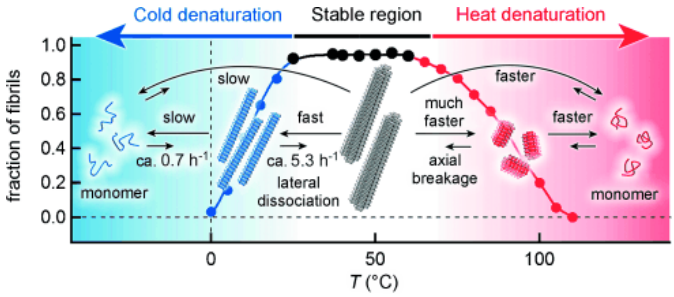

Fig. 2 Schematic of defibrillization of α-synuclein upon either cold or hot denaturing. Reprinted with permission from Ref. 91. Copyright 2014, Wiley-VCH Verlag GmbH &Co..

Whilst amyloid fibrils of many peptides such as β_2-microglobulin and $A\beta_{1-40}$ or $A\beta_{1-42}$ undergo heat-induced breakup, cold denaturation (dissociation into monomers) was additionally observed for α-synuclein (Fig. 2).[91] CD spectroscopy was used to monitor the loss of β-sheet structure on cooling (to 0 °C), and the temperature dependence was analysed, along with additional isothermal titration calorimetric (ITC) measurements, to provide thermodynamic information. This suggests that cold denaturation results from the burial of charged residues in the core of α-synuclein fibrils, opposite to the case of protein folding.[91] The dissociation of amyloid fibrils under cold conditions is exemplified by a study on α-synuclein in supercooled water at -15 °C.[86]

The denaturation of insulin under extreme temperature conditions up to 140 °C was probed via CD and ThT fluorescence experiments.[92] Amyloid structure was gradually replaced with random coil structure above 80 °C until no amyloid structure was detected at 140 °C. Fibrillization was observed when the sample was cooled down to 100 °C and incubated showing that even exposure to very high temperature, which favours full unfolding, does not lead to completely irreversible denaturing.[92]

2.2.3 Organic reagent-induced fibrillation

Protein denaturing agents such urea, salts or guanidinium hydrochloride or surfactants (e.g. SDS) may cause amyloid fibril formation. For example, many studies on amyloid fibril formation by the prion protein PrP have involved chemical denaturants that promote non-native conformational states.[93] Alcohol co-solvents generally lead to an increase in β-sheet structure associated with fibril formation of peptides and proteins. On the other hand, high concentrations of hexafluoroisopropanol (HFIP) or 2,2,2-trifluoroethanol (TFE) inhibit aggregation (and are widely used to disperse peptides and proteins in an unaggregated form). Acetonitrile is also reported to have an effect in inhibiting fibrillization.[7]

In a further example, the formation of fibrils (so-called protein nanofibers) by the extracellular matrix (ECM) adhesion protein fibronectin was observed after incubation at 37 °C in water/ethanol mixtures.[94] The fibrils were used as scaffolds to deposit *N*-hydroxysulfosuccinimide (NHS) modified CdSe–ZnS core–shell quantum dots (QDs) with potential applications as biophotonic nanohybrid materials. Fibrinogen also forms fibrils by incubation at pH 2, and these were used as templates for biomineralization.[95]

2.2.4 Metal ion-induced fibrillation

Metal ions are associated with amyloid deposits in several neurodegenerative disorders including Alzheimer's, Parkinsons and prion diseases. Metal ion coordination (through residues such as histidine) may cause inter-peptide crosslinking (Fig. 3 shows possible structures) and in turn influence oligomerization and fibrillization. In Parkinson's disease, elevated levels of copper and iron ions are found in the cerebrospinal fluid and Lewy bodies (which are intracellular inclusion bodies containing β-sheet rich aggregates of α-synuclein).[96] An early characteristic of prion disease is metal imbalance and Cu^{2+} has been found in scrapie isolates and confers prion strain type.[96] Furthermore, copper ions, found in trace quantities in the bloodstream, are known to bind to PrP *in vivo* and *in vitro* and to influence PrP levels in the brain. Aggregation of Aβ in Alzheimer's disease may also be promoted by metal ions.[97-101] Metal ions (e.g. Cu^{2+}, Fe^{3+}, Zn^{2+}, Al^{3+}…) were found to be co-localized at abnormally high concentration with senile plaques in AD brains.[102-106] Furthermore, Aβ rapidly aggregates in the presence of physiological concentrations of Zn^{2+} at pH 7.4.[107-109] In addition, metal ion-mediated amyloid formation is thought to be associated with inflammation in AD patients. For example, Cu^{2+}-induced aggregation was enhanced at mildly acidic pH values associated with inflammation.[109] The apparent interdependence of metal ions and amyloid assembly in AD opens up potential therapeutic targets. For instance, treatment with metal ion chelators can reduce the deposition of Aβ in brains.[110-113] The majority of studies to date have focused on metal ions ability to enhance Aβ fibrillation (e.g. Cu^{2+}, Zn^{2+} Al^{3+} and Fe^{3+}).[114] However, some studies have proposed that under certain conditions copper,[111, 115, 116] and zinc[111, 115] (but not iron[111]) ions are non-fibrillogenic. It should be noted however that amorphous and/or oligomeric aggregates may still be promoted through increased intramolecular bridging. This was exemplified by a study of different fragments of Aβ peptides, some of which promote fibrillization whilst others reduce fibril formation.[116] Apart from Aβ, di- and tri-valent metal ions have been shown to cause significant increases in the rate of fibril formation of α-synuclein and there appears to be a correlation to ion charge density.[117] The binding between protein and metal ions occurs via metal-ligand supramolecular interactions, which has been studied in detail for model metal ions by Bolisetty et al. both by molecular dynamic simulations and binding isotherms.[118]

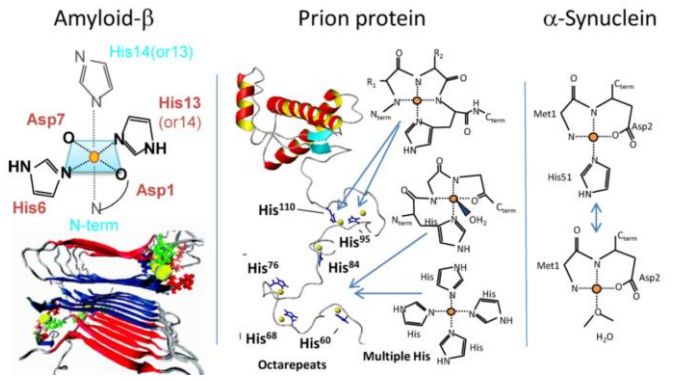

Fig. 3 Proposed modes of metal ion binding involved in the aggregation of the three proteins or peptides indicated. Reprinted with permission from Ref. 96. Copyright 2012, Elsevier Ltd.

The subject of peptide self-assembly triggered by metal ions has been reviewed in depth.[119] Many artificial ligands for metal ions have been incorporated into peptide-based molecules, and in addition the influence of metal ions on peptides incorporating natural ion-binding residues (histidine, cysteine, tryptophan or glutamic acid) has been examined. Self-assembly into different structures including α-helix based structures, β-turns etc has been reviewed,[119] but this is outside the scope of the current review.

2.2.5 Biopolymer-induced formation

Proteoglycans are an essential component of the ECM and they have important effects on amyloid aggregation *in vivo* and these have been investigated *in vitro*. Glycosaminoglycans (GAGs) or proteoglycans are thought to be associated with AD since sulfated GAGs such as heparin or chondroitin sulfate are present in neuritic plaques, neurofibrillary tangles and vascular amyloid deposits.[113, 120-122] Binding of some sulfated GAGs can prevent the proteolytic degradation of fibrillar Aβ. Sulfated GAGs can interact with histidine residues on peptides such as Aβ. Interestingly, sulfated GAGs can promote fibril formation due to a charge templating effect.[123] It has been reported that the sulfate spacing in heparin and several other GAGs is ideal for β-sheet formation (with associated 4.8 Å strand spacing), but this is not the case for some other polysaccharides.[123] In parallel studies, it has been reported that heparin or heparin sulfate can accelerate the fibrillization of Aβ *in vitro*,[121] probably due to electrostatic binding to a specific domain in the $A\beta_{11-28}$ region.[124] The influence of uncharged polysaccharides on fibril formation has been less studied, although one study suggests that glycogen can promote β-sheet formation of the prion protein.[125]

In a few cases, the inhibition of amyloid fibrillization by polysaccharides has been reported, for instance κ-carrageenan forms a complex with positively charged β-lactoglobulin which partly hindered high temperature fibril formation.[126] Uncomplexed β-lactoglobulin still formed fibrils, but protein-carrageenan complexes did not. Chitosan and poly(vinylsulfate) have an inhibitory effect on $A\beta_{1-42}$ fibrillization.[123] The influence of proteoglycans on amyloid fibrillization is reviewed elsewhere.[7, 114]

Linse's group has investigated the effects of polyamino acids and polyelectrolytes on Aβ fibrillization.[127] They investigated the kinetics of $A\beta_{1-42}$ aggregation using ThT fluorescence measurements and observed a concentration dependent accelerating effect on the aggregation process from all positively charged polymers examined (polyglutamic acid and polyacrylic acid). In contrast, no effect was seen for the negative polymers polylysine or poly(ethylenimine) or poly(diallyldimethyl ammonium chloride) or the neutral polymers polythreonine.[127]

The interaction between nucleic acids and amyloid fibrils has been investigated by several groups. DNA is known to be a powerful promotor of fibrillization due to electrostatic interactions with negatively charged residues on the DNA. Complexation of DNA with two arginine-containing molecules - one bola-amphiphile and one PA, has been examined.[128] Both of these peptide-based compounds self-assemble into layered β-sheet structures with incorporated DNA, the structural integrity of the DNA being maintained.

In another example, it was shown that DNA origami nanotubes can sheathe transthyretin fragment amyloid fibrils formed within them.[129] A DNA origami construct was used to form 20-helix DNA nanotubes with sufficient space for the fibrils inside.

2.2.6 Nanoparticle induced/inhibited amyloid fibrillation

Nanoparticles can significantly influence amyloid formation because they may catalyse fibril formation due to increased local protein concentration or they may inhibit aggregation when there is strong binding or a large particle/protein interaction surface area.[130] In the context of high local amyloid concentration, nanoparticle/amyloid hybrids are have been proposed as model systems to understand amyloid formation under crowded conditions relevant to those observed *in vivo*.[131] The effects of nanoparticles on amyloid formation may also be related to aspects of protein adsorption on nanoparticles in the blood stream, with relevance to nanoparticle toxicity.[132] The ability of a nanoparticle to influence amyloid aggregation is dependent on the stability of the protein and its intrinsic aggregation rate.[130] Amyloid fibrillization in the presence of nanoparticles with varying hydrophobicity and other surface chemistries has been examined. Polymeric nanoparticles can either increase or decrease the fibrillization of amyloid proteins, depending on the nanoparticle hydrophobicity and the unfolding behaviour of the protein and the hydrogen bonding capacity of subunits within it.[133]

Polymeric nanoparticles (uncharged acrylamide-based copolymers) inhibit the fibrillization of $A\beta_{1-40}$, an observation ascribed to the binding of Aβ (in monomeric or oligomeric form) to the nanoparticles.[134] The binding mainly affects nucleation, and the lag time was found to be strongly influenced by the copolymer composition. The binding is due to a combination of hydrophobicity (controlled via copolymer composition) and hydrogen bonding between polar groups on the polymer and in Aβ.[134] In the case of cationically (amide)

 This journal is © The Royal Society of Chemistry 20xx

functionalized polystyrene nanoparticles, inhibition of fibrillization is observed for high particle surface area, whereas fibrillization is accelerated for low particle surface areas due to reduction of the lag phase.[135]

Inorganic nanoparticles can function as Aβ fibrillization inhibitors, although this was demonstrated with cytotoxic CdTe nanoparticles.[136] On the other hand, it seems that TiO_2 nanoparticles can promote Aβ fibril formation by reducing the nucleation period,[137] however, the precise mechanism is unclear. Polyoxometalates which comprise inorganic early transition metal clusters also inhibit the aggregation of Aβ.[138] Surprisingly, inorganic nanoparticles based on porous silica have been shown to penetrate the brains of fruit flies (*D. melanogaster*), without exhibiting neurotoxic effects and potentially enabling delivery across the blood-brain barrier (BBB).[139] BBB permeability can be modeled using the parallel artificial membrane permeability assay, which measures passive diffusion of small molecule through an artificial lipid membrane.[140, 141]

There is growing evidence that metal nanoparticles may act as seeds for amyloid nucleation and growth,[142] an observation which can be relevant for amyloid related neurodegenerative diseases in the light of the fact that nanoparticles may be able to pass through the BBB. For instance, nucleation of amyloid oligomers has been reported on gold nanorods,[143] for a model synthetic bacterial protein which was functionalized with a hexa-histidine tag for binding to the gold surface. Conformational changes in the bound protein were probed using surface-enhanced Raman spectroscopy (SERS) and the nucleation was ascribed to the formation of immobilized pre-amyloidogenic monomers.[143] Gold and silver nanoparticles have been shown to accelerate fibril growth of the NNFGAIL peptide from human islet amyloid polypeptide and the prion protein Sup35 peptide GNNQQNY in physiological aqueous solutions.[144] Large-scale molecular dynamics simulations highlight the role of the structural reorganization of the peptide corona around gold nanoparticles as being the rate-limiting step in the aggregation process.[145]

Both metal ions and metal nanoparticles could promote the formation of amyloid fibrils, but the nature of their binding with proteins is different. Metal nanoparticles adhere with amyloids basically by electrostatic interactions and surface tension reduction, while metal ions bind to amyloids via supramolecular metal-ligand interactions.

2.2.7. Interface- and mechanical force-mediated amyloid formation

It has been suggested that fibrillization kinetics can be influenced during mixing by mass transfer effects. In addition, mixing leads to shear forces, which can influence the growth of fibrils by perturbing the equilibrium between soluble protein molecules and proteins incorporated into fibrils, since fibrils can fragment and create new nuclei.[146] The possibility to fragment fibrils by mechanical forces has been commonly exploited to produce monodisperse short amyloid fibrils by sonication of long filaments. For instance, Chatani et al. studied this process for β_2-microglobulin.[147] However, (ultra)sonication is not always required to produce low dispersity (in width) amyloid fibrils as exemplified by the protocol used by the Mezzenga group to prepare well defined β-lactoglobulin fibrils, which does not involve sonication.[148]

The influence of shear on the structure and mechanical properties of amyloid fibrils of this protein has been investigated using both controlled (steady shear in a Couette cell) or uncontrolled (stirring) shear flows. It has been observed that distinct morphologies (with different mechanical behaviour) can be obtained depending on the shear conditions.[149] Couette shear induces amyloid fibril formation in β-lactoglobulin starting from spheroidal seed-like species.[150] In contrast, bovine serum albumin undergoes irreversible unfolding (without amyloid formation) in Couette flow.[151] The influence of mechanical stress (linear shaking) on the fibrillization kinetics and morphology of glucagon has been examined.[152] Studies of this type highlight the need for great care in the interpretation and comparison of amyloid formation kinetic data.

Many amyloid-forming proteins and peptides have surfactant-like properties and are active at the air-water interface. This leads to the possibility to use amyloid fibrils as emulsifying agents.[153, 154] For example, a designed β-sheet forming peptide containing alternating phenylalanine and charged residues was able to act as a water-oil emulsifier.[153] Fibrillization of α-synuclein is enhanced at the air-water interface compared to that at a solid-liquid interface because fibrils are selectively adsorbed at the air-water interface.[155] Fibril nucleation is observed even without the presence of seeds although fibril elongation is faster in bulk when seeds are added at sufficient concentration.[155] A designed coiled-coil peptide forms α-helices at the air-water interface which can transform into β-sheets, either with intrinsic slow kinetics or stimulated by the addition of metal ions such as Zn^{2+}.[156] At the interface, increasing peptide conformation or parallel alignment (by compression) of the α-helical intermediates (which tends to pre-align β-strands), has the greatest effect on β-sheet aggregation. The metal ions actually hindered aggregation of this peptide in bulk but not at the interface.[156]

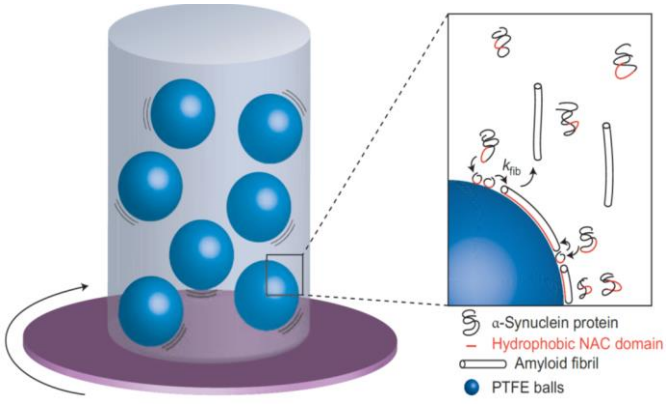

Fig. 4 Formation of amyloid fibrils by α-synuclein. A solution was agitated in the presence of particles of hydrophobic PTFE, slightly

hydrophilic PMMA or chemically inert glass; experiments with air injected at the top of the cuvette were also performed. Inset: Proposed mechanism of the fibrillization. The aggregation of proteins into fibrils (at the rate constant kfib), caused by association of the protein hydrophobic NAC domains, is enhanced in the presence of hydrophobic PTFE interface. Reprinted with permission from Ref. 158. Copyright 2010, Nature Publishing Group.

The presence of hydrophobic interfaces can influence the fibrillization of amyloid-forming proteins. Pronchik *et al*. studied the fibrillization of α-synuclein using a standard fluorescence dye technique used to assay amyloid formation.[157] The kinetics of fibrillization in dilute aqueous solutions of the protein were monitored as a function of incubation time, the samples being subjected to agitation in the presence of different types of particles of 1-2 mm in diameter (Fig. 4).[158] The particles were made of borosilicate glass which is largely inert, polymethylmethacrylate (PMMA) which is slightly hydrophilic or polytetrafluoroethylene (PTFE) which is hydrophobic. Some samples were also agitated in the presence of controlled volumes of air (which is hydrophobic). The fibrillization kinetics were found to depend strongly on the number of PTFE particles, i.e. to the hydrophobic surface area. The inverse lag time also increased in a non-linear fashion with the number of PTFE particles. Further nucleation and growth of fibrils was induced by addition of PTFE particles to a sample containing fibrils that had already developed upon agitation in the presence of PTFE particles. An increase in dye fluorescence was observed in the presence of air, although fibrils were not observed using AFM. In the case of glass particles, no fibril formation was observed. Fibrillization was observed using PMMA particles, but to a much lower extent than with PTFE particles. As a further control, quiescent samples were examined and these showed no increase in ThT fluorescence in the absence of agitation. The fibrillization kinetics were proportional to the PTFE surface area, but not to the surface area of glass or PMMA. The contact angle of PTFE decreases dramatically in the presence of protein, showing that the protein coats the PTFE surface progressively reducing the amount of available catalytically active interface. Moreover, the fact that addition of more PTFE particles leads to re-initiation of growth indicates that saturation of adsorption had not occurred since fibril-capable protein was still present in solution. Accelerated fibrillization was also observed in the presence of air, although the morphology of fibrils was different (globular aggregates were observed). These results clearly show the importance of hydrophobic interfaces in accelerating the fibrillization of the amyloid-forming protein α-synuclein. These findings provide an important insight to the understanding of the issues of sample-to-sample reproducibility that plague *in vitro* studies of amyloid fibrillization. Variability in morphology resulting from mixing in the presence of hydrophobic interfaces may also be important since fibril polymorphism, resulting for instance from sonication, has a profound effect on toxicity.[159]

The effect of lipid membranes on amyloid aggregation has been examined for several peptides including Aβ and α-synuclein.[160, 161] The importance of lipid interactions with Aβ is highlighted by the fact that apolipoprotein E, ApoE, (especially the ε4 allele) a key genetic risk factor for AD, is involved in lipid metabolism.[162, 163] Lipid membranes have a number of important roles in modulating amyloid fibrillization. These include: (partially) unfolding the peptide, increasing the local concentration of peptide bound to the membrane, orienting the bound protein in an aggregation-prone manner and variation of penetration depth into the membrane affecting the nucleation propensity.[164] Lipid rafts are implicated in Aβ dimer and oligomer formation,[165-167] and may provide platforms for selective deposition of different Aβ aggregates (this also depends on the ordering of the lipids within the membranes which may be different in the rafts[168]).[169] Further information on the interaction of Aβ with membranes is available elsewhere.[114]

Lipid membranes are influenced by amyloid peptides and *vice versa*. Advanced fluorescence imaging techniques enabled membrane disruption caused by native and mutant forms of α-synuclein to be examined.[170] It has been shown that[171] α-synuclein partially inserts into the outer leaflet of the lipid bilayer[172] and it was thought that this was due to interaction with anionic lipid membranes.[171, 173] However, it has been demonstrated that the protein is able to remodel lipid membranes from vesicles to tubules, even when the lipid membrane has no net charge.[171]

The cross-interaction of IAPP and Aβ peptides at lipid membranes has also been investigated.[174] Mixed fibrils are formed at the anionic lipid raft membranes.[174]

2.3 Aggregation mechanisms and kinetics of proteins and peptides

2.3.1 Aggregation mechanisms of unfolded and folded proteins

In the previous sections we discussed the effect of several physicochemical parameters on the conversion of soluble monomeric peptides and proteins into insoluble amyloid fibrils. In most of these systems, the formation of amyloids is the consequence of an aggregation process under kinetic control. In this perspective, amyloid formation differs from other types of protein aggregation phenomena that are under thermodynamic control, such as protein oligomerization, precipitation and liquid-liquid phase separation. In the light of this observation, the kinetics and the mechanisms of amyloid formation play a key role in determining the properties and the functions of the final fibrillar products. Therefore, in order to design amyloid products with tailored functions, the understanding of the microscopic mechanisms underlying the aggregation process represents a crucial component.[154]

This task exhibits several challenges, since the formation of amyloids is the consequence of a complex aggregation network represented by several elementary reactions of nucleation and growth (Fig. 5a).[175, 176] The formation of amyloids is triggered initially by primary nucleation processes, which generate the first nuclei from soluble monomers. These nuclei can be represented by a variety of different small soluble species, which can be defined with different terminologies depending on their size, structure and reactivity. In the context of this section we define generically this broad class of small assemblies as oligomers.

 This journal is © The Royal Society of Chemistry 20xx

Some of these species are non-reactive and off-pathway with respect to the transition into amyloids and accumulate in the system, while other oligomers are on-pathway and can further grow into protofibrils and eventually into mature filaments.[177-179]

In the vast majority of amyloid systems fibril growth occurs via elongation reactions, where a monomeric unit is incorporated at the end of an existing fibril via a diffusion motion over an energetic barrier.[180] This process can in principle be reversible. However, the dissociation of monomers from fibrils is typically negligible, given the high thermodynamic stability of the fibrillar structure. In a very few cases, fibril growth can occur via fibril-fibril aggregation, as observed for amphiphilic peptides exhibiting complementary defects at the fibril ends.[181]

In addition to primary nucleation reactions, secondary nucleation processes have been increasingly identified in the aggregation of several amyloidogenic peptides. Such secondary nucleation processes involve typically the fragmentation of fibrils induced by either thermal energy or mechanical forces.[146, 182] These breakage events multiply the number of fibrils and increase the concentration of reactive fibril ends which can recruit monomers and elongate. Another common secondary nucleation process, originally identified in seminal studies on sickle haemoglobin,[183] involves the generation of new oligomers catalysed by the presence of the surfaces of existing fibrils.[184-187] Such surface-induced secondary process has been demonstrated to account for most of the production of toxic species during the aggregation of the peptide Aβ[185] and, under certain conditions, also of α-synuclein.[188] Importantly, these mechanisms of aggregation, commonly identified *in vitro*, are recently starting to find correlations also in *in vivo* studies performed using worms[189] and mice models[190].

The generic aggregation mechanism described above applies to both unfolded and globular proteins forming amyloids. A key difference between these two classes of proteins, however, is related to the monomeric form responsible for initiating and propagating aggregation. Indeed, short peptides and largely unstructured proteins are typically prone to form amyloid fibrils without the requirement of major conformational changes.[54, 191] In contrast, the formation of amyloids from proteins that are largely folded follows typically a pre-aggregation event that triggers the conversion of the native form into an aberrant conformation that is more aggregation-prone.

One of the most common events is protein misfolding, i.e. the conformational change of the initially folded state into an unfolded or partially-folded intermediate.[192-194] This is the case for instance for insulin,[195-198] lysozyme,[199, 200] β_2-microglobulin,[201, 202] enzyme superoxide dismutase (SOD1),[203] and light chain immunoglobulin,[204] which have been observed to form fibrils under conditions that promote the formation of partially folded species.

Other reactions that can trigger the formation of amyloids from globular proteins involve the truncation of the protein[205] or the hydrolysis of the original polypeptide sequence into smaller fragments. For instance, lysozyme[206, 207] and β-lactoglobulin[206, 208, 209] have been shown to form amyloid fibrils under acidic conditions after the hydrolysis of the full-length protein into smaller peptides. In particular, two classes of peptides can be identified based on their reactivity: a series of peptides which converts over time into amyloids and a second sub-class which does not aggregate and remains soluble.[208, 209] An analogous system is represented by the amyloidogenic peptides $A\beta_{1-40}$ and $A\beta_{1-42}$, which are generated from the enzymatic cleavage of the amyloid precursor protein (APP).[114] The higher aggregation propensity of short peptides with respect to the precursor globular protein is not surprising, since steric constraints disfavour the thermodynamic stability of amyloid fibrils with respect to the soluble state for polypeptide sequences longer than 100 residues.[54] Indeed, for large globular proteins such as immunoglobulins the formation of amorphous fractal-like aggregates rather than fibrils is typically more favoured.[210-212]

The formation of individual amyloid filaments can be followed by additional supramolecular events, leading to the generation of 2D and 3D amyloids. These additional processes include lateral fibril-fibril association[206] as well as the formation of nematic phases[213, 214] and gels[154, 215]. This rich phase behaviour opens a route to finely tune the morphology and the mechanical properties of supramolecular fibrillar hydrogels and other soft materials by carefully controlling the individual events underlying the aggregation process. This observation highlights once more the importance of identifying the aggregation mechanisms to allow rational design in structure-function studies of amyloid materials.

An attractive strategy to modulate the aggregation mechanisms in a tailored way consists of introducing into the system suitable reactive species. For instance, aggregation reactions can be seeded by adding pre-formed fibrils or other non-native species, which can trigger the aggregation of physiological monomers following prion-like mechanisms. As discussed previously, other important heterogeneous nucleation events involve the presence of air-water interfaces,[155] hydrophobic surfaces[157, 216] and vesicles,[160] which are particularly prone to trigger the formation of amyloid fibrils, although the exact mechanisms underlying these effects are only starting to be elucidated.

We conclude this paragraph by highlighting two emerging directions in amyloid mechanistic studies: a first activity is aimed at increasing our understanding of the microscopic steps underlying the generation of the oligomers.[217] This topic is clearly relevant to understand the toxicity associated with the aggregation process in biological systems, and it is also crucial to clarify safety issues associated with the use of amyloid biomaterials for healthcare applications. A second important direction is the description of the behaviour of proteins at high concentrations, which underlies several biotechnological and biological applications. Indeed, under these conditions, the quaternary state of proteins is governed by a complex physics, since the increase of the protein concentration can both change the phase diagrams and accelerate the rate of nucleation and growth reactions by increasing the activities of the reagents. There is therefore the need to correlate the thermodynamic phase behaviour with the kinetic aspects of the aggregation processes.

2.3.2 Identifying aggregation mechanisms from kinetic studies

In order to identify the microscopic aggregation mechanisms in a particular system, it would be convenient to fully characterize the large class of intermediate species populated during the aggregation process. However, several of these intermediate species are transient and present at low concentrations, and therefore challenging to characterize experimentally. Indeed, biophysical assays for structural studies are typically well suited to characterize only the initially soluble monomeric state and the final insoluble fibrillar aggregates.

To address this limitation, in analogy with other branches of chemistry and protein biophysics, chemical kinetics is emerging as a powerful tool to investigate amyloid aggregation mechanisms at the molecular level from the measurements of macroscopic rate laws.[146, 193, 218] By recording the global aggregation profiles at different protein concentrations, the reaction orders can be extracted, and compared with integrated laws based on mathematical models describing different microscopic mechanisms.[219] One of the greatest advantages of this method is the possibility to extract information on multiple microscopic events of nucleation and growth from a limited number of experimental macroscopic read-outs, which typically include the monomer conversion or the total amount of aggregates formed during time.

For instance, high-throughput assays have been well established to monitor the formation over time of the total fibril content. A conventional method is based on a ThT fluorescent assay,[220, 221] which relies on the increase of the fluorescence yield of the dye upon binding to the characteristic β-sheet structure of the fibrils. The time evolution of the total fibril content typically exhibits a sigmoidal profile, where a lag-phase is followed by an exponential growth regime and eventually by a plateau related to the consumption of soluble monomer. It is important to note that the microscopic reactions described in the previous section are present during all the stages of the aggregation process, even at the early beginning of the reaction. Indeed, although it may be tempting to consider the lag-phase as a waiting time, this period represents the time required by the fibrils to reach a critical concentration that is detectable by the experimental assay.[222, 223]

The application of chemical kinetics in amyloids has been hampered for a long time by the complexity of the non-linear aggregation scheme described in the previous paragraph, which has challenged the derivation of analytical rate laws. Moreover, the high sensitivity of amyloids to several physicochemical factors complicates the establishment of robust kinetic assays, which often suffer from irreproducibility issues. Advances in theoretical analysis,[146] and the development of optimized experimental protocols,[224] however, have recently opened the possibility to apply the kinetic platform to several amyloidogenic systems, leading to the identification of the aggregation mechanisms under a broad range of conditions.

An attractive advantage of kinetic studies is the high sensitivity in detecting, also with high resolution, changes in the aggregation mechanisms that derive from the modulation of the reagent composition or of intrinsic and extrinsic factors.[160, 185, 188, 189, 225-227]

Of particular interest is the analysis of the changes in the aggregation mechanisms in the presence of inhibitors of amyloid formation. This information is particularly important in the biomedical context of the search for drugs to fight against amyloid-related disorders, where a kinetic inhibition of the aggregation process can represent an effective strategy to avoid the onset and development of the associated disorders over a characteristic life span.[114] It is becoming apparent, however, that this approach cannot be achieved simply by a generic inhibition of the aggregation process but requires a specific intervention aimed at targeting specific microscopic events that are most responsible for the formation of toxic species, in particular oligomers.[228] In this context, the application of chemical kinetics is fundamental to identify the specific processes that are affected by the presence of different modulators.[228, 229]

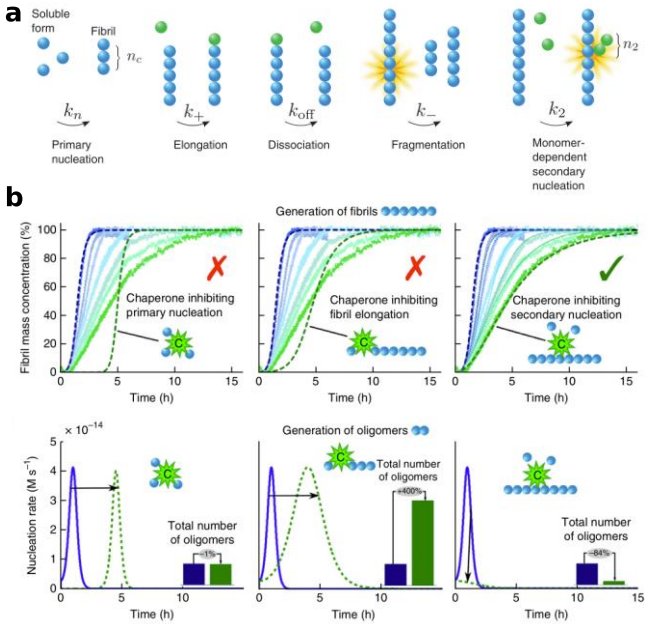

Fig. 5 a) Individual microscopic events underlying the aggregation mechanisms of amyloids; b) The identification of the aggregation mechanisms and the specific intervention on targeted microscopic reactions is fundamental for the rational design of tailored functions. This concept is illustrated here with the example of the peptide $A\beta_{1-42}$, for which the generation of particularly active species can be modulated by inhibiting different microscopic steps. Reprinted with permission from Ref. [225]. Copyright 2015 Nature Publishing Group.

A recent example of the importance of this activity has been demonstrated with the peptide $A\beta_{1-42}$: the application of chemical kinetics and the understanding of the microscopic mechanisms underlying the aggregation process has opened the possibility to tune in a controlled way the generation of specific intermediates characterized by a particularly high level of toxicity, as shown in Fig. 5b.[225] This platform allowed the identification of a biological molecule which can selectively supress the secondary nucleation reaction and therefore the generation of the oligomers. By contrast, specific targeting of primary nucleation and elongation rate, although equally efficient in delaying the formation of the fibril amount (top panels) cannot deplete the

This journal is © The Royal Society of Chemistry 20xx

oligomer formation (bottom panels). This outcome would have not been achievable by means of experimental characterization only, and highlights the importance of theoretical mechanistic frameworks in structure-activity studies of amyloids.

It is envisioned that in the near future improvements in experimental assays to detect oligomers[217, 230, 231] will enable researchers to perform kinetic studies specific to these species, thereby improving the understanding of the microscopic steps responsible for the formation of these important intermediates.

2.3.3 Aggregation mechanisms and fibril length distribution

In the previous paragraphs we discussed the importance of identifying aggregation mechanisms in amyloids and we described the use of chemical kinetics as one of the major tools to perform this operation. A particularly important aspect of these activities that deserves special attention in material sciences is the characterization of the time evolution of the fibril length distribution. Indeed, fibrils with different lengths are associated with drastically different mechanical properties and activities, including different toxicity in biological systems.[232]

From an experimental point of view, different techniques have been successfully applied to characterize the fibril length of amyloids. Single-molecule imaging techniques, including AFM,[209, 233-237] EM[225] and super resolution fluorescence microscopy,[238, 239] provide a high level of resolution by analysis of a large number of individual filaments. Alternative bulk methods have also been recently developed based on the indirect evaluation of the fibril length from the measurement of physicochemical properties such as the rotational[240] or translational diffusion coefficient[241, 242] or the sedimentation coefficient.[243-247]

In addition to the improvements in the experimental characterization, recent progress in the analytical treatment of kinetic models has allowed the derivation of compact expressions describing the dependence of the fibril length distribution on key kinetic parameters.[248, 249] Experimental information on the full length distribution provides a large number of constraints for the comparison between model simulations and experimental data. Thereby, the robustness and the refinement of the derived aggregation mechanisms are significantly increased with respect to kinetic analysis that relies only on the comparison with a limited number of average quantities of the fibril population. These more refined models lead to a better understanding of the relationship between aggregation mechanisms, fibril length distribution and product functions.

3 Atomic to mesoscopic structure of protein and peptide amyloids

In the above part, we demonstrated and discussed the various self-assembly and aggregation mechanisms of amyloid forming proteins and peptides. It is clear that the small differences in molecular aggregation and self-assembly are responsible for the formation of a wide variety of amyloid nanostructures. Recently, Luo and co-workers reviewed recent advances in the protein assembly for the fabrication of various nanostructures by biotechnological and chemical strategies.[250] Although that review does not focus specifically on amyloid fibrils, it reviews the state of the art on the use of proteins assembly as versatile platforms for designing attractive functional nanostructures. In this section, we will focus on the atomistic to mesoscopic structures of a number of amyloid assemblies, including molecular oligomers, 0D aggregates (nanoclusters, nanoparticles, nanotriangles, squares, and loops), 1D aggregates (protofibrils, nanofibrils, nanoribbons, and nanotubes), 2D aggregates (sheets, films, and membranes), and 3D amyloid plaques and scaffolds.

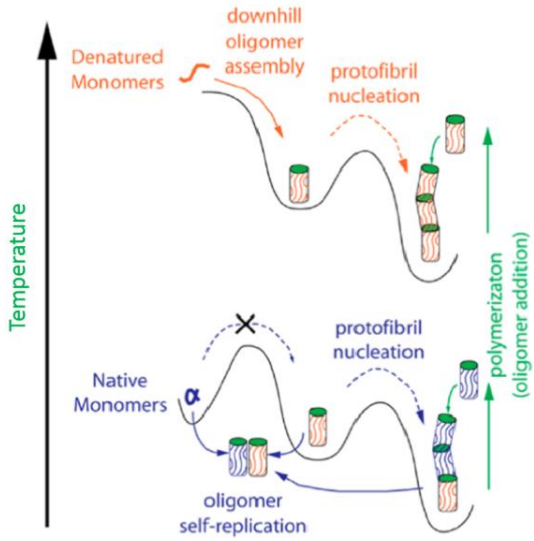

Fig. 6 Schematic assembly pathways of lysozyme oligomers at both denaturing and native temperatures. Reprinted with permission from Ref. 257. Copyright 2014, American Chemical Society.

3.1 Amyloid oligomers

Due to their ubiquitous presence in the brains of patients suffering from many neurodegenerative diseases and their apparent cytotoxicity *in vitro,* insoluble peptide and protein amyloid aggregates were assumed to be the cytotoxic culprit in these diseases.[251] However, new evidence suggests that prefibrillar soluble amyloid oligomers with low molecular weight could be the primary toxic species responsible for neuron death in both Alzheimer's and Parkinson's disease.[114, 252, 253] Although there is no universal consensus on what constitutes an amyloid oligomer they can typically be considered to possess some or all of the following biochemical and biophysical characteristics.[254] They are molecular aggregates with β-sheet rich structures composed of between 2-30 assembled monomers. They possess various sizes and morphologies, and are soluble in aqueous solutions. Their morphology is polymorphic and time-dependent and can aggregate into long, stable mature amyloid fibrils. Previously, a number of excellent review articles on the structure, formation mechanism, and toxicity of natural and artificial amyloid oligomers have been reported.[114, 255, 256]

A range of techniques including AFM,[257] EM,[258] attenuated total reflection (ATR)-FTIR,[259] NMR,[260] and single particle confocal microscopy,[261] have been used to investigate oligomeric structures and the conformational transition between oligomers and mature

fibrils. Mulaj et al. combined ThT fluorescence assays, static and dynamic light scattering (S/DLS), AFM, and ATR-FTIR to assess the stability, kinetics, and structure of hen egg-white lysozyme during its transition from oligomeric species to protofibrils and nanofibrils.[257] They found that the amyloid oligomers and protofibrils but not latter stage filaments were responsible for the amyloid growth at both physiological and denaturing temperatures, as shown in Fig. 6. Their results led them to suggest that at physiological temperatures amyloid seeds cannot form spontaneously from native lysozyme monomers. Oligomer self-replication from native monomers at physiological temperature is required to promote protofibril nucleation and further assembly into mature nanofibrils (bottom part of Fig. 6), which can also be created by using the denatured monomers and thus elevated temperatures (upper part of Fig. 6). This study outlined the self-replication ability of amyloid oligomers and protofibrils as distinct assembly pathways, and is important for understanding the molecular mechanisms and aggregation behaviour of both pathological and functional amyloid materials.

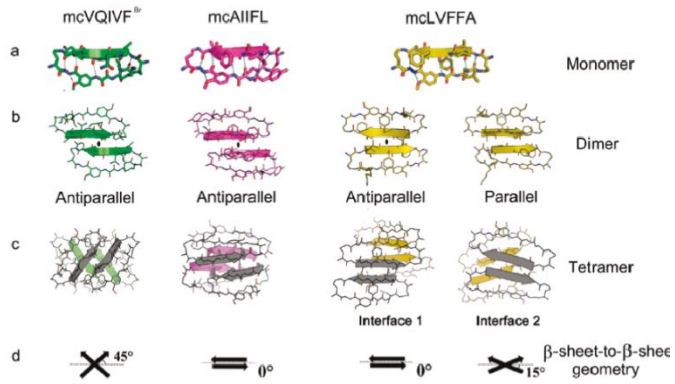

Fig. 7 (a-c) Crystal structure of macrocyclic peptides with (a) monomer, (b) dimer, and (c) tetramer. (d) Several interaction modes of dimers to form a tetramer. Reprinted with permission from Ref. 254. Copyright 2011 American Chemical Society.

X-ray crystallography and computer simulations have been widely utilized to investigate the atomic structure of amyloid oligomers that can assemble into crystalline morphologies.[254, 262, 263] Liu and co-workers designed a series of macrocyclic peptides based on Aβ and Tau proteins (associated with AD) that formed amyloid oligomers with a crystalline morphology.[254] Fig. 7 shows the atomistic structures of three macrocyclic peptides, mcVQIVFBr, mcAIIFL, and mcLVFFA, as monomers (Fig. 7a), dimers (Fig 7b) and tetramers (Fig 7c) as determined by X-ray crystallography and atomistic simulations. In the monomers, the interactions between the neighbouring strands are limited to the backbone hydrogen bonding (a typical β-sheet structure). For the dimers, the formed intermolecular β-sheets could be aligned in either parallel or antiparallel orientations via hydrogen-bonding interactions. In addition, tetramers could be formed by the complementary side-chain interactions of dimers with different molecular packing geometries, as shown in Fig. 7c and d. These findings are helpful for understanding the assembly of amyloidogenic oligomers at the atomic level and offer clues for the design of structure-based therapeutics against amyloid diseases. More recently, the same authors solved the crystal structure of a toxic amyloid oligomer of an 11-residue segment (KVKVLGDVIEV) from the Aβ protein.[262] Separately, Domanska et al. demonstrated the utility of nanobodies to trap and characterize the crystalline intermediates of β_2-microglobulin amyloids by X-ray crystallography.[263]

Amyloid oligomers with distinct molecular structure and morphology can be created by altering the assembly environment (e.g. temperature, pH etc) and changing the pathways of monomer aggregation. Alternatively, aggregation can be modified by promoting interactions between protein/peptide monomers with additional biomolecules (eg. non-amyloid proteins or macromolecular sugars).[264] Elucidating the structure of these oligomeric species at the atomic level will promote the understanding of formation mechanisms and toxicity of amyloid structures.

3.2 0D amyloid aggregates

By 0D objects we refer to aggregates/clusters, in which there is not a dominant dimensional feature, as in 1D or 2D objects, but for which self-limiting size is observed, differently from 3D aggregates. Numerous 0D amyloid aggregates have been generated *in vitro*. Observed morphologies include nanoparticles,[265-268] nanospheres,[269, 270] loops, triangles, squares, and rings.[271-273] In this section, we will review the main preparation strategies for these nanostructures and their corresponding formation mechanisms.

3.2.1 Nanoparticles and nanospheres

Prefibrillar amyloid structures such as spheroidal aggregates (nanoparticles and nanospheres), similar to the molecular oligomers introduced previously, have been frequently proposed to be a highly cytotoxic species in many neurodegenerative diseases.[265, 274] Silveira and co-workers degraded large prion protein (PrP) aggregates into smaller PrP nanoparticles with sizes ranging from 17 to 27 nm,[265] and then characterised the PrP nanoparticles with DLS, non-denaturing gel electrophoresis, and TEM. Their finding suggested that the PrP nanoparticles with masses equivalent to 14-28 PrP molecules are the most infectious initiators for prion diseases. In another study, El Moustaine et al. formed amyloid nanofibrils and nanoparticles from recombinant PrP at high pressure.[266] This study provided insight into the initial molecular processes that lead to misfolding and eventually self-assembly into higher order structures.

This journal is © The Royal Society of Chemistry 20xx

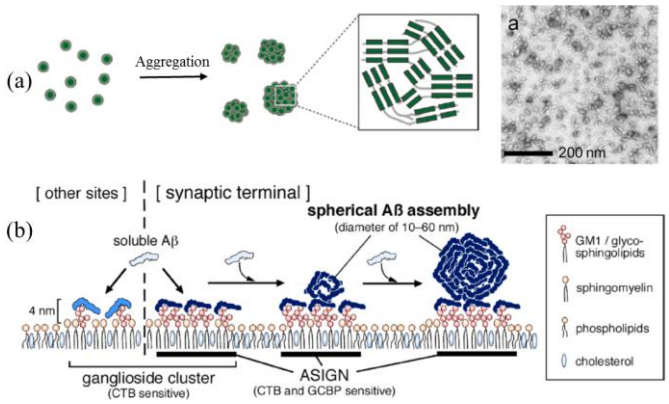

Fig. 8 Typical strategies for creating 0D amyloid (a) nanoparticles and (b) nanoclusters: (a) Aβ oligomer self-aggregation, (b) lipid bilayer membrane-induced Aβ assembly. CTB is cholera toxin B subunit. ASIGN is Aβ-sensitive ganglioside nanocluster. Images (a,b) are reproduced with permission from (a) Ref. 268, Copyright 2014, American Chemical Society, and (b) Ref. 270, Copyright 2013, American Chemical Society.

Other strategies besides elevated pressure and degradation of larger aggregates have been investigated for amyloid nanoparticle fabrication. Fändrich et al. reported the creation of $A\beta_{1-40}$ amyloid peptide nanoparticles by a simple self-aggregation method (Fig. 8a).[267,268] Typically, $A\beta_{1-40}$ with a concentration of 2.5 mg/mL was first dissolved in 100% HFIP, and the solution was diluted 10-fold with ultrapure water after 10 min incubation. Amyloid nanoparticles with sizes ranging from 15 to 30 nm were formed after a further 15 min incubation, as shown in the TEM image in Fig. 8a. In another study, Guo and co-workers reported that it is theoretically possible for triphenylalanine (FFF)-based peptides to self-assemble into nanospheres using the large-scale coarse-grained molecular dynamics simulations.[269] The simulations showed that the FFF nanospheres were formed and stabilized by peptide-peptide electrostatic, vdW interactions and strong peptide-solvent interactions.

Matsubara and co-workers demonstrated that $A\beta_{1-40}$ peptides can be induced to self-assemble into nanospheres on synapse-mimicking lipid membranes (Fig. 8b).[270] They showed that Aβ binding and assembly was promoted on GM1 lipid domains. This was found to be due to the presence of an Aβ-sensitive ganglioside nanocluster (ASIGN) within the glycosphingolipids (GM1) domain. The corresponding AFM images indicate that a thin Aβ layer and Aβ nanospheres were formed simultaneously. This study outlines a possible lipid mediated assembly mechanism of Aβ proteins that may occur in the AD brain.

3.2.2 Annular oligomers: Loops, triangles, squares, and rings

Other more complex 0D amyloid nanostructures have also been observed for a variety of amyloidogenic sequences, and include loops, triangles, squares, and rings.

Conway and co-workers reported the creation of annular oligomers of α-synuclein when comparing the aggregation behaviour of wild-type (WT) and a homo-mutant form (A53T) of α-synuclein connected to early-onset Parkinson's disease.[271] The nanoscale annular oligomers were formed from equimolar mixtures of WT and A53T protein. It was found that the acceleration of oligomerization but not fibrillization is a shared property of α-synuclein mutations, which suggests that the nonfibrillar intermediates, including annular oligomers, may be critical in pathogenesis. Elsewhere, Hatters et al. reported the preparation of annular oligomers from the aggregation of human apolipoprotein C-II (ApoC-II).[272,273] CD indicated a time-dependent increase in the amount of β-sheet structure. After incubation for 48 h, the amyloid aggregates were measured with transmission electron microscope (TEM) and AFM, and ordered closed loops with a diameter of 50-75 nm were observed. The above studies demonstrated an alternative folding pathway of human apolipoproteins. Two loop formation models, the wormlike chain and random-walk approaches confirmed that the formation of annular oligomers is critically dependent on the fibril flexibility, which allows the fibrils with appropriate lengths to bend back and anneal end-to-end to form a loop.[273] In addition, Wong et al. found that another apolipoprotein, ApoA-I, can also form loop-like structures with a periodicity in the range 25-60 nm.[275]

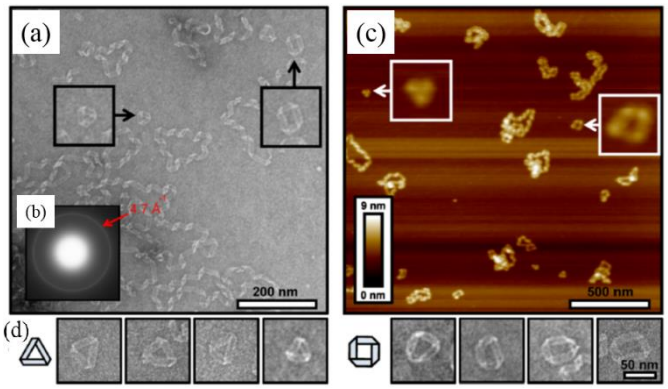

Fig. 9 Amyloid triangles, squares and loops of ApoC-III. (a,b) TEM image of loops and electron diffraction pattern, (c) AFM image of loops, and (d) TEM images of triangles and polyhedra. Reproduced with permission from Ref. [276]. Copyright 2014, American Chemical Society.

Recently, de Messieres et al. reported that ApoC-III protein can aggregate into 0D amyloid triangles, small squares and loops.[276] The formed amyloid loops (Fig. 9a and 9c) show ribbon-like structures consistent with helical twist, which is similar to the loop structures formed by α-synuclein,[271] ApoC-II,[272, 273] and ApoA-I.[275] The corresponding electron diffraction pattern (Fig. 9b) shows a typical interstrand spacing for the β-sheet conformation, suggesting the amyloid loops are formed by the self-assembly of β-sheets. Other amyloid structures including triangles and squares were also observed, as shown in Fig. 9d.

The formation of loop-like structures in amyloid oligomers is related to the structures and properties of constituent proteins. For example, the apolipoproteins (i.e. ApoA-I, ApoC-II, and ApoC-III) have similar helical conformation in an annular morphology as when they are bound to lipid membranes,[277] and all three proteins are found on high-density lipoprotein

and can mediate lipids to form plaques with a similar size and shape to lipoprotein particles.

Studies have suggested that the formation of annular amyloid structure maybe related to the "channel hypothesis".[278] This hypothesis proposes that cell death in neurodegenerative diseases occurs via a disruption of cellular homeostasis due to unregulated calcium (and other ion) transport across the cell membrane. This is thought to occur due to the presence of annular oligomers of Aβ peptides or proteins (e.g α-synuclein) that insert themselves into the cell membrane and creating aberrant ion channels. Ding et al. found that annular α-synuclein protofibrils could be produced when incubating spherical amyloid oligomers in solution or allowing them to adsorb onto *ex vivo* brain derived lipid membranes.[279] In their study, two distinct oligomeric morphologies were formed, namely spherical and annular protofibrils. The annular protofibrils were formed by incubating spherical oligomers for prolonged periods. In addition, membrane-associated annular protofibrils were observed by binding the spherical protofibrils to brain-derived lipid membranes. Further studies indicated that annular oligomers of α-synuclein resulted in a more rapid formation of pores or ion-permeable channels than the soluble monomeric α-synuclein, providing strong evidence for the neurotoxicity of small annular α-synuclein oligomers.[280-282] Kayed et al. studied the formation of annular Aβ and α-synuclein protofibrils in solution and on lipid membranes and proposed a possible formation mechanism of the annular protofibrils at the surface of lipid membranes.[283] Their mechanism states that spherical oligomers first interact with the membrane, and then the additional oligomers are recruited to the lipid bilayer, conjugate with the bound oligomers to form a β-barrel pore.

Whilst the "channel hypothesis" does provide a compelling explanation for neurotoxicity via uncontrolled calcium influx into cells, little direct evidence has been provided either *in vitro* or *in vivo.* Additionally a number of alternative mechanisms by which amyloid oligomers can induce similar cell membrane disruption have been proposed. These include membrane thinning,[284] excessive membrane tubulation,[285, 286] or membrane extraction through amyloid-lipid co-aggregation.[170, 287] Further research into the mechanisms driving the assembly of annular amyloid oligomers, both in solution and on model cell membranes will help to elucidate the importance and relevance of the "channel hypothesis" in relation to the alternative proposed mechanisms of cell membrane deregulation by amyloid oligomers.

3.3 1D amyloid superstructures

In this section, the self-assembly and formation of 1D peptide and protein nanofibrils, twisted and untwisted nanoribbons, helical ribbons and nanotubes are introduced and discussed in detail.

3.3.1 Amyloid protofilaments, protofibrils and nanofibrils

Here, we will focus on the formation and superstructures of amyloid protofibrils and nanofibrils,[288] we will place particular emphasis on fibrils possessing twisted, helical, and chiral morphologies.[289]

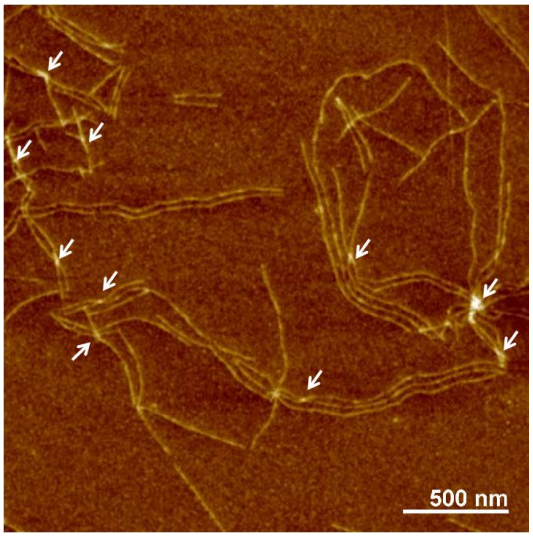

Fig. 10 Individual protofilaments of β-lactoglobulin aligning and starting to attach at specific points to form first protofibrils and finally mature fibrils. Reproduced with permission from Ref. [240]. Copyright 2011 Royal Society of Chemistry.

In general, all 1D amyloid superstructures are found to have a highly hierarchical morphology in which constitutive 1D fibril precursors combine to form mature amyloid structures. The terminology used for the 1D fibrillar precursors is not consistent through the literature, with the terms protofilaments or protofibrils loosely interchangable in most of the reports. Here we will adopt the view that protofilaments are the simplest mature 1D building block of amyloids, while protofibrils are a form of amyloid which has not yet reached the mature fully-formed stage. According to this terminology, protofilaments form individually first, then assemble into loosely packed protofibrils which further assemble into more ordered mature amyloid fibrils. Fig. 10 shows an example of such a process through individual snapshots resolved by AFM.[240] The white arrows highlight the points at which different protofilaments started to attach and overlap to form protofibrils.

Mature (1D) amyloid fibrils are then generally formed from a number of intertwined protofilaments each being 2-5 nm in diameter and up to a few μm in length.[235] Variations in the packing of these protofilaments result in a wide variety of morphologies all with potentially different functions. Insight into the packing mechanisms can be achieved with various nanoscale analytical techniques.

For example, Stroud et al. studied the structure and properties of oligomers of $A\beta_{1-42}$ with XRD, TEM, CD, FTIR, and chromatography.[290] They found that the peptide molecules could stack into short protofilaments consisting of pairs of helical β-sheets, which wrapped around each other to form a superhelical structure. In another example, Dearborn and co-workers utilized cryo-TEM and scanning transmission electron microscopy (STEM) to study the *in vitro* self-assembly of α-

 This journal is © The Royal Society of Chemistry 20xx

synuclein.[291] They found that protofibrils have a typical size with length of 7.5 nm and width of 2.5 nm.

In the following of this section we will discuss the various 1D morphologies observed and how they may affect their biological, biomedical or nanotechnological functions.

3.3.2 Twisted ribbons and helical ribbons

Many multi-filamentous morphologies have been observed including twisted ribbons, helical ribbons and rippled structures. Twisted ribbons are characterized by a saddle-like (Gaussian) curvature; helical ribbons on the other hand are characterized by a mean curvature but zero Gaussian curvature: in other words, they can be wrapped around a cylinder. The transition from twisted to helical ribbon in amyloid is now well understood and been reviewed already extensively.[154, 292] In general, a twisted to helical transition is observed upon increase in the number of protofilaments (width to thickness ratio), as a consequence of a different way to store bending and torsional energy by twisted vs helical ribbons. Helical ribbons can finally close into nanotubes eliminating the extra energy associated with edge line tension. This mechanism and the associated entire series of transitions have been observed both in peptide and protein-based amyloids.[29, 206, 293] More common, however, is the presence of one individual polymorphic form observed at distinct timepoints.

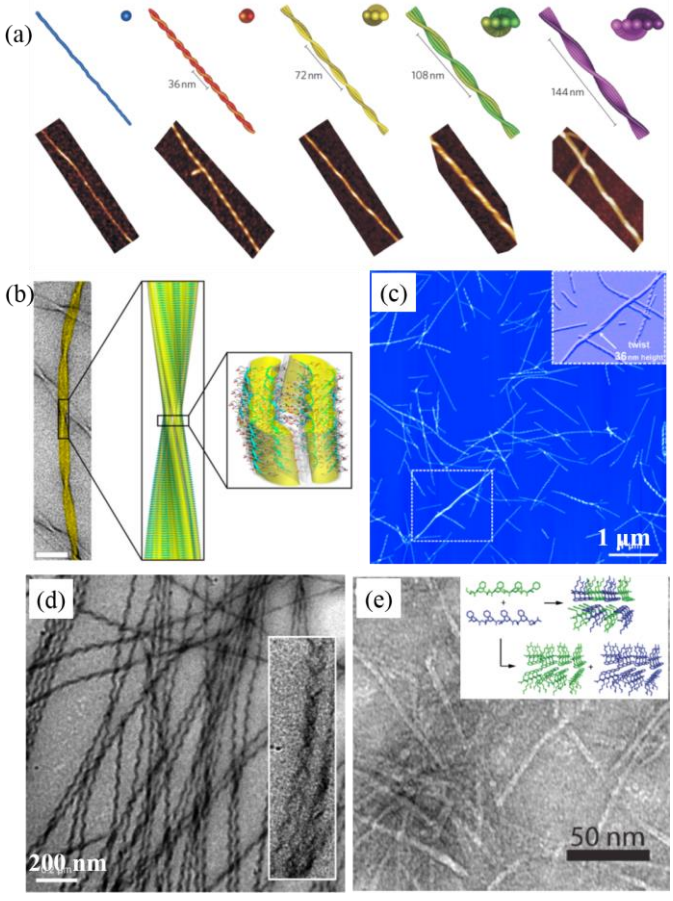

Fig. 11 Twisted and helical amyloid ribbons: (a) Left-handed β-lactoglobulin nanofibrils with multistranded twisted filaments. Reprinted with permission from Ref. 233. Copyright 2010, Nature Publisher. (b) Cross-β amyloid $TTR_{105-115}$ fibril with triplet atomic-resolution structure. Reprinted with permission from Ref. 294. Copyright 2013, National Academy of Sciences. (c) Twisted right-handed helical ILQINS hexapeptide ribbon. Reproduced with permission from Ref. 297. Copyright 2014, American Chemical Society. (d) Twisted double-helical peptide ribbon, Reprinted with permission from Ref. 298. Copyright 2009, Wiley-VCH Verlag GmbH & Co. (e) Amyloid-inspired rippled β-sheet ribbons by the co-assembly of enantiomeric amphipathic peptides. Reprinted with permission from Ref. 299. Copyright 2012, American Chemical Society.

α-synuclein fibrils have been shown to co-exist as left- and right-handed helical ribbons with differing pitches.[77] Adamcik et al. examined the different stages of aggregation throughout heat-denatured β-lactoglobulin amyloid fibril assembly with single-molecule AFM and theoretical analysis.[233] They found that the mature fibrils have a multistranded left-handed twisted morphology. Fig. 11a presents the typical AFM images and corresponding coarse-grain molecular dynamics reconstructions of the left-handed helical β-lactoglobulin fibrils. The β-lactoglobulin nanofibrils were shown to have persistence lengths of between 1-4 µm and maximum heights of 2, 4, 6, 8, and 10 nm for 1, 2, 3, 4, and 5 twisted filaments, respectively. In addition, the helical pitch of nanofibrils showed clear proportional increase from 35-135 nm with increasing filament number. This work provided a general model for understanding amyloid fibril assembly into a twisted ribbon morphology. In another study, Fitzpatrick and co-workers investigated atomic structure and assembly of fibrils formed from the $TTR_{105-115}$ peptide. As with α-synuclein and β-lactoglobulin, $TTR_{105-115}$ was found to assemble into mature fibrils via hierarchical assembly of β strands of peptide molecules into protofilaments which further intertwined to form mature fibrils with a twisted ribbon structure (Fig. 11b).[294]

In general, there is a well-defined linear relationship $L \propto n$ between the periodicity L of twisted ribbon amyloids and the number of constitutive protofilaments, n.[233] Using coarse grained simulations, Assenza et al. showed that the relationship between twisted ribbon periodicity and the number of protofilaments has a pseudo-linear behavior at small n, i.e. $L \sim (3n^2-7)^{1/2}$. When the number of protofilaments increases and the fibrils approaches maturity the relationship with periodicity approaches a truly linear behaviour.[295] This has led to the conclusion that this behaviour is a universal mesoscopic signature of amyloid fibril polymorphism.

Twisted and helical ribbons with different structures have also been created by selecting specific peptide sequences and controlling their molecular self-assembly. For example, Uesaka et al. investigated the self-assembly of the histidine (his)-containing helical peptides of the form A_3-His_n-B, where A is a hydrophilic polysarcosine chain, and B is a hydrophobic helical dodecapeptide.[296] Dependent on the pH of the peptide solutions the molecular assemblies formed different morphologies including twisted ribbons, helical ribbons, and nanotubes. The A_3-His_2-B peptide formed twisted ribbons, helical ribbons, and nanotubes at pH 3.0, 5.0, and 7.4, respectively, whilst A_3-His-B only formed helical

ribbons at pH 3.0. The pH dependent morphological changes were explained by variations in electrostatic repulsion, which in turn affected the molecular packing of the peptides. This study showed a very effective pH-responsive strategy for creating adjustable 1D amyloid structures by controlling the intermolecular interactions.

Lara and co-workers reported that a hexapeptide (ILQINS) identified as being an amyloidogenic sequence in left-handed helical ribbons formed from hen egg white lysozyme self-assembles into right-handed helical ribbons and crystals.[297] At short incubation times multi-stranded right-handed helical ribbon structures were observed (Fig. 11c). At longer incubation times the right-handed ribbons were almost entirely replaced by aggregates with a crystalline structure. Hamley and co-workers demonstrated the formation of left- and right-handed twisted helical amyloid ribbons by assembling the peptide fragment (KLVFF) modified with two β^2-Alanine residues ($\beta^2A\beta^2A$-KLVFF), as shown in Fig. 11d.[298] In some cases, the left- and right-handed twisted helices were intertwined into a double-helix amyloid ribbon, as shown in the inset image. The formation of helical ribbons is ascribed to both functional motifs of the designed peptide, in which the KLVFF motif is responsible for the self-assembly to cylindrical fibrils, and the β-amino acids are crucial for the formation of helical nanoribbons. A sequence of twisted fibrils, helical ribbons and nanotubes were observed as kinetic states during the aggregation of the capped version of this peptide, globular structures also being observed as the initial state.[293] The closure into nanotubes was very slow, being observed only after several weeks.

Swanekamp and co-workers reported the formation of rippled β-sheet $_{L/D}$-cofibrils from the coassembly of two enantiomeric amphipathic peptides, $_L$-$(FKFE)_2$ and $_D$-$(FKFE)_2$, as shown in the inset of Fig. 11e.[299] The $_L$-$(FKEF)_2$ peptide self-assembled in water into left-handed helical fibrils, whilst the $_D$-$(FKFE)_2$ peptide self-assembled into enantiomeric right-handed fibrils (TEM image of Fig. 11e). The equimolar mixing of $_L$-$(FKFE)_2$ and $_D$-$(FKFE)_2$ created a new fibril type, which contains alternating $_L$- and $_D$-peptides in a rippled β-sheet orientation.

Lashuel and co-workers demonstrated the creation of polymorphic β-sheet quaternary structures including fibrils and ribbons by using a small number of peptidomimetics.[300] They found that the distribution of quaternary amyloid structures could be adjusted by manipulating the pH, buffer conditions, and ionic strength. Their study indicated that it is possible to control both the self-assembly of designed peptide structures and their lateral interactions to create untwisted amyloid ribbons.

Adamcik and co-workers created large multistranded amyloid ribbons from the microtubule-binding fragment (**VQIVYK**PVDLSKVTSKCGSLGNIHHK, known as R3) of Tau protein.[301] Tau does not aggregate spontaneously *in vitro*, but it undergoes aggregation in the presence of polyanions such as heparin.[302] The peptide motif, **VQIVYK**, plays critical roles for the self-assembly and formation of β-sheet amyloid aggregates of Tau. Therefore, the self-assembly of R3 in both the presence and absence of heparin was investigated. In the presence of heparin, R3 fibrils with a normal twisted fibrillar morphology were rapidly formed as seen by AFM, TEM and strong ThT binding. In the absence of heparin, aggregation was much reduced, as evidenced by decreased ThT binding, however amyloid ribbons consisting of large numbers of laterally associated protofilaments were observed (Fig. 12a). Increasing incubation times up to 1 week demonstrated the continuous growth of the multifilamentous ribbons eventually forming giant multistranded amyloid ribbons with 2D laminated structures (composed of over 45 laterally associated protofilaments of 350 nm total width).

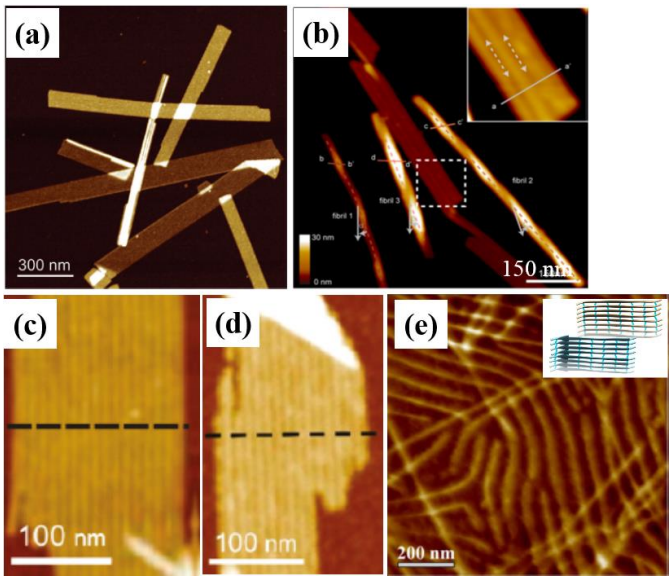

Fig. 12 Multistranded amyloid ribbons: (a) Tau protein R3 ribbon, Reprinted with permission from Ref. 301. Copyright 2016 Wiley-VCH Verlag GmbH &Co. (b) Multistranded $hIAPP_{20-29}$ ribbon, Reprinted with permission from Ref. 303. Copyright 2013, National Academy of Sciences. (c,d) Lysozyme (c) and β-lactoglobulin (d) ribbons, Reprinted with permission from Ref. 206. Copyright 2011, American Chemical Society. (e) Amelogenin ribbon, Reprinted with permission from Ref. 305. Copyright 2016, Nature Publishing Group.

Recently, Zhang et al. studied the self-assembled structures of $hIAPP_{20-29}$, the amyloidogenic core fragment relevant to type-II diabetes, by quantitative nanomechanical AFM.[303] They provided strong evidence of the coexistence of fibrils with flat ribbon and helical ribbon morphologies, as shown in Fig. 12b. As in the work of Adamcik et. al.,[301] the ribbons show clear striations along their long axis, indicating the presence of multiple parallel protofilaments (inset of Fig. 12b). AFM-based force-volume and nanoindentation measurements indicated that the flat ribbon structure has higher stiffness than helical ribbons, suggesting that the core of the helical ribbons were hollow.

Some proteins, such as lysozyme,[206] β-lactoglobulin,[206] and amelogenins,[304-306] can also form multistranded amyloid ribbons over time. Lara et al. introduced a general self-assembly mechanism for converting hydrolysed globular lysozyme and β-lactoglobulin into multistranded amyloid ribbons (Fig. 12c and d).[206] After long periods of time (up to 100 hours) multistranded ribbons with widths up to 173 nm were observed due to a modular lateral assembly of around 17 protofilaments. This study provided novel insight into the fibrillation mechanisms of globular proteins and amyloid polymorphism. Recently, Carneiro and co-workers showed that recombinant human full-length amelogenin protein (rH174) can self-assemble into amyloid-like ribbons both *in vitro* and *in vivo*.[305] In the presence of calcium and phosphate, rH174 assembled into

 This journal is © The Royal Society of Chemistry 20xx

highly aligned ribbons on glass substrate (Fig. 12e) with widths of 23 nm regular peak-to-peak distance of approximately 69 nm.

The above studies show that multistranded amyloid ribbons can be fabricated from a range of proteins or amyloidogenic peptides (i.e. R3, KLVFF, and VQIVYK). Examples such as this increase our understanding of how peptide sequences and the reaction conditions affect the final morphology of the assembled structures. A detailed knowledge of the factors underpinning assembly into mature fibrils should allow the routine rational design of amyloid forming peptides containing specified amino acid sequences additional to the amyloidogenic core. This will enable us to tailor the structure and function of the fabricated assemblies for a range of applications. Up until now such there are only a few examples of such functionalized peptide sequences,[307, 308] largely due to the difficulty in predicting the amyloidogenicity of the modified peptides.

3.3.3 Amyloid nanotubes

Amyloid protein and peptide nanotubes are a particularly interesting class of amyloid nanostructure, due to their uniform dimensions, hollow architecture, and potential for modification, which have led to many potential applications for materials science, nanotechnology, and biomedicine. A comprehensive review of the synthesis and bionanotechnological applications of various protein and peptide nanotubes is available,[309] in which the structure, design and corresponding nanotube assembly mechanisms of proteins (lysozyme, Hcp1, TRAP, and others) and surfactant-like peptides have been demonstrated and discussed. In this section, we will focus on the studies of several novel amyloid protein and peptide nanotubes first described after the publication of the above review.

Amyloid nanotubes can be created by either the closure of helical ribbons precursors as discussed above (section 3.3.2) or by molecular design of single proteins or peptide building blocks.[310-312] For example, Zhao et al. reported that a symmetric amphiphilic peptide with the sequence of KI_4K could assemble into nanotubes in aqueous solution.[311] The created peptide nanotubes have typical diameters in the range of 80-160 nm and lengths on the order of µm. In addition, they found that the peptide assemblies could be converted from nanotubes to nanofibrils by increasing the acetonitrile concentration in the assembly system. In another study, Brodin and co-workers reported the design and synthesis of protein nanotubes with adjustable diameters by using a single tetrameric Zn_8R_4 building block that created by mixing disulphide-linked protein dimer (R_2) with 4 equivalents of Zn^{2+}.[312] The formation and morphology of the nanotubes was mediated by altering the concentration of Zn^{2+} causing the rapid formation of nanotubes with a width of 48±3 and 20±2 nm, respectively. The initial formation of the Zn_8R_4 building blocks was crucial for the formation of nanotubes as the direct mixing of 10-fold Zn^{2+} with R_2 in the first step resulted in only amorphous aggregates. This work showed it is possible to kinetically dictate the self-assembly of protein building blocks to desired nanostructures by tuning the intermolecular interactions with metal coordination.

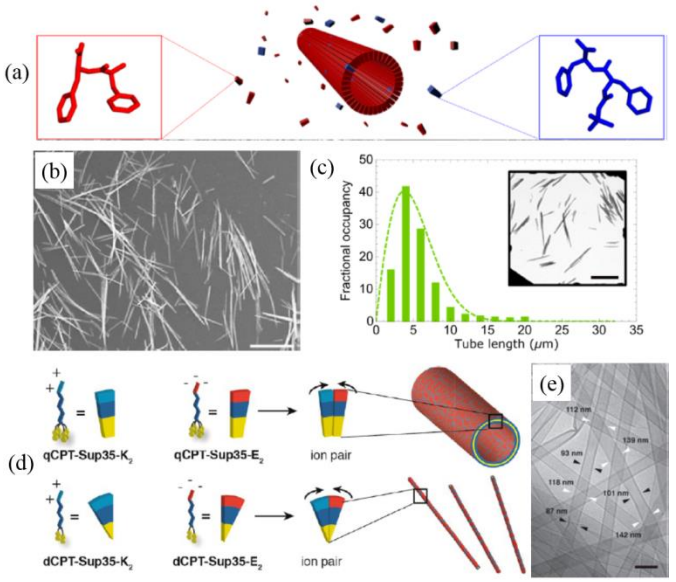

Fig. 13 (a-c) Supramolecular co-assembly for the formation of amyloid peptide nanotubes with controllable dimensions: (a) co-assembly mechanism of FF and Boc-FF, (b) SEM image of peptide nanotubes with a FF/Boc-FFF ratio of 5:1, and (c) Length distribution. Reproduced with permission from Ref. 313. Copyright 2016, American Chemical Society. (d,e) Co-assembly of amyloid amphiphilic peptide-based molecules to form multiwalled nanotubes: (d) co-assembly mechanism, and (e) TEM image of peptide nanotubes. Reproduced with permission from Ref. 314. Copyright 2014, American Chemical Society.

Amyloid nanotubes can also be prepared by the supramolecular co-assembly of two peptide-based building blocks.[313,314] The integration of two types of building blocks allows the fabrication of nanomaterials with complex structure and extended biophysical properties. Adler-Abramovich and co-workers formed peptide nanotubes with controllable physical dimensions[313] from the co-assembly of two diphenylalanine (FF) based building blocks. Aqueous solutions of FF and Boc-FF (N-(tert-butoxycarbonyl)-L-Phe-L-Phe-COOH), were mixed at various molar ratios (Fig. 13a). Increasing the Boc-FF concentration in the co-assembly system resulted in a systematic decrease in the length of the assembled nanotubes as shown in Fig. 13b and c. This work revealed a simple and effective strategy for creating peptide nanotubes with controllable length distribution through the co-assembly of two peptide building blocks, providing a template for molecular engineering at the nanoscale.

Lin and co-workers produced multi-walled amyloid nanotubes by mixing two oppositely charged drug-peptide amphiphilic molecules.[314] The peptide moiety GNNQQNY, a key β-sheet forming sequence derived from the yeast prion Sup35, was modified by an anticancer drug camptothecin (CPT) to design the drug-peptide building blocks. Two lysine (K) and two glutamic acid (E) residues were added to the C-terminal of the drug-peptide chain to adjust the overall amphiphilicity and pKa, as shown in Fig. 13d. They found that qCPT-Sup35-K_2 (here "q" means four CPTs are bound to the peptide moiety) and qCPT-Sup35-E_2 could co-assemble into nanotubes, but dCPT-Sup35-K_2 (here "d" means two CPTs are bound onto the peptide moiety) and dCPT-Sup35-E_2 could only co-assemble

into nanofibrils (Fig. 13d). When qCPT-Sup35-K_2 and qCPT-Sup35-E_2 were mixed, nanotubes with uniform morphology were clearly observed as shown in Fig. 13e. The created CPT-peptide nanotubes have an outer diameter of about 123 nm and wall thickness of approximately 25 nm, which suggest the presence of multiple bilayers in the assembled structure. Theoretically, the created drug-peptide nanotubes possess a 36% fixed CPT loading, and therefore could have promising application in drug delivery and cancer therapeutics.

3.4 2D amyloids (sheets, films, and membranes)

3.4.1 2D protein amyloids

Amyloid fibrils generally possess very high mechanical strength and adhere well to various substrates. These features make it possible to create 2D amyloid assemblies using simple post-assembly treatment techniques.

A number of different post-assembly processes have been investigated to fabricate 2D amyloid films. These include amyloid stacking,[315] filtration,[316] and self-assembly at the air-water interface.[317, 318] Lysozyme nanofibril films were created by stacking pre-formed nanofibrils onto a polytetrafluoroethylene film (Fig. 14a),[315] and β-lactoglobulin nanofibril films were fabricated via vacuum filtration of solutions of β-lactoglobulin nanofibrils (Fig. 14b).[316]

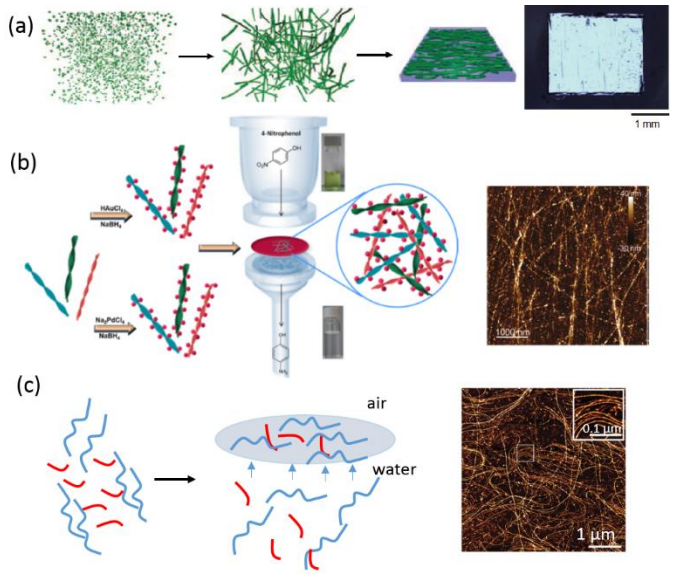

Fig. 14 Typical methods for the fabrication of 2D protein amyloids: (a) stacking, (b) filtration, and (c) self-assembly at air-water interface. Image (a-c) are reproduced by permission from (a) Ref. 315, Copyright 2010, Nature publishing Group, (b) Ref. 316, Copyright 2015, American Chemical Society, and (c) Ref. 317, Copyright 2016, Royal Society of Chemistry.

Jordens and co-workers reported the formation of β-lactoglobulin amyloid fibril films at an air-water interface.[318] The assembly mechanism was found to follow a complex non-equilibrium process leading to a crowded interface and a viscoelastic 2D film.[319, 320] The structure of the interface could be further defined by combining long protein nanofibrils with short protein linear aggregates, as shown in Fig. 14c.[317] Experiment and simulation results indicated that the short protein aggregates orient perpendicular to the long nanofibrils at very short distances and parallel to the axis of nanofibrils at intermediate distances, as shown in the AFM image in Fig. 14c. Liquid crystalline 2D bimodal systems such as this may have interesting technological applications but are complex and hard to control due to a large number of long-range non-covalent interactions affecting the self-assembly process. Thus studies such as this are very helpful to better understand and guide liquid crystal structures at an interface, and to unveil the process of formation of amyloid biofilms, as discussed later in this review.

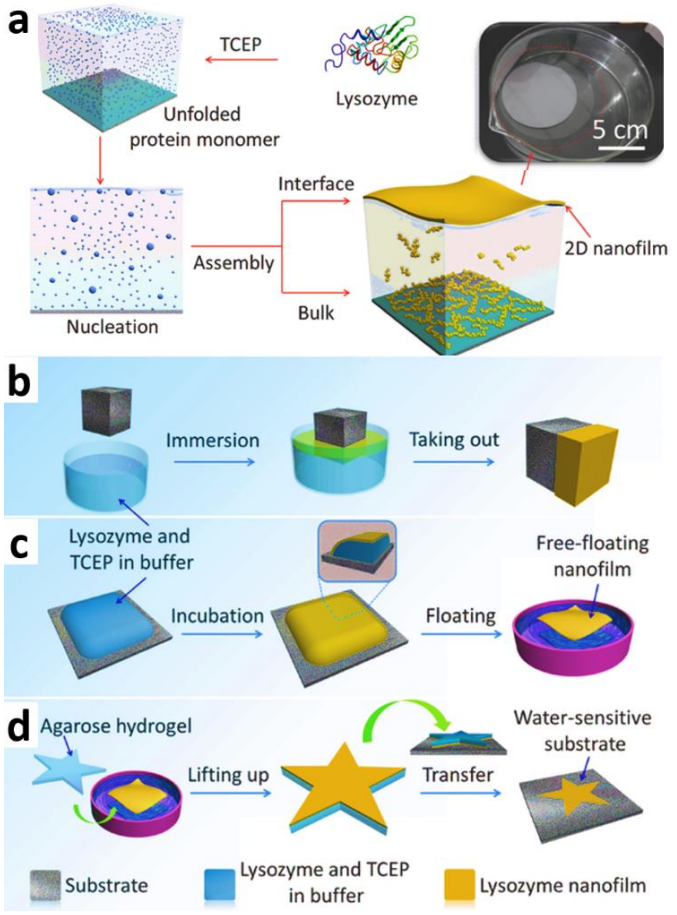

Fig. 15 (a) Schematic illustration of the proposed mechanism for amyloid nanofilm formation. (b-d) Schematic strategies for lysozyme fibril nanofilm formation (b) on the surface of immersed materials (solid/liquid interface) and (c) at the aqueous solution surface (vapor/liquid interface). (d) The contact-printing technique to deposit the free-floating amyloid nanofilm onto water-sensitive substrates Reproduced with permission from Ref. 321. Copyright 2015, Wiley-VCH Verlag GmbH & Co.

Recently, Wang et al. exploited the conformation change of lysozyme after breaking down its disulfide bond by tris(2-carboxyethyl) phosphine (TCEP) to induce heterogeneous nucleation and assembly (Fig. 15a).[321] The assembled lysozyme fibrils spontaneously concentrated at both the solid-water and water-air interfaces (Fig. 15a,b), and the films formed at the water-air interface could easily be converted to free floating films

This journal is © The Royal Society of Chemistry 20xx

(Fig. 15c) transferred to the surface of a hydrogel and contact printed onto a water sensitive substrate (Fig. 15d).

3.4.2 2D peptide amyloids

Amyloid nanofibrils fabricated from short peptide sequences have also been utilized to fabricate 2D structures including membranes,[322] nanosheets,[323, 324] and films.[325,326] This is typically achieved by adjusting the assembly conditions (ionic strength, pH or physical stimulations) to promote the formation of 2D substrates.

The Zhang group reported the spontaneous self-assembly of a self-complementary oligopeptide (EAK_{16}) to form a stable macroscopic membrane.[322] They found that peptides with alternating hydrophilic and hydrophobic amino acid residues readily form β-sheet structures and then aggregate into stable membranes dependent on the ionic strength of the solution. The assembled membranes have very high stability to heat and extreme pH (acid and alkaline) due to the formation of complementary ionic bonds between glutamic acid (E) and lysine (K) residues. This work paved the way for the fabrication of nanofibrous peptide structures with controllable self-assembly dependent on their sequence.

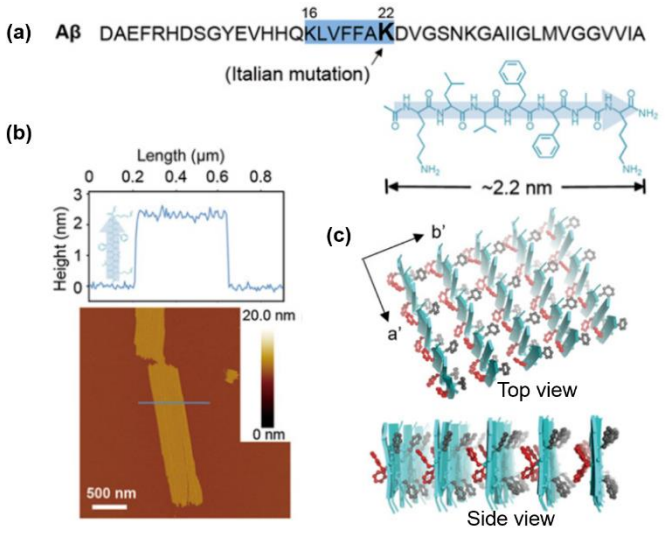

Fig. 16 a) Amino acid sequence of $A\beta_{1-42}$ and molecular structure of $A\beta_{16-22}$; b) AFM image and height analysis of self-assembled amyloid nanosheets; c) structural modal of the KLVFFAK nanosheet. Reproduced with permission from Ref. 323. Copyright 2015, National Academy of Sciences.

Dai and co-workers demonstrated the formation of amyloid nanosheets from a mutated form of $A\beta_{16-22}$ (KLVFFAK) (Fig. 16a).[323] The nanosheets were typically a few microns long, several hundred nm wide and around 2.2 nm thick (Fig. 16b). Increasing the ionic strength of the peptide solution promoted the formation of more uniform nanosheets. Based on their experimental observations and molecular dynamics simulations, the authors hypothesised that the peptide molecules within the nanosheet stand upright to form a monolayer (peptide length = 2.2 nm). The nanosheet then grows in two dimensions along both the fibril axis (a') via the main-chain hydrogen bonds and the zippering axis (b') via the side-chain steric hydrophobic interactions (Fig. 16c). This work shows that the functionality of amyloid nanosheets can be tuned by replacing the amino acid side chains at the periphery but retaining the core nanosheet-forming sequence (LVFFA). In another study, Hamley and co-workers reported that the amphiphilic peptide $(Ala)_6Arg$ could self-assemble into 3 nm-thick peptide sheets at low concentration in aqueous solutions.[324] The self-assembly of the peptide and the formation of sheets are driven by the amphiphilic sequence design of the peptide molecule with unique conformation and the electrostatic properties of the arginine headgroup.

Physical stimulations can also mediate the self-assembly of peptide molecules and promote the subsequent formation of 2D amyloid films. For instance, Pan and co-workers developed a simple, effective and environmentally friendly method of fabricating nanofibrous films from $A\beta_{16-22}$, via argon glow discharge.[326]

3.5 3D amyloid plaques and scaffolds

3D insoluble deposits in the brain (i.e. Lewy Bodies in PD, and Aβ plaques or Tau tangles in AD) are major pathological hallmarks in many neurodegenerative diseases.[327] These deposits typically have length scales spanning from several to a few hundred microns and are composed predominantly of amyloid fibrils, with other assorted biomolecules (lipids, sugars etc). Currently visualization of these deposits (often *post mortem*) represents one of the only definitive methods to diagnose a number of diseases including Alzheimer's or Parkinson's. Therefore, a considerable amount of research has focused on developing *in vivo* and *in vitro* brain imaging protocols to detect and observe these deposits. A number of different imaging techniques including magnetic resonance imaging (MRI),[328] positron emission tomography (PET),[329] near infrared (NIR) imaging,[330] and FTIR microscopy,[331] have been utilized to investigate the formation and growth of amyloid plaques. Benseny-Cases and co-workers used micro-FTIR spectroscopy to observe the in-situ co-localization of amyloid senile plaques in tissue samples of human brains affected by Alzheimer's disease.[331] They found that the oxidization of lipid in tissues is associated with the aggregation of peptides and the formation of amyloid plaques. The tissue samples from non-Alzheimer's disease samples showed lower level of lipid oxidation, which indicated that the oxidative capacity of amyloid peptides or proteins may play a crucial role in the formation of amyloid plaques.

In addition to natural amyloid plaques, artificial amyloid 3D structures (multilayers,[332] and microgels[333, 334]) have been reported. Qin et al. utilized an Aβ peptide derivative with a diphenylalanine moiety (Ne-RGDFF-OH) to create peptide nanofibrils that assembled into supramolecular hydrogels at both pH 8 and 6.5.[332] The self-assembly of the designed peptide was defined by three distinct motifs. The naphthyl group (Ne) provides the hydrophobic force to enhance the self-assembly ability in aqueous solutions, the FF motif serves as the core amyloidogenic sequence, and the RGD sequence (a

sequence found in the ECM protein fibronectin) acts as both an acceptor and a donor of hydrogen bonds. In addition, the RGD sequences can promote biocompatibility and cell attachment. Their results indicated that the designed peptide nanofibrils could be further adjusted into catenulate microfibers (forming a row or chain), multilayered amyloid plaques, and hydrogels by controlling the drying conditions of the amyloid nanofibril solution.

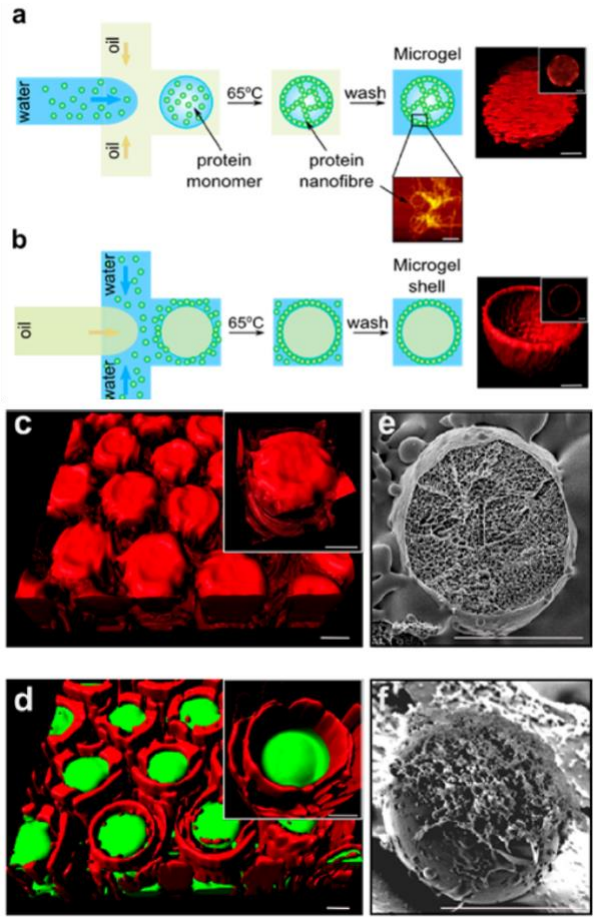

Fig. 17 Synthesis of amyloid 3D lysozyme microgels from amyloid fibril networks: a) water-in-oil microgels, and b) oil-in-water microgels. (c-f) Typical (c,d) 3D reconstructions of the confocal images and (e,f) cryo-SEM images of a) water-in-oil and b) oil-in-water microgels, respectively. Reproduced with permission from Ref. 334. Copyright 2015, American Chemical Society.

Amyloid nanofibrils can be also fabricated to form 3D microgels.[333] Recently, the Knowles group established a class of microgels based on amyloid protein fibrils by combining their inherent self-assembly process with microscale structuring techniques.[334] Both water-in-oil and oil-in-water microgels were prepared by forming microdroplets of a concentrated aqueous solution of lysozyme protein, as shown in Fig. 17a and b. For the formation of water-in-oil microgels, a microfluidic device was fabricated to create microdroplets of lysozyme solution encapsulated in an immiscible oil phase (Fig. 17a). After incubation, protein monomers assembled into protein nanofibril gels, which were recovered from the oil phase by extensive washing. Confocal fluorescence microscopy (Fig. 17c) and cryo-SEM (Fig. 17e) images indicated that networks of protein nanofibrils were formed in the interior of the microgels. When the phases are reversed (i.e water-in-oil becomes oil-in-water) hollow microgels were formed (Fig. 17b). The corresponding confocal fluorescence microscopy (Fig. 17d) and cryo-SEM (Fig. 17f) images showed that in this case the lysozyme monomers were located at the oil/water interface, and thus the fibrillar network structure was formed on the outer shell of the oil-in-water microgels. Protein microgels based on amyloid nanofibrils may have interesting applications for enhanced drug delivery due to their high biocompatibility and biodegradability.

3.6 Summary on the characteristic length scale of various amyloid structures

In parts 3.1-3.5, we have comprehensively reviewed the formation of various amyloid structures with morphologies including pre-fibrillar oligomers, nanoparticles, fibrils, films, and plaques. The various amyloid systems discussed and their dominant morphologies, length scale and assembly conditions are presented in Table 1.

Table 1 Summary of the types, species, length scales, and formation conditions of amyloid nanostructures.

Amyloid Type	Species	Length Scale	Assembly Condition	Ref
oligomers	lysozyme	Monomer to fibril	pH=3, 70°C	257
	cyclic peptide	monomer, dimer, tetramer	20 mM PBS, pH 7	254
	KCKCLGDVIEV	6-mers/2.2 nm	--	262
	β2-microglobulin	--	pH=7.5, 20 mM Tris	263
0D				
NPs	PrP	17-27 nm	self-assembly	265
NPs	Recom-PrP	20 nm	self-assembly	266
NPs	$A\beta_{1-40}$	15-30 nm	self-aggregation	268
sphere	FFF-peptide	10-13 nm	self-assembly	269
sphere	$A\beta_{1-40}$	10-60 nm	membrane-assembly	270
loop	α-synu-A53T	H=2-4 nm, D=23-55 nm	self-assembly	271
loop	ApoC-II	H=2.1 nm, W=12 nm, D=50-75 nm	self-aggregation in PBS buffer	272
triangle	ApoC-III	D=35-77 nm	NaPi buffer	276
1D				
protofibril	β-lactoglobulin	H=3 nm, L= 500 nm	pH=2, 90 °C, D_2O	240
protofibril	$A\beta_{1-42}$	13-28 nm	PBS, 37 °C	290
protofibril	α-synuclein	L=7.5, W=2.5 nm	HEPES, 37 °C	291
helical fibril	β-lactoglobulin	L=0.5-15 μm, H=2-6 nm	pH=2, self-assembly	233
fibril	$TTR_{105-115}$	H=7-16 nm, L=1-3 μm	aceton/water, pH=2	294
ribbon	ILQINS	W=63-87 nm, L=5.57 μm	pH=2, 90 °C	297
ribbon	$\beta^2A\beta^2$AKLVFF	W=17.5 nm	self-assembly	293, 298
cofibril	$(FKFE)_2$	D=8.2±1.0 nm, L= a few 100 nm	self-assembly in water	299
ribbon	R3	W=147 nm, L=a few μm	self-assembly in buffer	301
ribbon	$hIAPP_{20-29}$	H=7.4 nm, L=several 100 nm	self-assembly	303
nanotube	KI_4K	D=80-160 nm, L= a few μm	self-assembly in water	311

This journal is © The Royal Society of Chemistry 20xx

nanotube	Zn_8R_4	D=20-48 nm, L= a few μm	Zn^{2+}-induced assembly	312
nanotube	FF, Boc-FF	L=10 μm	90 °C , H_2O, assembly	313
nanotube	CPT-Sup35	D=123±28 nm, L= a few μm	1:1 MeCN/H_2O	314
2D				
film	lysozyme	a few mm	stacking	315
film	β-lactoglobulin	adjustable	filtration	316
film	β-lactoglobulin	adjustable	self-assembly at air-water interface	317
nanosheet	$Aβ_{16-22}$	H=2.3 nm, W=500 nm, L= a few μm	self-assembly	323
sheet	A_6R	thick=3 nm, L/W= a few 100 nm	self-assembly in solution	324
3D				
plaques	$Aβ_{1-42}$	Several-100 μm	aggregation	331
multilayer	Ne-RGDFF-OH	hydrogel	assembly at pH 8/6.5	332
microgels	lysozyme	2-60 μm	microdroplet	334

In addition, referring to previous reports by Knowles and Mezzenga,[32, 33] an illustrative chart of amyloid materials across all relevant length scales is shown in Fig. 18.

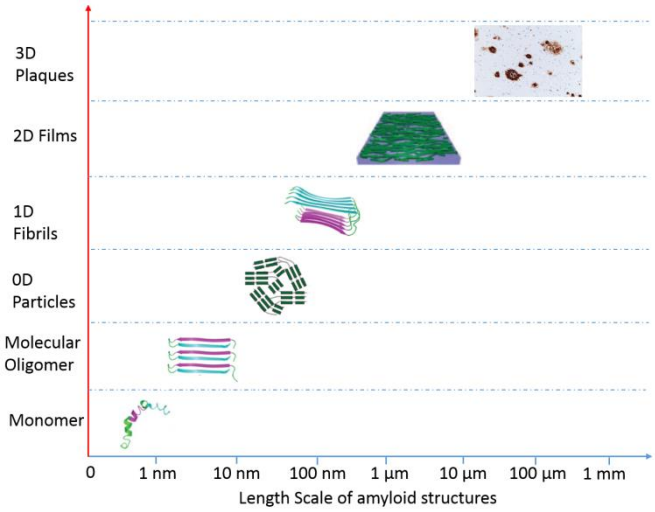

Fig. 18 Length scale of various amyloid structures from monomer to oligomers, 0D, 1D, 2D, and 3D.

4 Manifold functionality of biological and artificial protein/peptide amyloid materials

In this section, we will present and discuss the fabrication of biological (biofilms) and functional hybrid amyloid materials.

4.1 Fabrication and functions of biological amyloids

Natural protein and peptide amyloid materials show higher stability, mechanical strength, and increased resistance to protease biodegradation compared to their corresponding protein and peptide monomers. These properties have been utilised in nature to create "functional" amyloids with beneficial physiological functions. Numerous examples of functional amyloid systems have been found in bacteria, plants and mammals.[335-338] Additionally, the above physical characteristics make synthetic amyloids attractive structural components for the formation of functional biomaterials with wide ranging applications.

4.1.1 Amyloid-based biofilms

Biofilms are complex bacterial communities embedded in a predominantly proteinaceous ECM which protects bacteria from the surrounding environments.[339] Amyloid protein fibrils have been identified as a major structural component of many biofilms.[340] To better understand the fundamental processes underpinning biofilm formation, amyloid formations in bacterial biofilms (curli fibrils) have been investigated for growing films of E. coli.[14, 341] In the formation process of the biofilm, CsgA subunits are secreted by E. coli and self-assemble into amyloid curli fibrils, whilst CsgB subunits serve as nucleator proteins to anchor the curli fibrils to the bacterial membrane (Fig. 19a).[14]

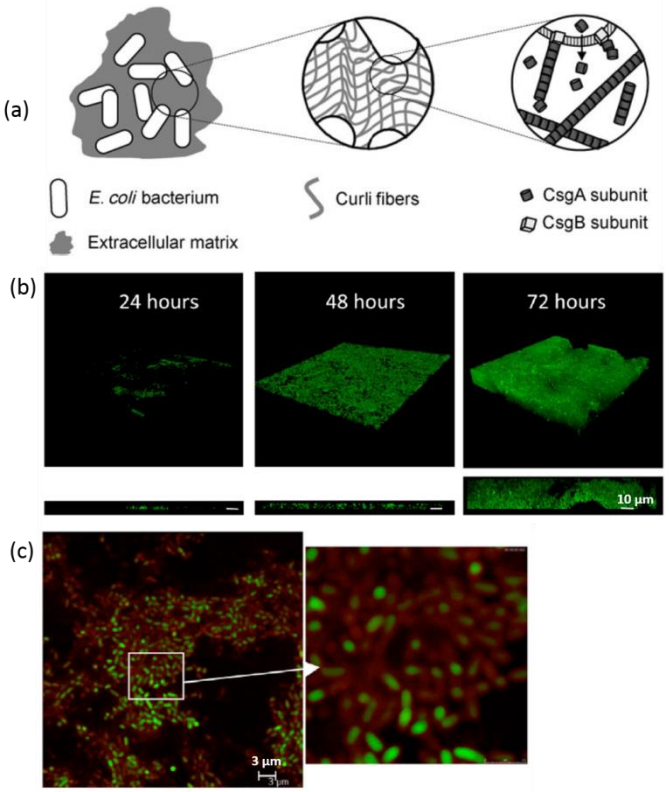

Fig. 19 (a) Formation mechanism of curli fibrils in E. coli biofilm. Reprinted with permission from Ref. 14. Copyright 2008, Wiley-VCH. (b) 3D projection (upper) and side view (lower) CLSM images of S. Typhimurium biofilms with growth period of 24, 48, and 72hs. (c) CLSM image of 72 h biofilm with DNA staining. Reproduced with permission from Ref. 345. Copyright 2015, Elsevier Inc.

Biofilm formation can also be affected by a range of other protein subunits other than CsgA and CsgB.[342-344] For example, Ostrowski et al. found that a small protein named YuaB serves both an exopolysaccharide and an accelerator for mediating the formation of TasA amyloid fibrils during biofilm formation.[342] Herbst et al. investigated the formation of biofilms with the Gram-negative bacterium, *P. aeruginosa*, and found that the proteome of this bacterium is tightly associated with amyloid

fibril formation, the distribution of fibrils, biofilm formation, and proteolytic activity.[344] Studies have also shown that DNA may play an important role in the formation of biofilms, Gallo and co-workers reported the formation and roles of curli-DNA composites in *S. Typhimurium* pellicle biofilms formed at the air-liquid interface (Fig. 19b).[345] Microscopy images of the 72 h *S. Typhimurium* biofilms showed high concentrations of stained DNA (Fig. 19c), indicating that extracellular DNA (eDNA) either released by dying bacteria or actively released into the ECM serves as an important component for the formation of these biofilms. Furthermore, ThT fluorescent assays showed that eDNA accelerates the polymerization of curli fibrils, inhibiting their degradation by DNAase and creating potent immunogenic complexes, which were seen to activate a number of different immune cell types. This work highlighted a role of curli-DNA composites in stimulating the innate and the adaptive immune system.

The formation of amyloid-based biofilms can be mediated by adjusting the physiochemical environment of the growing bacteria. For instance, Wu and co-workers investigated the formation of biofilms of *E. coli* at the air-liquid interface,[346] and found that the curli fibrils present in the biofilms result in a significant increase in their strength, viscoelasticity, and electrical resistance. The same authors studied the effects of chemicals such as dimethyl sulfoxide and ethanol on amyloid biogenesis and biofilm formation. They showed that the presence of these small molecules increased the formation of the *E. coli* biofilm.[347] Other environmental signals (e.g. ionic strength and pH) can also affect the formation of biofilms. Taglialegna et al. reported that the Bap protein of *S. aureus* assembles into functional amyloid nanofibrils and can be induced to form a biofilm matrix at low pH and in the presence of low concentrations of Ca^{2+} ions.[348] Increased Ca^{2+} concentration favours a more stable Bap conformation leading to the inhibition of amyloid formation. This relationship between Ca^{2+} concentration and amyloid formation could have implications in the design of antibacterial materials and therapeutics.

4.1.2 Amyloid hydrogels and aerogels

Hydrogels are water swollen polymeric networks formed by long range non-covalent interactions of self-assembled nanofibrils. Amyloidogenic proteins and peptides have been shown to make useful molecular building blocks for the design and synthesis of hydrogels.[349] Due to their relative ease of synthesis and biocompatibility these hydrogels show a wide variety of applications in diverse fields including: cellular therapies, drug delivery, and tissue repair.[67, 350] In order to successfully fabricate amyloid hydrogels two conditions must be met. First, the protein or peptide monomers must have the ability to form amyloid fibrils in aqueous solutions and second, the fibrils must be able to be synthesised at sufficient concentration to promote gelation.[19]

Amyloid hydrogels have been formed from a variety of amyloid proteins including elastin,[351] α-synuclein,[352] lysozyme,[353, 354] and β-lactoglobulin.[355-357] Bhak et al. reported the synthesis of amyloid hydrogels derived from α-synuclein fibrils with a curled morphology (so called CAF, or curly amyloid fibrils). They showed that CAF hydrogels have potential applications as a matrix for enzyme entrapment.[352] In their study, they found that under normal self-assembly conditions (200 rpm, 37 °C, and 100 h), α-synuclein preferred to form straight amyloid fibrils (SAF) that did not readily form hydrogels (Fig. 20a). CAF that did undergo gelation were created by isolating α-synuclein granules formed in the middle of the lag phase of the aggregation pathway. The granules were subjected to centrifugal membrane filtration to form CAFs (Fig. 20b). These hydrogels were characterised via ThT binding assays and confocal microscopy (Fig. 20c). The authors proposed that these α-synuclein hydrogels could have potential applications in fields as diverse as tissue engineering, drug delivery, nanofiltration, and biosensing. Knowles and co-workers fabricated lysozyme hydrogels loaded with drugs.[315] The addition of beta-adrenoceptor antagonists into the lysozyme hydrogel altered the nanostructure of lysozyme amyloids and affected drug release profiles. This study suggests that hydrogel-based drug carrier architecture can be adjusted to obtain desirable release performance by careful selection of structural promoters and disruptors of amyloids.

Bolisetty et al. discussed the gelation of β-lactoglobulin amyloid fibrils and proposed that β-lactoglobulin fibrils could undergo both an isotropic-nematic and a sol-gel phase transition with increasing fibril concentration or ionic strength.[357] This work sheds light on the dynamic behaviour of biological colloidal system and opens new directions in the fabrication of amyloid gels.

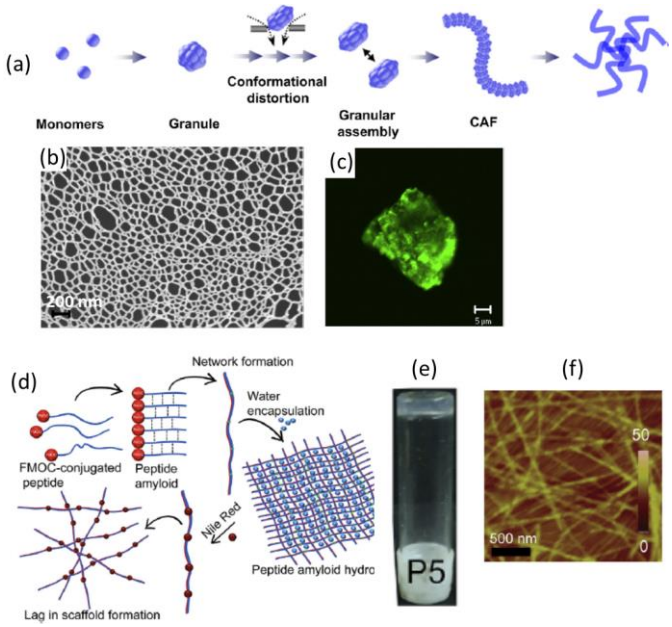

Fig. 20 (a-c) Amyloid protein nanofiber hydrogel: (a) formation mechanism, (b) SEM and (c) fluorescence images. Reproduced with permission from Ref. 352. Copyright 2010 Elsevier Ltd. (d-f) Amyloid peptide nanofiber hydrogel: (d) formation mechanism, (e) optical image of hydrogel, and (f) AFM image. Reproduced with permission from Ref. 19. Copyright 2015 Elsevier Ltd.

Hydrogels have also been prepared from Aβ amyloid fibrils. Jacob et al. studied the formation of self-healing amyloid hydrogels from a series of peptides based on the high

This journal is © The Royal Society of Chemistry 20xx

aggregation prone C-terminus of $A\beta_{1-40}$ and $A\beta_{1-42}$.[19] They found that a number of sequences only formed hydrogels when the amino acid sequence was conjugated to an aromatic Fmoc protecting group. Additional long range aromatic stabilisation (π-π stacking) offered by the Fmoc groups (Fig. 20d) was found to be a major driving force promoting gelation of these peptides. The addition of a fluorescent dye (Nile Red) into the peptide amyloid hydrogel inhibited gelation, suggesting that Nile Red blocks exposed hydrophobic sites on the formed amyloid fibrils and reduces their non-covalent interactions. The corresponding optical (Fig. 20e) and AFM (Fig. 20f) images identify the formation of amyloid hydrogels with 3D structure composed of nanoscale fibrous networks.

The additional stabilisation offered by the conjugated Fmoc group allows very short peptide fragments from Aβ to form amyloid-like hydrogels. For instance Fmoc-dipeptide hydrogels (FF and KK) have been formed based on β-sheet self-assembly and intermolecular π-π association.[358] Hydrogels have also been formed through the self-assembly of non Fmoc containing short peptides.[359-361] Tena-Solsona et al. demonstrated that the self-assembly and co-aggregation of tetrapeptides containing alternate aromatic and polar amino acid residues (Z-FDFD, Z-DFDF, and others, where Z denotes a benzyloxycarbonyl group) can lead to hydrogel formation, which can be used to screen positively charged Lys residues involved in amyloid misfolding.[359] In a further study, pH-responsive hydrogels were formed from Z-FDFD, Z-FKFK, and Z-KFKF.[360]

An interesting extension of the hydrogel, is its "dry" homologue, the so-called aerogel. In a recent study, Nystrom et al. demostrated that β-lactoglobulin amyloids can form ultralight aerogels composed solely of β-lactoglobulin amyloid fibrils and air.[362] This new material is among the lightest materials ever created and fully epxloits the rigidity and versatily of β-lactoglobulin amyloid fibrils. To create the dry form, the water content of β-lactoglobulin amyloid hydrogels was solvent-exchanged with ethanol to produce an alchogel. Then, exploiting the fact that ethanol is fully miscible with supercritical CO_2, they removed the liquid phase by supercritical CO_2 processing, leading to the final amyloid aerogels. Excitingly, these aerogels can be used to template the formation of hybrid materials with unique properties, leading, for example to the lightest form of gold ever produced to date. These gold aerogels were formed by combining β-lactoglobulin amyloid fibrils and gold single crystals and fabricating the aerogels as outlined above. The resultant aerogels contain no more than two percent solid mass. Beside being the lightest gold material ever produced, the gold aerogels have additonal properties unseen in solid gold, such as photonic, fluorescent and catalytic properties. This example and the others preceding it illustrate the endless possibilities available when designing materials using amyloids as building blocks.

4.2 Fabrication and functions of artificial amyloid-based hybrid materials

Amyloid fibrils generally display multiple, identical, and periodically spaced binding sites for small molecules along their surface. This makes them an exciting prospect for the design of amyloid materials functionalised with specific chemistries post-assembly. In this section, we will introduce the preparation and fabrication of 1D, 2D, and 3D functionalised or hybrid nanomaterials.

4.2.1 1D amyloid-based hybrid materials

Lysozyme, Aβ, curli proteins and a number of other systems have been used to fabricate 1D amyloid hybrid systems. Whilst amyloids make ideal substrates for hybridisation with additional functional materials, care must be taken that additional materials do not modify amyloid aggregation altering the balance of hydrophobic and electrostatic interactions within the forming fibrils.

4.2.1.1 Amyloid-nanoparticle

One of the most studied amyloid hybrid systems is the amyloid-nanoparticle hybrid. Such hybrids allow the fabrication of nanoparticle-decorated amyloids with specified material properties. Alternatively, nanoparticles have been used as therapeutic targets for disease related amyloids with the aim of inhibiting amyloid aggregation. Typically, the formation of amyloid-nanoparticle hybrids is based on metal or metal compound nanoparticles.[363-365] Bolisetty et al. reported the synthesis of hybrids formed by dispersing negatively charged iron oxide (Fe_3O_4) magnetic nanoparticles in positively charged β-lactoglobulin solutions at acidic pH. Depending on the pH, different hybrid aggregates are formed, at pH 3 amyloid fibrils with their surface decorated with nanoparticles were observed and at pH 4.5 only spherical nanoclusters were observed.[366] Liao et al. studied the influence of gold nanoparticles (AuNPs) on Aβ fibrillation and found that they could alter the observed fibrillization pathways.[367] AuNPs added to preformed Aβ fibrils, caused fragmentation of the fibrils. AuNPs possessing negative surface potential inhibited Aβ fibrillation and redirected assembly into off-pathway intermediates. Such anionic AuNPs could potentially have applications as AD therapeutics preventing assembly into toxic species.[367]

More complex nanoparticles have also been investigated. For instance, Yoo et al. reported that thioglycolic acid-stabilized CdTe nanoparticles are capable of efficient inhibition of amyloid formation.[136] Inhibition occurred as CdTe nanoparticles preferably bind to oligomers but not monomers, halting the aggregation process at this stage. This paper highlights a potential issue with such amyloid inhibitors; indeed, preventing fibrillization may be relatively simple, but if it is at the expense of creating more amyloid oligomers, extreme care must be taken to ensure that the oligomers formed are not themselves highly cytotoxic. Other nanoparticles have also been used to reduce amyloid aggregation kinetics. Anand et al. designed capsaicin-capped silver nanoparticles (AgNPs) to suppress albumin aggregation.[364] Interestingly, assembly inhibition was not observed in the presence of isolated capsaicin molecules or unmodified nanoparticles, suggesting a co-operative effect between the silver nanoparticles and capsaicin coating.

Polymeric nanoparticles have also been shown to affect the fibrillation kinetics of amyloid fibrils. Brambilla et al. showed that

PEGylated nanoparticles with long *in vivo* retention times bind strongly to the $A\beta_{1-42}$ peptide.[368] Structural analysis revealed that binding occurred through a non-specific binding of the PEG polymer on the surface of the NP (Fig. 21a). Simulations revealed that the PEG chains wind around the helical peptide between residues 1-25 and more loosely interact with the helix at residues 26-42 and at the β-turn (Fig. 21b and c). To evaluate the role of oxygen atoms in the PEG, it was replaced with a fully alkylated polymer chain. This fully saturated polymer chain did not wind around the helix (1-25) but bound only with the termini of both helices, clearly indicating the importance of the oxygen atoms in such polymers.

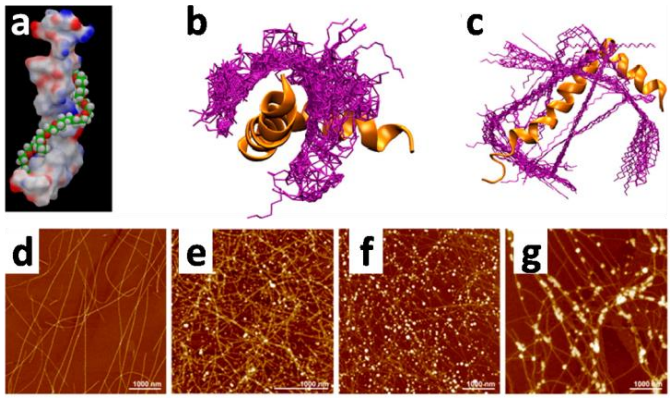

Fig. 21 (a) Atomistic model of a PEG chain docked to $A\beta_{1-42}$. The chain interacts with both hydrophobic as well as hydrophilic residues of the peptide and forms a spiral structure. (b) Best 50 conformations of the PEG chain (purple) docked to $A\beta_{1-42}$ (orange), and (c) alkyl PE chain (purple) docking on $A\beta_{1-42}$ (orange). Images (a)-(c) are Reproduced with permission from Ref. 368. Copyright 2012, American Chemical Society. (d-g) AFM (bottom row) images of the β-lactoglobulin amyloid fibrils (d) and fibrils decorated by gold (e), silver (f), and palladium (g) nanoparticles after the respective metal salt reduction by $NaBH_4$. Images (d)-(g) are reproduced with permission from Ref. 370. Copyright 2014, American Chemical Society.

Amyloid fibrils have also been used for metallization and mineralization experiments, and the fabrication of amyloid-nanoparticle nanohybrids. Previously, Wei and co-workers showed it was possible to functionalise the surface of amyloid-like fibrinogen nanofibrils with AuNPs.[369] Bolisetty et al. were able to decorate β-lactoglobulin amyloid fibrils (Fig. 21d) with Au (Fig. 21e), Ag (Fig. 21f), and Pd (Fig. 21g) NPs via metal salt reduction by $NaBH_4$.[370] Hamley et al. examined the labelling of amyloid nanofibrils created from the self-assembly of a surfactant-like peptide $Ala_{10}His_6$ (hexa-histidine connected with an oligo-alanine sequence) with NTA functionalized AuNPs in the presence of Ni.[371] Pazos and co-workers reported a one-pot synthesis for the nucleation of uniformly sized and spatially ordered AgNPs using supramolecular nanofibrils formed by peptide-amphiphiles.[372] Aldehyde moieties at the N-terminus could reduce two silver ions to form Ag_2 clusters without the need for an external reducing agent or additives to control the nucleation process.

4.2.1.2 Amyloid-quantum dots

Similar to nanoparticles, QDs have been shown to inhibit amyloid fibrillation. Xiao et al. reported that N-acetyl-L-cysteine capped QDs (NAC-QDs) are capable of disrupting the fibrillation of insulin amyloid assemblies due to hydrogen bonding between the NAC-QDs and the fibrils.[373] Ng et al. suggested that NAC-QDs may act as neuro-protective agents through fibrillation inhibition and a reduction in the formation of reactive oxygen species.[374]

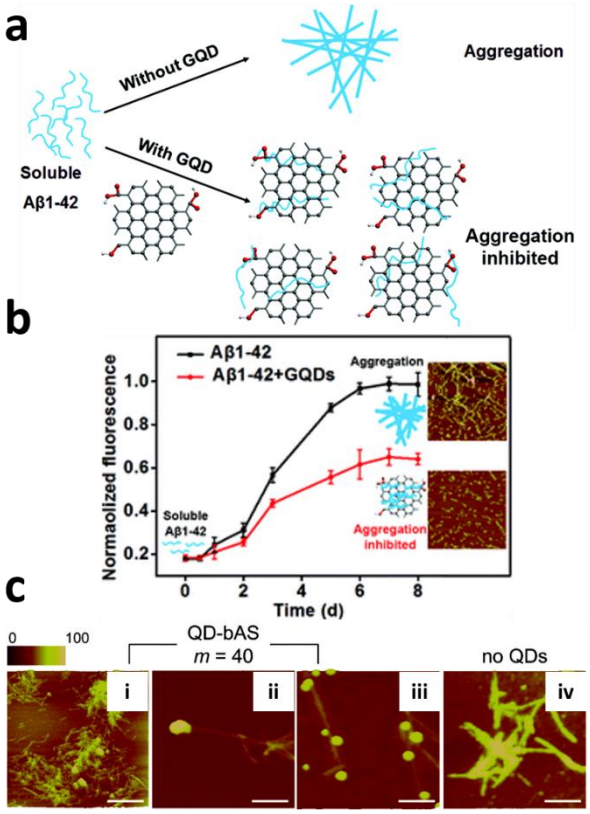

Fig. 22 (a) Schematic representation of the GQDs used for inhibiting the aggregation of $A\beta_{1-42}$ peptides. (b) The kinetics of $A\beta_{1-42}$ aggregation as monitored by the thioflavin T fluorescence in the absence of GQD or presence of GQD. Reproduced with permission from Ref. 375. Copyright 2015 Royal Society of Chemistry. (c) AFM images of the fibrils obtained from mixtures of (i-iii) QD-bAS (QD/bAS = 1/40), and (iv) α-synuclein alone. Scale bars: 10 µm. Reproduced with permission from Ref. 376. Copyright 2009, American Chemical Society.

Liu et al. demonstrated graphene QDs (GQDs) can efficiently inhibit the aggregation of Aβ peptides.[375] This is thought to be either due to binding of the negatively charged GQDs to the central hydrophobic motif and/or positively charged histidine residues present on $A\beta_{1-42}$ (Fig. 22a and b). Further studies revealed that the inhibition efficiency of the GQDs decreased with increasing surface negative charge, indicating that the hydrophobic interactions are likely to be dominant. In some cases, QDs can accelerate the aggregation of amyloid proteins. Roberti et al. demonstrated that the aggregation of α-synuclein at high concentrations was enhanced by adding multivalent QDs (Fig. 22c).[376] This is likely due to aggregation seeding initiated by the high local concentrations displayed at the surface of the QDs. Fig. 22c (i-iii) shows that the QDs functionalised with biotinylated α-synuclein (bAS) are incorporated into α-synuclein fibrils resulting in increased aggregation.

This journal is © The Royal Society of Chemistry 20xx

The inherent fluorescence of QDs opens many new potential applications for amyloid fibrils-QD hybrids, for example they could be used as fluorescent biosensors, or for bioimaging or diagnostics. NHS modification of CdSe-ZnS core-shell QDs has been used to detect the formation of amyloid protein fibrils in solution by fluorescent measurements after binding to the fibrils.[94] Quan et al. reported a red-emitting fluorescent probe constructed by PEGylated QDs further functionalized with benzotriazole (BTA) that facilitated the targeting to the β_2 position of Aβ fibrils with high affinity, enabling the sensitive detection of amyloid fibrils.[377] Due to a combination of the greater fluorescent quenching of QDs and the higher affinity of the BTA, QD-PEG-BTA probes were able to achieve more sensitive detection than conventional thioflavin derivatives. Su et al. used peptide nanofibrils decorated with QDs as an intracellular fluorescent imaging agent.[378] Cellular internalization of the nanofibril-QD hybrids was promoted by increased interactions between the cationic fibrils and the slightly negatively charged outer leaflet of the cell membrane. In a further study, they created novel functional hybrid materials based on the conjugation of GO, peptide nanofibrils, and GQDs.[379]

4.2.1.3 Amyloid-hydroxyapatite

Due to broad functionalization possibilities, long contour lengths, exceptional mechanical properties, accurately controlled growth and ease of synthesis, amyloid fibrils are ideal candidates to act as biomimetic materials, performing similar biological functions to fibrous networks such as fibronectin or collagen. *In vivo* bone regrowth occurs in the presence of collagen-hydroxyapatite (HA) composites, thus in the fields of tissue engineering and regenerative medicine there is a strong desire for biomaterials that can mimic the properties of these composites.[380] The Stupp group demonstrated that one-dimensional cylindrical and fibrillar nanostructures were able to direct the growth of oriented HA crystals, while flatter nanostructures failed to reproduce the orientation found in biological systems.[74, 380] By adjusting pH, concentration and ionic strength, Wei et al. prepared amyloid-like fibrinogen fibrils in the absence of Ca^{2+} and thrombin.[95] These fibrils were mineralised to form amyloid-HA composites proving that self-assembled fibrinogen nanofibrils can mimic collagen and serve as a building block for HA-based biomaterials for bone tissue regeneration applications. Wang et al. fabricated a HA scaffold via layer-by-layer assembly of graphene oxide (GO) nanosheets and preformed fibrinogen nanofibrils.[381] After 7 days of mineralization in simulated body fluid, the GO-nanofibril surface was uniformly covered with branch-like apatite minerals that didn't appear on a bare GO substrate. Therefore, it appears that the amyloid nanofibrils provided a structural foundation and surface functional groups for the growth of HA crystals. A second generation of amyloid peptide nanofibrils was designed with specific motifs present on the surface of the fibril to provide the nucleation sites for HA mineralization.[382] Using these fibrils and GO nanosheets, they fabricated a nanohybrid scaffold designed to promote mineralisation. The second generation nanohybrids enhanced nanoscale apatite crystal growth leading to the formation of HA spheres with a diameter of 4 μm.

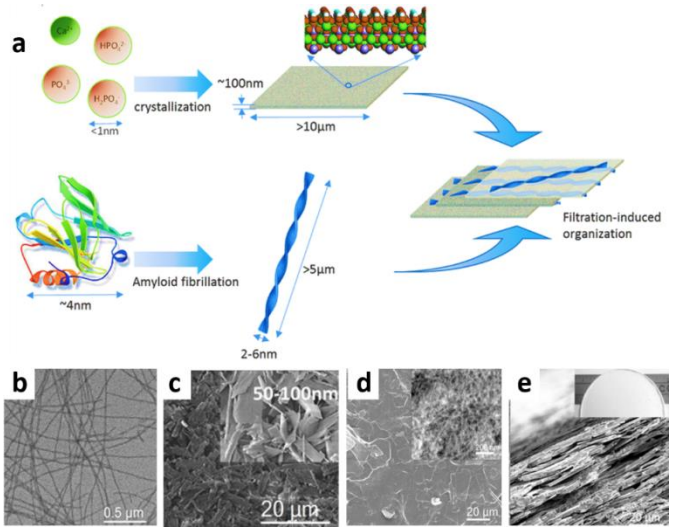

Fig. 23 (a) Schematic representation of the fabrication of bone-mimetic composites based on amyloid fibril and HA platelets. (b) TEM image of β-lactoglobulin amyloid fibrils. (c-e) SEM image of HA platelets (c), surface (d) and fracture sections (e) of the amyloid-based composite with 60 wt% brushite platelets. Reproduced with permission from Ref. 383. Copyright 2014, Wiley-VCH Verlag GmbH & Co.

In order to be useful biomimetic scaffolds for bone re-growth, amyloid-HA hybrids should not only promote mineralization but they must also display the high levels of mechanical stiffness required to provide the load bearing ability of newly formed bone. Adopting a simple filtration procedure, Li et al. fabricated a highly laminated structure composed of β-lactoglobulin and/or lysozyme amyloid fibrils and HA platelets (Fig. 23a).[383] The formed fibril network possessed a homogenous and compact surface and the resultant biomimetic bone grown on the networks had similar Young's modulus and density to human bone (Fig. 23b-e). More importantly, these scaffolds promoted the growth of human osteoblast cells, providing a compelling example of amyloid-based biomimetic bones.

4.2.1.4 Amyloid-carbon materials

Various carbon nanomaterials including fullerenes (C_{60}), carbon nanotubes (CNTs), graphene, and GO have been investigated for their ability to inhibit amyloid assembly.[384, 385] Due to the presence of multiple benzene rings in the majority of carbon nanomaterial structures, hydrophobic interactions are thought to play a key role in the inhibitory ability of carbon nanomaterials. In a comprehensive review, Li and Mezzenga discussed how C_{60}, CNT and GO affect amyloid fibrillation and the formation of amyloid-carbon material hybrids.[384] It is expected that the conformation and chemical behaviour of the Aβ peptide will change in the presence of single-walled carbon nanotubes (SWNTs) due to the adsorption of the peptide onto the hydrophobic surface of the SWNTs. Importantly, the cytotoxicity of cells cultured in the presence of SWNTs coated with Aβ peptides was drastically reduced compared to cells cultured with the Aβ peptide alone.[386]

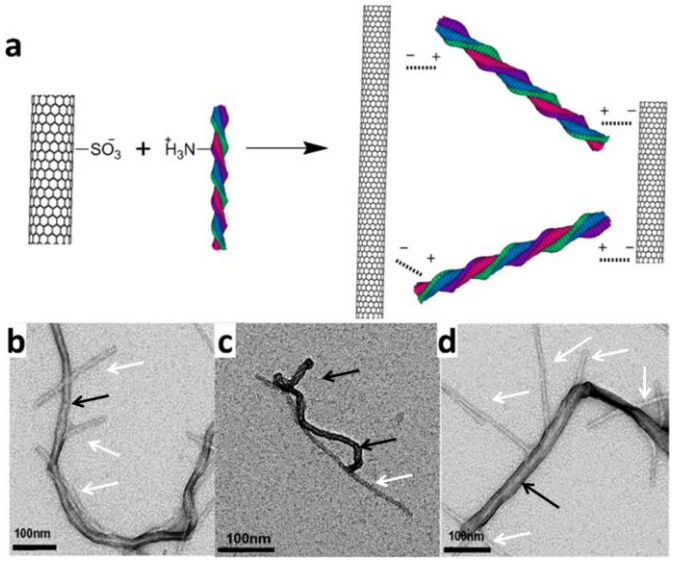

Fig. 24 Formation of amyloid nanofibril-MWNT hybrid: (a) Schematic illustrations of functionalization of CNTs with amyloid fibrils. (b-d) TEM images of hybrids consisting of functionalized MWNTs (black arrows) and amyloid fibrils (white arrows) at 0.1 wt % with (b and c) covalent and (d) noncovalent functionalization. Reproduced with permission from Ref. 355. Copyright 2012, American Chemical Society.

To enhance the binding of amyloids to carbon nanomaterials, attempts have been made to modify the nanomaterials with reactive polymers or small molecules. For example, Li and Mezzenga introduced sulfonic functional groups on the surfaces of multi-walled carbon nanotubes (MWNTs) promoting interactions with β-lactoglobulin fibrils (Fig. 24a).[355] The negatively charged functionalised MWNT surfaces promote complex formation with the positively charged β-lactoglobulin fibrils. Beside complementary chemistry, other factors such as the persistence length (of both MWNTs and fibrils) and ionic strength are important for the fabrication of hybrid amyloid-carbon materials. If the persistence lengths of both MWNTs and amyloid fibrils are not similar, the mismatch leads to a misalignment of the fibrils along the MWNTs contour lengths due to a high content of SO_3^- (Fig. 24b and 24c). However, an appropriate content of SO_3^- would make individual MWNTs match several amyloid fibrils at different positions, as shown in Fig. 24d.

The surface modification of carbon nanomaterials plays an important role in the design of multifunctional amyloid-carbon material composites.[381, 382, 387] For instance, positively charged lysozyme fibrils can bind to GO sheets, providing binding sites for negative charged AuNPs.[388] The charges from GO and lysozyme become partially nullified, making the hybrids ideal platforms for immobilizing additional molecules such as enzymes to afford additional functions.

Mahmoudi et al. found that the large available surface area of GO sheets is able to delay the process of Aβ fibrillation via adsorption of amyloid monomers.[389] In addition, the protein coating layer can create a protective shell on the surface of the GO sheets, resulting in an increase in the amyloid assembly lag time. Yang et al. reported that graphene nanosheets could penetrate and extract a large number of peptides from pre-formed amyloid fibrils.[390] This leads to the intriguing question of whether graphene or GO sheets could have therapeutic applications and potentially reverse the amyloid formation process in neurodegenerative diseases. However, it is likely that such therapies would either need to be injected directly into the brain or be able to cross the BBB, factors that complicate the development of such therapeutics. Very recently, Castelletto and co-workers reported the fabrication of a hybrid biomaterial based on the co-operative self-assembly of polysaccharide sodium alginate with PA (C_{16}-KKFF) and subsequently adding GO.[391] The created hybrid biomaterial showed excellent bioactivity and high mechanical strength.

4.2.1.5 Amyloid-biomacromolecules

Functionalizing amyloid fibrils with specific biomolecules such as proteins and sugars may have significant biomedical applications. For instance, networks of amyloid based materials can be produced that mimic various biological tissues such as muscles or the cornea.[392, 393]

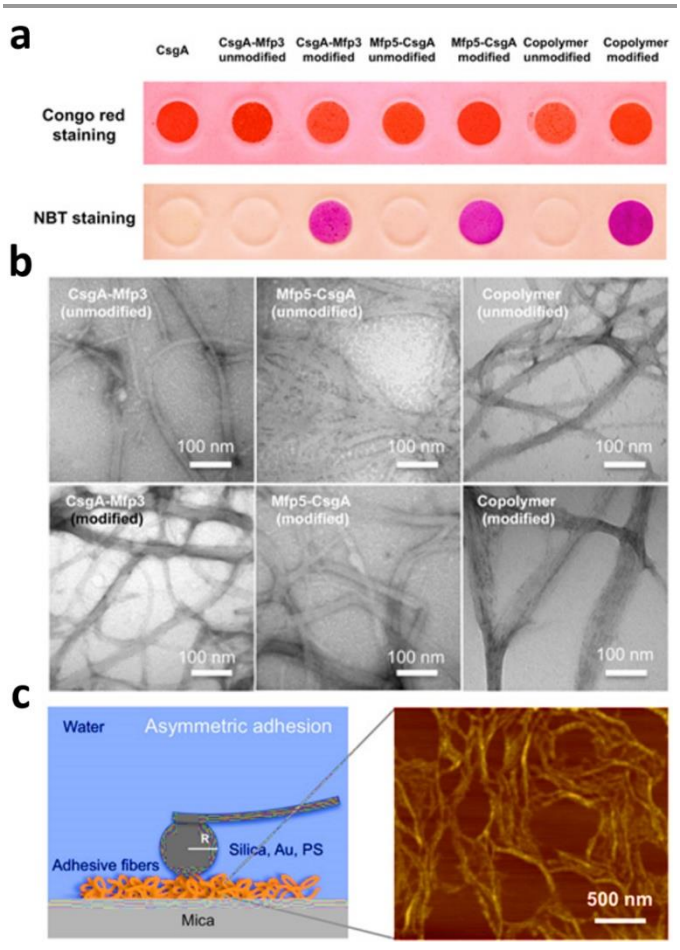

Fig. 25 (a) CR and NBT assays confirm the amyloidogenic features and the formation of amyloid-DOPA hybrid. (b) TEM images of unmodified and modified amyloid nanofibrils with biomolecules. (c) Schematic presentation of the measurement of the adhesion force between amyloid nanofibrils and biomolecules with AFM force spectroscopy. Representative AFM image showing modified Mfp5-CsgA fibres 1 h after deposition on a mica surface. Reproduced with permission from Ref. 394. Copyright 2014, Nature Publishing Group.

This journal is © The Royal Society of Chemistry 20xx

Zhong et al. reported strong underwater adhesives constructed by co-polymers of tyrosine containing mussel foot proteins (Mfps) of Mytilus galloprovincialis and CsgA protein (which forms curli fibrils in *E. coli*).[394] The co-polymers all formed fibrous structures, but the nitro blue tetrazolium (NBT) assay turned purple (to confirm the presence of the adhesive moiety DOPA) only when the Mfps proteins were modified with tyrosinase (which converts tyrosine residues to DOPA) (Fig. 25a and b). To assess the underwater adhesion of the adhesive fibres, AFM tips modified with silica, gold or polystyrene surfaces were used. The strongest adhesion was found with silica tips and tyrosinase-modified fibres, suggesting that the amyloid domains of the adhesive fibres not only provided a high surface area for contact but could also modulate how the Mfp domains interact with the substrates and achieve different adhesion levels (Fig. 25c). In another case, Dubey et al. identified that amyloid nanofibrils can promote co-aggregation of other proteins, which also explained the mechanism of coexistence of two amyloid-linked diseases in individual patients.[395] However, both aggressive co-aggregation and cross-seeding reactions between different proteins occurred only at 70 °C.

There are many studies based on physiochemical properties and functions of amyloid fibril based materials.[396] Nikiforov et al. studied electromechanical coupling of amyloid fibrils in both prokaryotic and eukaryotic cells.[397] They found that the mechanical properties of the fibril and the electrical double layer at the fibril- water interface are responsible for its electromechanical response. Ling and co-workers combined regenerated silk fibrils from *Bombyx mori* (*B. mori*) fibroin with amyloid fibrils produced *in vitro* from β-lactoglobulin.[398] By either adding inorganic nanoparticles or by selectively removing one of the fibrous constituents via enzymatic reactions, they further explored how the Young's moduli, porosity and stimuli-responsive features of the resulting hybrid materials can be controlled. The authors also showed that these membranes could be used for molecular-weight dependent separation, pointing at possible future applications of these porous scaffolds as protein-based separation membranes.

4.2.2 2D amyloid-based hybrid materials

The Young's modulus of many amyloidogenic 2D films are similar to those of many rigid proteinaceous materials found in nature, (e.g. keratin and collagen).[315] Thus, when functionalized with additional biologically relevant molecules, 2D amyloid-hybrid materials can be fabricated that mimic both chemical and structural facets of biology.

Based on amyloid fibrils and silk fibroin fibrils, Ling et al. designed a multifunctional membrane decorated with magnetic nanoparticles.[398] The formed membrane was transparent and homogenous under cross-polarized light, with β-strands of silk fibroin running parallel to the film plane and the amyloid fibrils in a perpendicular orientation (Fig. 26a and b) as detected by Wide-angle X-ray scattering (Fig. 26c-e). The addition of positively charged magnetic nanoparticles resulted in the fabrication of a homogenously distributed film combining dual magnetic and moisture responsiveness (Fig. 26f and g). Hydration of the membrane resulted in a reduction in rigidity and allowed for cyclic shape printing and recovery on repeated wetting and drying cycles. Upon applying a magnetic field to the hydrated film the membrane underwent a bending motion and maintained its shape after removal of the field and drying. Layer-by-layer deposition of silk proteins and amyloid fibrils has also been employed to create an immunosensing platform capable of detecting $A\beta_{1\text{-}40}$.[399] Multilayers containing 1, 3 and 5 bilayers of silk fibroin and $A\beta_{1\text{-}40}$ fibrils were fabricated that showed linear responses to increasing $A\beta_{1\text{-}40}$ antibody concentrations via cyclic voltammetry.

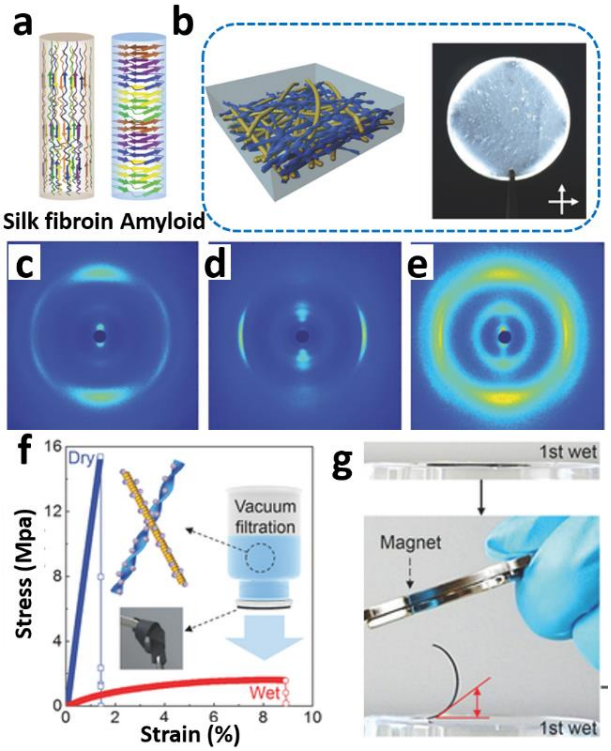

Fig. 26 (a) Schematic orientation of β-sheets and β-strands in silk fibroin fibrils and amyloid fibrils. (b) Schematic illustration and cross-polarized light observation image of silk fibroin fibrils and amyloid fibrils composite film. (c-e) 2D-WAXS patterns of the films containing (c) 100% silk fibroin fibrils, (d) 100% amyloid fibrils and (e) 5:5 silk fibroin fibrils:amyloid fibrils. (f) Magnetic functionalization and tensile properties of the film (silk fibroin fibrils:amyloid fibrils:magnetic nanoparticles weight ratio of 70:10:20), as prepared by vacuum filtration. (g) Shape-memory properties of the magnetic composite film when exposed to the combined presence of an external magnetic field and water. Reproduced with permission from Ref. 398. Copyright 2014 Wiley-VCH Verlag GmbH & Co.

Wu et al. used the previously discussed amyloid-GO immobilization platform to immobilise Au nanocatalysts and enzymes.[388] This integrated system maintained the catalytic activity of the immobilized AuNPs, and was used as an electrochemical sensor for colorimetric glucose sensing. Yan et al. also reported a new approach combining electron-induced molecular self-assembly with simultaneous metal nanoparticle formation.[400] The peptide motif KLVFF ($A\beta_{16\text{-}20}$) was combined with metal ions and assembled into membranes in the presence of an argon plasma. The argon plasma resulted in the reduction of the metal ions forming homogenously dispersed metal NPs that decorated the underlying film of amyloid fibrils.[326] Such

hybrid amyloid-nanoparticle films may have important applications in heterogeneous metal catalysis. This has been recently demonstrated with amyloid-nanoparticle porous membranes, capable of securing a continuous flow of a feeding solution which undergoes instantaneous heterogeneous catalysis within the hybrid membranes.[316]

2D amyloid hybrids have also been used to elucidate a better understanding of the mechanisms of bacterial biofilm formation. Nguyen et al. fused functional peptide domains onto the CsgA protein, resulting in a self-assembled network of curli fibres resembling the wild-type system.[401] This molecular engineering strategy should provide diverse artificial functions to synthetic hybrid amyloid biofilms. Additional peptide sequences could be introduced to the biofilm to provide various functionality including biomineralization, substrate adhesion, and protein immobilization. Using similar strategies, robust 2D materials with programmed functions could be fabricated with applications as large-scale engineered biomaterials.

4.2.3 3D amyloid-based hybrid materials

Utilizing amyloid-based molecules as building blocks to develop 3D functional materials with well-defined architectures and chemistry is a growing area of interest.[402, 403]

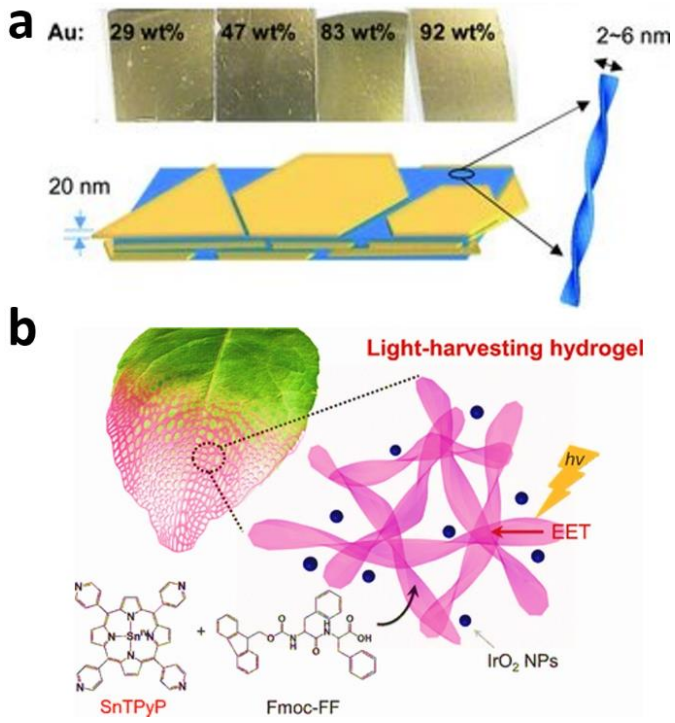

Fig. 27 (a) layered organization of amyloid fibrils and gold platelet hybrid nanocomposites. Reproduced with permission from Ref. 404. Copyright 2013, Wiley-VCH Verlag GmbH & Co. (b) An illustrative description of the development of a photoluminescent peptide-QD hydrogel through the self-assembly of Fmoc-FF building blocks and their PL quenching associated with the enzymatic detection of analytes. Reprinted with permission from Ref. 406. Copyright 2014, Wiley-VCH Verlag GmbH & Co.

3D hybrid amyloid materials are typically designed based on one or several kinds of lower dimensional materials. For example, Lara and co-workers fabricated 3D structures from single crystal nanoplatelets, protein nanotubes and ribbons.[29] By changing the procedure by which water is removed from the system, the same building blocks can be organized into organic-inorganic hybrid films of unique physical properties, composed of well-organized layered 2D single crystal gold nanoplatelets and 1D amyloid fibrils (Fig. 27a).[404] Adhikari and Banerjee incorporated graphene and reduced graphene oxide (RGO) into amyloid networks resulting in stable transparent hydrogels.[405] In this system, two kinds of Fmoc protected dipeptides, namely, Fmoc-YD-OH and Fmoc-FD-OH formed composite hydrogels without the presence of any external stabilizing agent. The hydrogels were stabilized via inherent π-π interactions between the Fmoc group, the aromatic side chains of Tyr and Phe residues and the RGO sheets. A number of stimulus-responsive amyloid hydrogels have also been investigated. For instance, by combining MWNTs decorated with sulfonic groups and β-lactoglobulin nanofibrils pH-responsive hydrogels were fabricated that reversibly form gels at acid pH.[355]

Metallized and small molecule modified nanofibrils also offer the possibility to create hydrogels for applications in nanotechnology. In a recent study conducted by the Stupp group,[372] bacterial growth was inhibited by hydrogels formed from peptide nanofibrils decorated with AgNPs. Kim et al. formed meso-tetra(4-pyridyl) porphine (TPyP) and Fmoc-diphenylalanine (Fmoc-FF) composite nanofibrils.[406] The four pyridyl groups at the meso-functional position of TPyP and carboxylic and hydroxyl groups of Fmoc-FF promoted hydrogel formation (Fig. 27b).

5 Various applications of amyloid-based hybrid nanomaterials

Thanks to their unique physiochemical properties, amyloid based nanomaterials, have many potential applications in a number of fields including biomedical engineering, tissue engineering, energy storage and catalysis. In this section we will review some of the most promising and exciting examples of where amyloid materials have been incorporated into functional devices.

5.1 Biomedical engineering

Historically, research on amyloids has largely focused on obtaining an improved understanding of the mechanisms causing toxicity in neurodegenerative diseases. However, in more recent times there has been a growing interest in using non-toxic amyloid assemblies for biomedical engineering applications.[33, 407] Some of the key studies in this area will be outlined in this section.

Due to the regular distribution of labile groups on their surface, many amyloid fibrils are amenable to functionalization with a broad range of moieties and molecules. For instance, Bolisetty et al. showed that amyloid fibrils can be used to enhance nanoparticle transfection into living organisms by incubating gold, silver, and palladium nanoparticle-decorated amyloid fibrils in the presence of living dendritic or MCF7 cells and confirmed their ability to cross the cell membrane and be uptaken into living cells (Fig. 28a).[370] Mains et al. explored lysozyme amyloid hydrogels loaded with a series of small

This journal is © The Royal Society of Chemistry 20xx

molecule beta adrenoceptor antagonists such as atenolol, propranolol and timolol.[354] Atenolol was shown to disrupt β-sheet content within the hydrogel whilst propranolol had the opposite effect and timolol had little effect. This research highlighted the need for careful selection of structure promoters and disruptors for drug delivery applications. The conjugation of amyloid fibrils with drug compounds may also be a useful strategy to create long-acting drug depots and provide controlled release systems preventing rapid clearance from the body.[17]

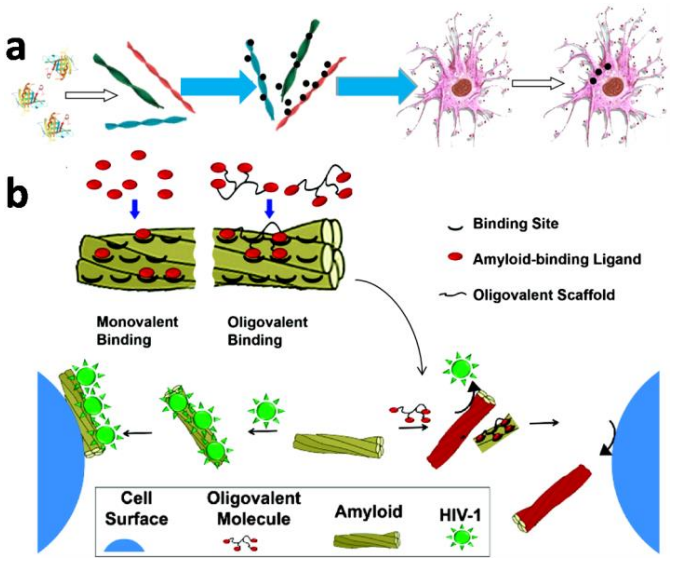

Fig. 28 (a) Schematic representation of the internalization and transport of metal nanoparticle-decorated amyloid fibrils into living cancer cells. Reprinted with permission from Ref. 370. Copyright 2014, American Chemical Society. (b) Proposed coating mechanism of SEVI fibrils with amyloid-binding oligomers. These coatings prevent the direct interaction of HIV-1 with SEVI fibrils and prevent SEVI-mediated enhancement of viral infection in cells. Reprinted with permission from Ref. 413. Copyright 2012, American Chemical Society.

Cheetham et al. designed a drug-peptide conjugate from Tau fibrils and the anticancer drug CPT (mCPT-mal-Tau), which formed discrete, stable, well-defined nanofibrils and nanotubes capable of quantitative drug loading.[408] The drug loading in the peptide nanostructures increased from 23% in non-fibrous controls to 38%. The corresponding drug release experiments indicated that the self-assembled drug-loaded peptide nanostructures released the bioactive form of the drug and enhanced the *in vitro* efficacy against a number of cancer cell lines.

Further examples of amyloid based drug delivery systems include a camptothecin (KCK-CPT) prodrug, that self-assembles initially into nanotubes, and upon complexation with hyaluronic acid into arrays of nanofibrils which form micelles upon dilution.[409] The hyaluronic acid-coated micelles were then seen to undergo efficient endocytosis into cancer cells *in vitro* where they were degraded back to the nanofibrous morphology in the endosome. Finally, the KCK-CPT prodrug was converted to the active form by glutathione (GSH) in the cytoplasm, inducing apoptosis in the cancer cell. Waku and Tanaka showed that self-assembling peptide nanofibrils can be used as potential delivery agents for vaccines.[410, 411] Highly antigen-loaded nano-assemblies were formed by conjugating antigens to β-sheet-forming peptides. The antigen-loaded peptide nanofibrils were taken up more efficiently by murine RAW264 cells compared to monomeric cell penetrating peptide-modified antigenic peptides, possibly because their size is more suitable for cellular uptake. Improved intracellular antigen delivery using a system such as this may promote a more efficient induction of the immune response required for effective vaccination to occur.

Due to their small size and nanoscale regularity, amyloid oligomers have been explored as potential nanomaterials for improved targeting and medical imaging. By conjugating either fluorescent molecules or superparamagnetic iron oxide (FeO) particles with oligomeric Aβ, Kumar et al. observed that the oligomeric hybrids specifically targeted macrophages in an *in vitro* co-culture of peripheral blood mononuclear cells and macrophages.[268] Of particular interest might be both the visualization of disease-associated accumulation of macrophages *in vivo* by MRI and the imaging of atherosclerotic plaques to assess the extent of cardiovascular disease. Very recently, Lock and co-workers synthesised an anticancer drug, Pemetrexed (Pem), conjugated onto the peptide sequence (FE).[412] The PemFE conjugate spontaneously self-assembles into nanofibrils and hydrogels under physiological conditions. The location, distribution, recovery, and drug release of injected PemFE hydrogels was successfully monitored by chemical exchange saturation transfer (CEST) MRI. This work proposed a potential strategy to monitor the in vivo distribution and release of drugs by using supramolecular design and self-assembly.

Capule et al. reported that oligovalent amyloid-binding molecules can reduce the enhancement of human immunodeficiency virus-1 (HIV-1) infection. The designed amyloid binding molecules competitively bind to semen-derived enhancer of virus infection (SEVI) fibrils preventing SEVI-mediated enhancement of viral infection in cells (Fig. 28b).[413] Yolamanova et al. demonstrated that amyloid fibrils fabricated from a 12-residue peptide (enhancing factor C) boosted virus infection of HIV-1 by a factor of four compared to naturally occurring SEVI fibrils.[414] This reduced virus infection is due to the formation of an electrostatic 'nanobridge' between the virion and the cell. Such amyloid based nanomaterials may significantly improve our ability to direct retroviral gene transfer in basic research and clinical applications.

5.2 Tissue engineering

Materials that can accurately replicate the structure of the micro- and nano-scale fibrous network that surrounds many cell types, the ECM, have many applications in tissue engineering and cellular therapies. For instance, ECM mimicking scaffolds may aid the culture of large volumes of clinically relevant therapeutic cells *in vitro*, or be used as implantable scaffolds for cell growth and tissue regeneration *in vivo*. Networks of amyloid fibrils assembled from either natural proteins or synthetic peptides are promising candidates for such materials as they possess similar morphological and mechanical properties to the fibrillar proteins that make up the ECM (e.g. fibronectin, collagen, and laminin). Additionally, they can be inexpensive to produce in the large

volumes required for clinical applications and are well suited to chemical functionalization with peptide sequences (typically from ECM proteins) that may promote cell adhesion, growth or differentiation (in stem cells).

In 2004, the Stupp group integrated the IKVAV sequence (a cell binding sequence from laminin) with a PA system to fabricate nanofibrous hydrogels. The density of the IKVAV presentation on the surface of the nanofibrils was three orders of magnitude higher than for laminin in the ECM. Furthermore, neural progenitor cells cultured in these hydrogels were seen to efficiently differentiate into neurons.[415] Various other amyloid based systems decorated with cell adhesion sequences have also been reported. For instance, Gras *et al.* modified a 10-residue peptide fragment ($TTR_{105-115}$) of the amyloidogenic protein transthyretin (TTR) with the integrin binging sequence RGD from fibronectin. In addition to the RGD modified sequence two similar sequences were synthesised with additional tripeptides that have no reported biological activity (RAD and RGE). All three peptides retained their ability to form amyloid fibrils and supported cell growth when fibroblasts were cultured on adsorbed networks of the fibrils. Only the RGD presenting fibrils was able to disrupt fibroblast cell adhesion to a fibronectin coated substrate. This suggests that the RGD modified fibrils can competitively bind to integrin assemblies present on the cell membrane.[308] The biocompatibility of these modified $TTR_{105-115}$-RGD fibrils has been further explored using a number of membrane integrity and apoptotic markers.[416] Despite good cellular attachment (via specific RGD-integrin bonds), the materials were found to show fibril morphology and concentration dependent cytotoxicity after longer periods of time. Studies such as this highlight the importance of fully understanding how physical, morphological and chemical properties of amyloid based materials affect cellular interactions before they can be applied as biomaterials. In addition to $TTR_{105-115}$-RGD an analogous amyloidogenic peptide was synthesised with a more physiological cyclic RGDfK sequence attached ($TTR_{105-115}$-cRGDfK). Compared to the $TTR_{105-115}$-RGD fibrils the $TTR_{105-115}$-cRGDfK fibrils were seen to significantly promote cell adhesion and cell spreading through the development of integrin mediated focal adhesions between the cRGDfK ligands and the cell membrane.[307, 417] However, masking of the cRGDfK chemistry with a thin plasma polymer layer revealed that the addition of the bulky cRGDfK sequence results in nanofibrils with a topography less favourable to cell growth.[417] Thus, once again this highlights the importance of considering both chemical and topographical features when designing amyloid based biomaterials. In another interesting recent example, RGD-functionalized PAs have been used to create enzyme (matrix metalloprotease)-triggerered releasable free-standing collagen-rich films, produced by human stromal corneal fibroblasts.[418, 419] The PA coating was aligned by use of a lithographic process and this led to aligned collagen deposition, mimicking the alignment of collagen fibres in the cornea.

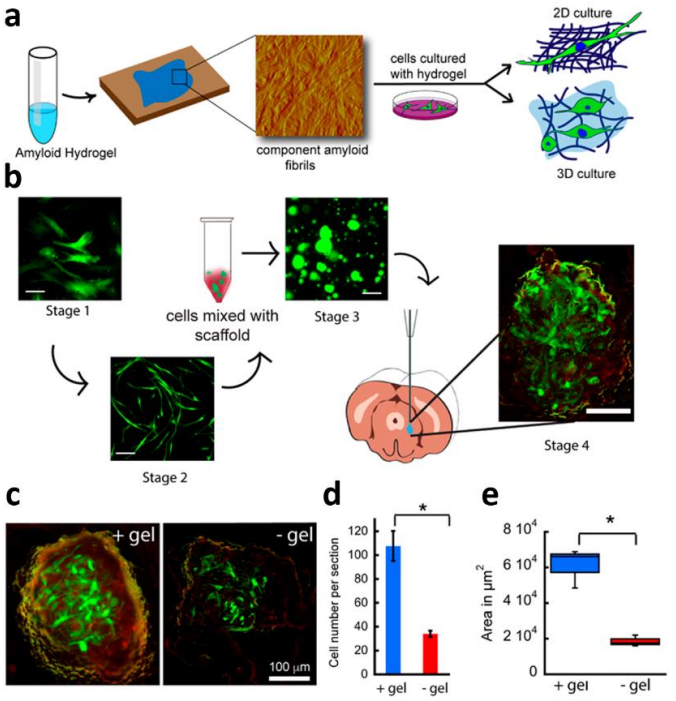

Fig. 29 Amyloid hydrogels for cell culture: (a) Schematic of amyloid hydrogels for 2D and 3D cell culture. (b) Schematic of the morphology of cells at each stage during the implantation. Stage 1: cultured cells for 24 h; stage 2: cells were primed with differentiation medium for 5 days; stage 3: cells then transplanted with hydrogel A5 into the mice brains, and stage 4: harvested brains. Scale bars: 200 µm for stage 1-3 and 100 µm for stage 4. (c) Implanted GFP-hMSCs with α-synuclein hydrogel (left) and without hydrogel (right) at the caudate putamen after 7 days in vivo. (d) Cell viability when implanted with and without hydrogel. (e) Box plot of the area with survived cells when transplanted with and without hydrogel. Reproduced with permission from Ref. 422. Copyright 2016, Nature Publishing Group.

3D scaffolds based on amyloid nanofibril systems functionalised with cell adhesion moieties have also been used as biomaterials that promote cell growth. Zhou et al. created hydrogels from a mixture of Fmoc-FF and Fmoc-RGD.[420] The rapid gelling system promoted the adhesion and 3D cell culture of encapsulated dermal fibroblasts through specific interactions with integrins on the cell membrane. Furthermore, by adjusting the ratios of Fmoc-FF and Fmoc-RGD in the system the concentration and ligand spacing of the RGD moieties in the hydrogel could be accurately controlled. Based on a similar gelation mechanism, a series of peptides based on Aβ were combined with Fmoc protecting groups.[19, 421] By adjusting the peptide sequence, concentration and the ionic strength, the mechanical properties of the formed gels could be controlled, which in turn was used to drive stem cell differentiation. In a similar study, Das and co-workers synthesized a new class of implantable α-synuclein-inspired peptide hydrogels with the ability to direct stem cell differentiation *in vivo* (Fig. 29a).[422] Mesenchymal stem cells (MSCs) were seeded into an α-synuclein based peptide hydrogel and transplanted into the brains of mice (Fig. 29b). After 7 days *in vivo*, the brains were harvested and sectioned and the cells implanted within the hydrogel showed increased evidence of neuronal differentiation compared to cells transplanted in the absence of the hydrogel (Fig. 29c).

This journal is © The Royal Society of Chemistry 20xx

Furthermore, the presence of the hydrogel resulted in increased cell number both within the caudate putamen (Fig. 29d) and substantia nigra of the implanted mice (Fig. 29e).

The section above highlights the considerable amount of research that has gone into designing bespoke amyloidogenic peptide sequences that self-assemble and display specific cell adhesion moieties on their surface. However, the design and synthesis of such sequences is non-trivial, and relatively expensive. Therefore, a different approach has also been investigated whereby inexpensive and abundant raw materials that are easily applicable to scale up to clinically relevant volumes required in the biomedical industry are used for the formation of amyloid based scaffolds. Healy et al. extracted crystalline proteins from fish eye lenses and studied the influence of temperature on their self-assembly into amyloid fibrils.[423] Furthermore, these fibrils were shown to be stable over a wide range of pH, over long periods of time and showed no significant cytotoxicity to Hec-1a endometrial cells.[424] This preliminary work suggests that crystalline nanofibrils should be further investigated as 2D or 3D biomaterials. Reynolds et al. fabricated amyloid fibril networks from lysozyme on solid supports with well-defined nanoscale surface features reminiscent of the topography of the ECM.[425] By masking the surface chemistry of the fibril networks with a thin layer of inert oligo (ethylene glycol) plasma polymer, they proved that the ECM mimicking nanotopography alone was enough to promote the attachment and spreading of a fibroblast cell line. In a following study, they showed that the attachment, spreading and cytoskeletal tension of cells could be controlled by adjusting the surface coverage of the amyloid fibril networks both in the presence and absence of serum proteins.[426]

Li et al. fabricated poly(N-isopropylacrylamide) (PNIPAM)-decorated amyloid fibrils from β-lactoglobulin. These decorated fibrils underwent a sol-gel transition below body temperature (32 °C).[427] This hybrid could be used as an injectable material at room temperature, while turning into a gel at body temperature. This finding may contribute to designing thermally controlled "smart" scaffolds for tissue regeneration applications.

5.3 Energy materials

The unique physiochemical properties of amyloid fibrils make them attractive materials not just in biomedical and regenerative medical fields. For instance, amyloid fibrils have been investigated as potential materials for next generation energy-harvesting devices,[428, 429] Lithium ion batteries,[23, 430] organic solar cells,[431] photovoltaic,[432] and catalyst materials.[316, 433]

Hanczyc et al. showed that amyloid fibrils of insulin, lysozyme and α-synuclein specifically enhance multiphoton absorption.[428] Channon et al. demonstrated a detailed mechanism of the light-harvesting function resulting from co-assembly of two independent luminescent moieties into amyloid-like fibrils.[429]

Similarly, light-harvesting peptide nanotubes were synthesized by the co-assembly of FF and porphyrin (Fig. 30a).[434] The dipeptide assemblies and porphyrin molecules mimicked the electron separator and mediator in natural photosynthetic systems, respectively. By incorporating PtNPs onto the surface of the FF/porphyrin nanotubes, self-metallization of PtNPs occurred, enabling an efficient separation and transfer of the exited electrons from the porphyrin to an electron mediator.

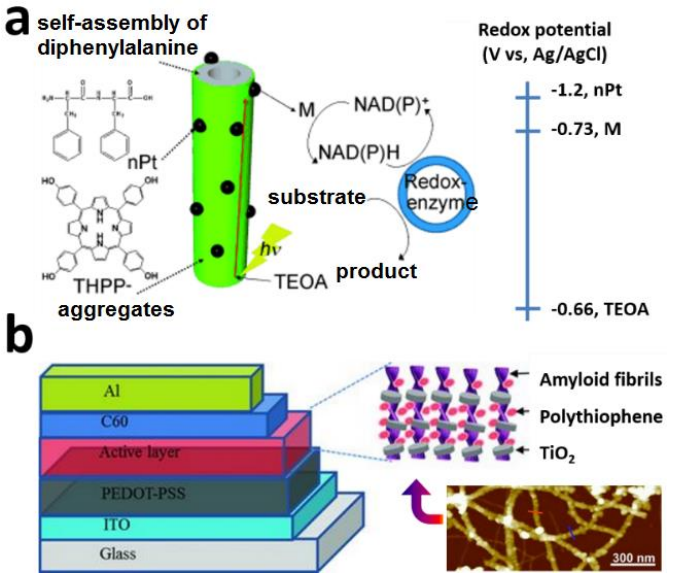

Fig. 30 (a) Biomimetic photosynthesis by light-harvesting peptide nanotubes. Reproduced with permission from Ref. 434. Copyright 2012, Wiley-VCH Verlag GmbH & Co. (b) Schematic diagram of the hybrid photovoltaic device prepared using an active layer composed of TiO_2-hybrid nanowires blended with polythiophene and AFM image of TiO_2 decorating the surface of the amyloid fibrils. Reproduced with permission from Ref. 432. Copyright 2012, Wiley-VCH Verlag GmbH & Co.

The Park group performed studies on the biomimetic mineralization of $FePO_4$ and Co_3O_4 nanoparticles on self-assembled diphenylalanine nanofibrils[23] and nanotubes.[430] They found that biomimetic inorganic-organic hybrid nanomaterials could act as promising cathode materials for rechargeable Lithium ion batteries with a high reversible capacity and good capacity retention during cycling.

Inganäs et al. demonstrated the integration of amyloid insulin nanofibrils into organic solar cells to enhance the transport properties of photovoltaic devices.[431] They found that the amyloid nanofibrils had a significant effect on the donor-acceptor material organization. At a specific ratio of nanofibrils, donors and acceptors the hybrid organic solar cells showed improved charge transport compared to the materials without added nanofibrils.

Bolisetty et al. utilized β-lactoglobulin amyloid fibrils as templates to successfully direct the synthesis of closely packed TiO_2 hybrid nanowires.[432] Due to the well-organized combination of electrostatic and hydrogen bond interactions, TiO_2 nanoparticles decorated the surfaces of the protein fibrils uniformly. Subsequently, the TiO_2-coated amyloid hybrid nanowires could be prepared into a photovoltaic active layer by spin coating a blended mixture of polythiophene-coated fibrils and amyloid-TiO_2 hybrid nanowires (Fig. 30b). Acar et al. demonstrated the amyloid peptide nanofibril templated synthesis of TiO_2 nanostructures via a bottom-up approach.[435] By staining the calcinated TiO_2 layer with an N719 photosensitizer

dye, they fabricated dye sensitized solar cells with high loading capabilities, and improved open circuit voltages exploiting the high surface area offered by the amyloid fibrils.

Amyloid fibrils also have important potential applications in heterogeneous catalysis. Bolisetty et al. prepared AuNPs and PdNPs respectively on β-lactoglobulin amyloid fibrils for catalytic reduction of 4-nitrophenol.[316] In another study, Chaves et al. reported a new biocatalyst based on the photo-immobilization of lipase onto amyloid fibrils via a photo-induced cross-linking reaction.[433] The resulting insoluble nanoscale biocatalyst showed higher enzyme stability than the soluble enzyme under several extreme conditions. Scott and co-workers demonstrated the preparation of amyloid (Fmoc-FF) peptide gel microparticles that are emulsified and stabilized with SiO_2 nanoparticles.[436] The amyloid matrix was used to immobilise the enzyme lipase B (CalB) and the catalytic performance assessed by monitoring the esterification of octanol in heptane. In the best performing system, the authors observed almost a 4-fold increase in catalytic activity compared to native CalB. Bio-catalytic amyloid microparticles such as these could be very useful for fabricating biosensors and bioinspired solar fuel devices.

5.4 Environmental science and technology

Amyloid fibrils have also found important applications in the environmental sciences. For instance, Bolisetty and Mezzenga reported that inexpensive and environmentally friendly β-lactoglobulin amyloid fibrils could be blended with activated carbon and filtered to form membranes capable of purifying a variety of contaminants from wastewater samples.[118] The initial study showed that these simple membranes provided remarkable levels of purification for water samples containing heavy metal, organic, and bacterial contamination. As shown in Fig. 31a, heavy metal ions purification occurred due to the presence of metal ion binding sites on the surface of the amyloid fibrils. After filtering, the content of potassium dicyanoaurate (I), mercury chloride and several other tested pollutants, was reduced by nearly three orders of magnitude (Fig. 31b and c). Leung et al. modified lysozyme amyloid fibrils with ethylenediamine to reduce their carboxyl content enabling the adsorption of toxic chromium(VI) ions in water.[437] These studies open up new possibilities in fabricating functionalised amyloid based materials that can efficiently scavenge pollutants from water supplies.

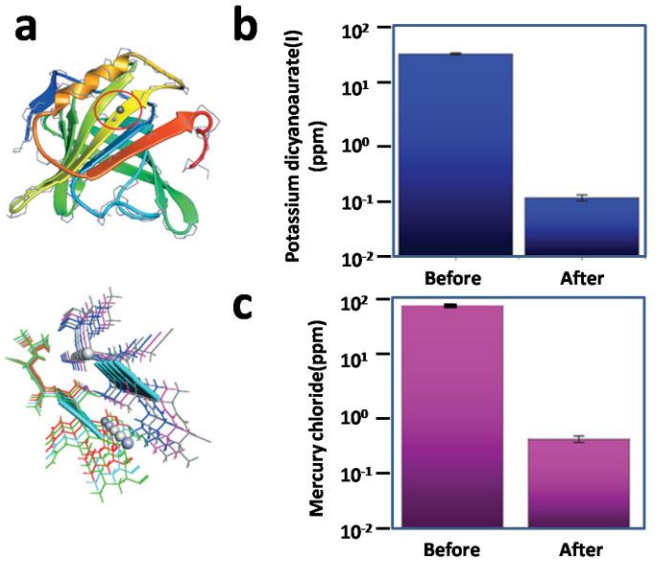

Fig. 31 Amyloid nanofibril-based materials for water purification. (a) Structure of the β-lactoglobulin protein with the heavy metal-binding motif highlighted, 121-cys, with a lead ion attached and the 121-cys-containing fragment (LACQCL) from β-lactoglobulin with docked Pb^{2+}. (b,c) Concentrations of heavy metal and radioactive pollutants before and after filtration through the amyloid fibril-activated carbon hybrid adsorber membrane: (b) Potassium dicyanoaurate (I); (c) Mercury chloride. Reproduced with permission from Ref. 118. Copyright 2016, Nature Publishing Group.

In a similar manner to the scavenging of waterborne contaminants outlined above, amyloid based materials could have applications as materials for capturing carbon dioxide from the atmosphere, thus helping to address the global threat of climate change. Li and co-workers reported that amyloid fibrils formed from the peptide sequence VQIVYK were capable of sequestering CO_2.[438] They found that the ε-amino group of lysine is uncharged at a high pH, which is thus capable of forming carbamate with atmospheric CO_2. The materials were able to capture CO_2 in the presence of water, which was later released by heating. In a further study, the same authors used VQIVYK capped with N-terminal acetylation and C-terminal amidation to increase fibril formation and promote the diffusion of small gaseous molecules.[439] Binding of carbon dioxide is thought to occur via carbamate formation with amine functional groups present in the lysine residues. In another design, they mutated the glutamine residue in position 2 to lysine, generating the hexapeptide VKIVYK.[438, 439] Although there was twice the number of amines in the designed fibrils, a two-fold increase in binding capacity of CO_2 was not observed, indicating that in these fibrils the amine groups are only partially accessible.

5.5 Electronic nanodevices

Inspired by the high efficiency of charge transport in biological systems, the possibility of introducing charged proteins and peptides in electronic devices has been suggested.[440] The unique hybrid conductivity behaviour makes self-assembled peptide nanostructures powerful building blocks for the construction of electronic nanodevices.[441] Carny et al. fabricated coaxial gold and silver nanocables by binding metallic NPs onto the self-

This journal is © The Royal Society of Chemistry 20xx

assembled peptide nanotubes via molecular recognition.[442] Dinca et al. successfully fabricated 3D structures from amyloid fibrils with potential application in molecular electronics.[443, 444] Amit et al. studied the conductance of the thiophene containing peptide (2-Thi) (2-Thi) VLKAA under a range of humidity conditions.[445] They found that the conductivity of the fibrils was increased at higher relative humidity, indicating proton transport rather than electron transport dominates the conductive behaviour. Compared with amyloids from the naturally occurring peptide AAKLVFF, the conductance of (2-Thi) (2-Thi) VLKAA was found to be much higher, and this was attributed to subtle changes in the folding structure.

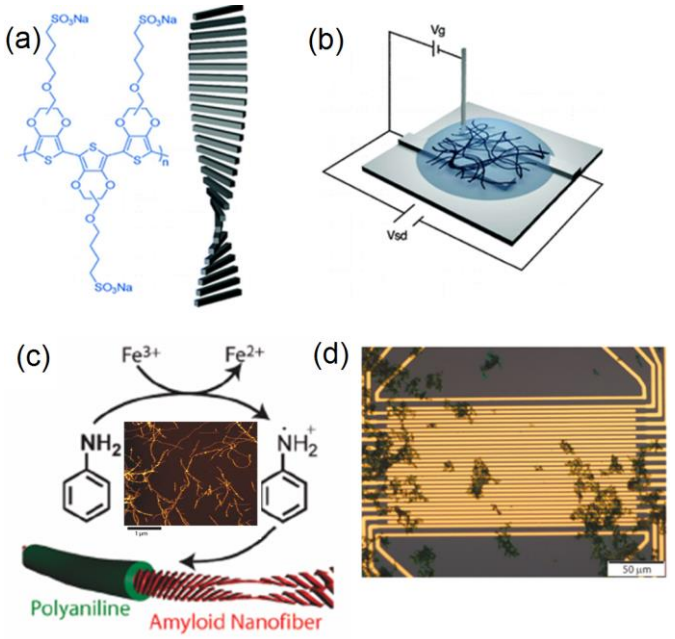

Fig. 32 Fabrication of amyloid-based transistors. (a,b) PEDOT-S amyloid nanofibrils based transistor: (a) molecular structure and (b) schematic picture the electrolyte gated transistor. Reproduced with permission from Ref. 446. 2008, American Chemical Society. (c,d) Amyloid-PAni hybrid nanofibril-based transistor: (c) synthesis and AFM image of PNF-PAni hybrid fibrils and (d) deposited hybrid fibrils on gold electrode array for conductivity measurements (PNF: peptide nanofibrils). Reproduced with permission from Ref. 447. Copyright 2015, American Chemical Society.

Self-assembled amyloid nanofibrils have found applications as building blocks for electrochemical transistors.[440] For instance, Hamedi et al. designed amyloid insulin fibrils coated with the highly conducting polymer alkoxy sulfonate poly(3,4-ethylenedioxythiophene) (PEDOT-S).[446] The assembled network was dispersed in an acetonitrile electrolyte and probed with a Pt gate electrode (Fig. 32a and b). The fabricated amyloid-PEDOT-S transistor showed high source-drain currents and also displayed repeatable switching characteristics with an on/off ratio of >40 when sweeping the gate between 0 and 0.5 V, clearly showing that PEDOT-S has not lost any electrical or electrochemical properties after self-assembly with amyloid fibrils. Furthermore, the nanowire networks showed ohmic connection to the metal, and no detachment during the electrochemical reactions. Meier et al. prepared conducting polyaniline (PAni) nanowires with a core-shell structure using amyloid nanofibrils as a template.[447] Adsorption of the conducting polymer to the fibrils was facilitated through binding between the hydrophobic aromatic functional groups on the PAni, and the exposed hydrophobic pockets on the surface of the growing fibrils (Fig. 32c). The resultant materials were deposited on an array of gold electrodes, as shown in Fig. 32d. The conductivity of coated hybrid fibrils was found to be far higher than that of uncoated fibrils. In another study, Tu and co-workers reported the fabrication of an electrochromic transistor based on PEDOT-decorated amyloid fibrils.[448] These studies show that amyloid fibrils provide an excellent structural template for the directed deposition of conducting polymers, which has major potential applications in the fabrication of next generation microelectronic devices.

Amyloid fibrils also exhibit promising electronic applications as organic light-emitting diodes (OLEDs).[449-453] For instance, amyloid insulin fibrils were conjugated with luminescent conjugated polymers, and used as the active layer in an OLED device.[449, 450] The introduction of amyloid fibrils into the fabricated OLED device resulted in a 10-fold increase of the external quantum efficiency.[450] In other studies, the same amyloid fibrils were functionalized with phosphorescent organometallic (Ir) complexes to fabricate red and yellow OLEDs.[451, 452] The conjugation of phosphorescent organometallic complexes with amyloid structures was seen to strongly improve the triplet exciton confinement and make it possible to fabricate white-emitting devices at low loading of phosphorescent complexes. More information on the modification of amyloid fibrils, as well as the fabrication and applications of OLEDs with fibrils have been discussed in a recent review article.[453]

5.6 Biosensor architectures

Amyloids have been shown to have promising applications in the design of novel biosensors. This is in part due to their high mechanical strength and chemical resistance to the surrounding milieu, their ability to detect nanoscale protein-ligand interactions and selectivity for low concentrations of biomolecule analytes.[454] For instance, self-assembled amyloid peptide nanotubes have been utilized to create novel electrochemical biosensing platforms for detecting hydrogen peroxide and enzymes.[455, 456]

Amyloids functionalized with ligands such as fluorophores, antibodies or enzymes can also be used for biosensing applications.[457] Glucose oxidase (GOx)-functionalized whey protein nanofibrils (WPNFs) were seen to promote the enzyme immobilization on screen-printed gold electrodes due to the large surface-to-volume ratio of the WPNF nano-scaffold.[458] Compared to simple physical enzyme adsorption, the produced cyclic voltammogram exhibited a distinct increase in the anodic peak current response when using WPNF nano-scaffolds. The anodic peak currents were even larger when using the thiol-functionalized WPNFs, due to increased binding of WPNF on the gold surface.

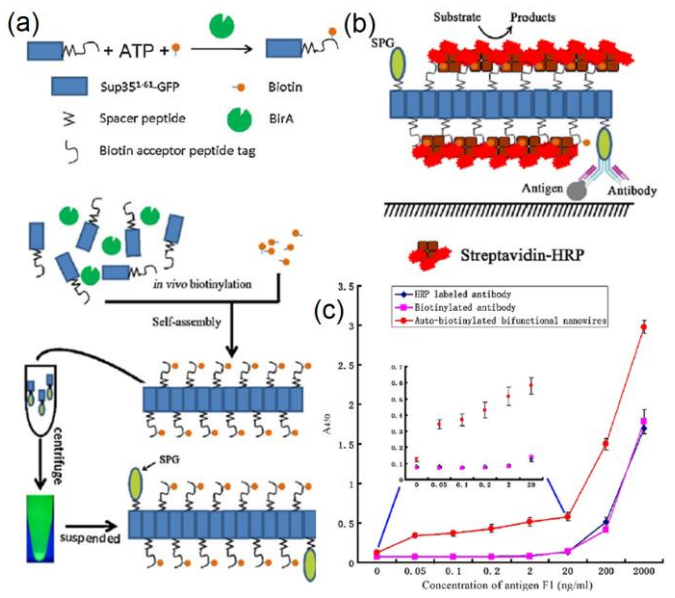

Fig. 33 Amyloid protein nanofibril-based immunosensors. (a) Schematic synthesis of Sup35-BAP nanofibrils. (b) Fabrication of immunosensor architecture via biotin-streptavidin interaction. (c) Improved sensing performance compared to non-fibril sensors. Reproduced with permission from Ref. 459. Copyright 2010, Elsevier Ltd.

Amyloid protein nanofibrils have shown potential for the fabrication of enzyme-linked immunosorbent assay (ELISA) immunosensors.[459, 460] For instance, Men and co-workers demonstrated the design of an auto-biotinylated bifunctional protein nanowires (bFPNw) based on the self-assembly of recombinant biotin-modified amyloid protein Sup35 (Fig. 33a).[459] The high concentration and regular arrangement of biotin molecules on the surface of the bFPNws allows any of the hundreds of commercially available diagnostic enzymes to be transferred to the surface of the immunosensor via the biotin-avadin reaction (Fig. 33b). These biosensors were able to detect Yersinia pestis F1 antigen with a 2000- to 4000-fold increase in sensitivity compared to traditional ELISAs (Fig. 33c). In addition, the bFPNw-based system was seen to amplify the detection signal, reduce the non-specific binding, and improve stability. In a similar example, gene fusion was used to express recombinant Sup35-E^2-GFP-MPH where E^2-GFP-MSH is fluorescent biosensor based on green fluorescent protein linked to the enzyme methyl parathion hydrolase. The self-assembled nanofibrils were able to detect the pesticide methyl parathion with a sensitivity around 10,000 times greater than free E^2-GFP-MSH.[460]

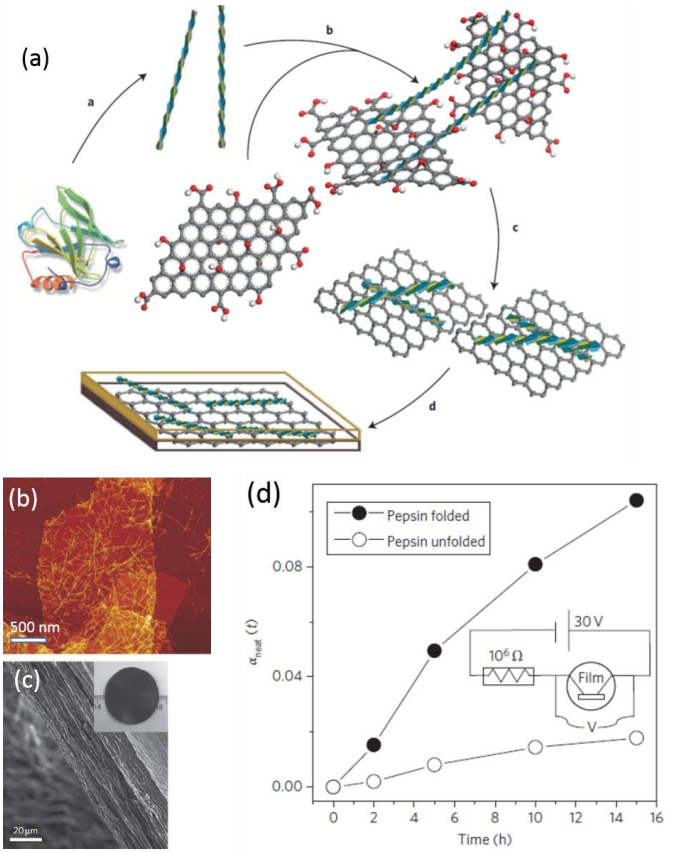

Fig. 34 Amyloid nanofibril-GO shape-memory materials. (a) Fabrication mechanism, (b) AFM of nanofibril-GO hybrid, (c) SEM image of nanofibril-GO hybrid film, and (d) Biosensors for enzymatic activity measurement. Reproduced with permission from Ref. 20. Copyright 2012 Nature Publishing Group.

Whilst gene fusion approaches such as those discussed above certainly show great promise for the design of amyloids that can act as enzymatic biosensors, their complexity and the specialised expertise required for their development may hinder their development. As an alternative amyloid β-lactoglobulin nanofibrils were combined with GO to fabricate biodegradable nanocomposites with shape-memory and enzymatic sensing properties[20] Free-standing nanofibril-RGO films were fabricated in a series of steps: after assembly of the fibrils and binding of the fibrils to the GO sheets, the GO sheets were reduced at high temperatures to RGO. RGO-fibril films were formed by vacuum filtration, as shown in Fig. 34a and b. The free-standing hybrid nanocomposite films possessed a film thickness of 40-60 μm (Fig. 34c) and displayed a remarkable and fully reversible shape-memory effect. In addition, the nanocomposites could be totally degraded by simple enzymatic reactions, or, under controlled enzymatic reactions, be used as a new class of biosensors to measure enzymatic activity (Fig. 34d).

5.7 Other functional nanomaterials

Besides the above mentioned biomedical and nanotechnological applications, amyloids fibrils have been used for the fabrication of other novel functional nanomaterials including liquid crystal

This journal is © The Royal Society of Chemistry 20xx

materials,[298, 461-465] photoluminescence and optical waveguiding materials.[466-468]

The formation of liquid crystal phase by amyloid fibrils is important for the fabrication of nanomaterials with hard structures, which could be reinforced by the rigid and anisotropic amyloid fibrils. Suspensions of amyloid fibrils frequently form liquid crystal phases due to long range non-covalent interactions between assemblies.[160, 321-325] For instance, Corrigan et al. demonstrated that the lysozyme nanofibrils readily form liquid crystal phases.[462] Zhao et al. created amyloid fibrils suspensions with isotropic-nematic coexistence by freeze-thaw cycling.[463] Han and co-workers found that FF rapidly self-assembles into nanowires with high aspect ratio in a volatile organic solvents, which showed a colloidal nematic liquid crystalline phase over a broad concentration range.[464] Hamley and co-workers showed that AAKLVFF nanotubes[465] and helical peptide βAβAKLVFF ribbons,[298] and other amyloidogenic peptides can form nematic liquid phases in organic solvent and water, respectively.

Self-assembled amyloids have been used for the synthesis of bioinspired functional materials for optical waveguiding. Ryu et al. reported the in situ conjugation of self-assembled FF nanotubes with the photosensitizers (4-acetylbiphenyl) and lanthanide (Tb^{3+} and Eu^{3+}) ions for fabricating novel photoluminescent nanotube materials.[466] Their finding indicated the FF nanotubes acted not only as a host matrix for lanthanide complexes, but also served as a photosensitizer. By careful adjustment of the composition of lanthanide complexes, various nanotubes with switchable colours (red, green, blue, cyan, and purple) were fabricated. In another study, Yan and co-workers demonstrated the optical waveguiding of self-assembled hexagonal FF microtubes and FF fibrous networks.[467, 468] The fabricated peptide nanotubes exhibited remarkable thermal stability and optical waveguiding, making them novel candidates to design and develop optical and electrical nanodevices.

6 Conclusions and outlook

In this review, we summarized the recent progress in both the fundamental study and applications of amyloid systems. We focused on the elucidation of the self-assembly mechanisms, hierarchical structure, physical properties of a series of amyloid nanostructures from molecular oligomers to 0D, 1D, 2D, and 3D nanomaterials. We elaborated on how the understanding at a very fundamental level of these salient features illuminates their application on the most diverse areas of artificial and biological materials. A wide range of strategies for fabricating natural and artificial amyloid-based materials were discussed. In addition, the various applications of amyloid-based hybrid nanomaterials for biomedical engineering, tissue engineering, energy materials, environment science, nanodevices, biosensors, and others were introduced and discussed in detail.

Looking to the future there are some areas which would benefit further research. More work should be focused on using computer simulation techniques such as molecular dynamics in order to understand the molecular mechanisms underpinning the formation of amyloid oligomers and other intermediates. Secondly, work should be performed to elucidate the selection rules and mechanisms responsible for the creation of 2D and 3D amyloid based materials. Multidimensional amyloid based nanomaterials show many promising applications for materials science and nanoelectronics. Currently, the controllable growth and formation of 2D and 3D amyloid structures is challenging and very difficult to predict due to a lack of fundamental knowledge. Thirdly, the exploitation of functional motifs from amyloid proteins to create biofunctional-specific amyloid nanostructures should be further investigated. In addition, it is possible to endow other functions like material recognition, biomineralization, and cell adhesion to the created amyloid nanostructures by inserting additional peptide motifs. Last but not least, it is to be hoped that the biocompatibility, biodegradation, and cellular toxicity of amyloid materials will be understood and tailored to a greater extent, as this could potentially unlock an extraordinary large numbers of applications in the field of biotechnologies and biomaterials.

In this respect, the contrast between the disease-relevant instances of amyloids and the various applications of amyloid-derived materials in a biological context, deserves some discussion, as this raises the question of the potential safety challenges of such materials. In general, the main discriminant in the selection of the amyloid building blocks should be the chemical nature of the peptides or proteins forming the amyloids. When the primary structure of the peptide/protein building block contains motifs from pathologically relevant amyloid-forming peptides, potential dangers need to be carefully considered up-front, although there are also examples where amyloids fibrils composed from fragments derived from pathological amyloidogenic proteins have been successfully used as cell scaffolds.[308] A very recent study, however, clearly points to a safe use of amyloid fibrils *in-vivo* - even in the context of food applications- when the fibrils are composed of hydrolyzed edible proteins.[469] Shen et al. have indeed used hybrids of β-lactoglobulin amyloid fibrils and iron nanoparticles to design a new efficient colloidal form of highly bioavailable nano-sized iron to be used in anemia treatment.[469] The trick used by the authors is to exploit the combined acidic and enzymatic environment present in the stomach to allow a fast dissolution of both the amyloid fibrils, digested by pepsin, and the iron nanoparticles, dissolved by the acidic pH, leading to a rapid dissolution of these hybrids into hydrolyzed milk proteins and highly bioavailable iron ions. This work convincingly demonstrates that if amyloid fibrils are made of edible building blocks and are administered through the gastrointestinal tract to enable correct digestion, they could even revolutionize fields such as pharmaceutics, food technology and nutrition, in which amyloid fibrils were never used before, tremendously widening the scope of applications of these fascinating materials.

Acknowledgements

GW thanks the financial supports from the Deutsche Forschungsgemeinschaft (DFG) under grant WE 5837/1-1. ZS acknowledges the financial supports from the National Natural

Science Foundation of China (Grant No. 51573013). NPR thanks the Australian Research Council (ARC) Training Centre for Biodevices at Swinburne University of Technology (IC140100023) for financial support. IWH would like to acknowledge EPSRC (UK) for Platform grant EP/L020599/1 and the Royal Society (UK) for a Wolfson Research Merit Award. EG thanks the support by a grant from the European Research Council BISON project.

Main abbreviations:

Nuclear magnetic resonance (NMR)
Circular dichroism (CD)
X-ray fiber diffraction (XRFD)
Thioflavin T (ThT)
Electron microscopy (EM)
Atomic force microscopy (AFM)
Small-angle x-ray scattering (SAXS)
Lower critical solution temperature (LCST)
Fourier transform infrared spectroscopy (FTIR)
Isothermal titration calorimetric (ITC)
Hexafluoroisopropanol (HFIP)
2,2,2-trifluoroethanol (TFE)
Extracellular matrix (ECM)
Quantum dots (QDs)
N-hydroxysulfosuccinimide (NHS)
Sulfated glycosaminoglycans (GAGs)
Blood-brain barrier (BBB)
Polymethylmethacrylate (PMMA)
Polytetrafluoroethylene (PTFE)
Islet amyloid polypeptide (IAPP)
Amyloid precursor protein (APP)
Amyloid β (Aβ)
Prion protein (PrP)
Attenuated total reflection (ATR)
Static and dynamic light scattering (S/DLS)
Prion protein (PrP)
Wild-type (WT)
Transmission electron microscope (TEM)
Magnetic resonance imaging (MRI)
Camptothecin (CPT)
tris(2-carboxyethyl) phosphine (TCEP)
Curly amyloid fibrils (CAF)
Graphene QDs (GQDs)
Hydroxyapatite (HA)
Graphene oxide (GO)
Single-walled carbon nanotubes (SWNTs)
Nitro blue tetrazolium (NBT)
Chemical exchange saturation transfer (CEST)
Peptide amphiphiles (PA)
Poly(N-isopropylacrylamide) (PNIPAM)
Poly(3,4-ethylenedioxythiophene) (PEDOT-S)
Organic light-emitting diodes (OLEDs)
Glucose oxidase (GOx)

Notes and references

1. A. Aguzzi and T. O'Connor, *Nat. Rev. Drug Discov.*, 2010, **9**, 237-248.
2. K. T. Weber, Y. Sun, S. C. Tyagi and J. P. M. Cleutjens, *J. Mol. Cell. Cardiol.*, 1994, **26**, 279-292.
3. L. Cen, W. Liu, L. Cui, W. J. Zhang and Y. L. Cao, *Pediatr. Res.*, 2008, **63**, 492-496.
4. A. C. Reymann, R. Boujemaa-Paterski, J. L. Martiel, C. Guerin, W. X. Cao, H. F. Chin, E. M. De La Cruz, M. Thery and L. Blanchoin, *Science*, 2012, **336**, 1310-1314.
5. T. P. J. Knowles, M. Vendruscolo and C. M. Dobson, *Nat. Rev. Mol. Cell Bio.*, 2014, **15**, 496-496.
6. M. P. Lambert, A. K. Barlow, B. A. Chromy, C. Edwards, R. Freed, M. Liosatos, T. E. Morgan, I. Rozovsky, B. Trommer, K. L. Viola, P. Wals, C. Zhang, C. E. Finch, G. A. Krafft and W. L. Klein, *Proc. Natl. Acad. Sci. U.S.A.*, 1998, **95**, 6448-6453.
7. O. G. Jones and R. Mezzenga, *Soft Matter*, 2012, **8**, 876-895.
8. T. Hard, *J. Phys. Chem. Lett.*, 2014, **5**, 607-614.
9. E. Andreetto, E. Malideli, L. M. Yan, M. Kracklauer, K. Farbiarz, M. Tatarek-Nossol, G. Rammes, E. Prade, T. Neumuller, A. Caporale, A. Spanopoulou, M. Bakou, B. Reif and A. Kapurniotu, *Angew. Chem. Int. Ed.*, 2015, **54**, 13095-13100.
10. A. J. Doig and P. Derreumaux, *Curr. Opin. Struct. Biol.*, 2015, **30**, 50-56.
11. M. R. Chapman, L. S. Robinson, J. S. Pinkner, R. Roth, J. Heuser, M. Hammar, S. Normark and S. J. Hultgren, *Science*, 2002, **295**, 851-855.
12. D. M. Fowler, A. V. Koulov, C. Alory-Jost, M. S. Marks, W. E. Balch and J. W. Kelly, *PLoS Biol.*, 2006, **4**, 100-107.
13. S. K. Maji, D. Schubert, C. Rivier, S. Lee, J. E. Rivier and R. Riek, *PLoS Biol.*, 2008, **6**, 240-252.
14. I. Cherny and E. Gazit, *Angew. Chem. Int. Ed.*, 2008, **47**, 4062-4069.
15. D. Romero, C. Aguilar, R. Losick and R. Kolter, *Proc. Natl. Acad. Sci. U.S.A.*, 2010, **107**, 2230-2234.
16. L. Adler-Abramovich, D. Aronov, P. Beker, M. Yevnin, S. Stempler, L. Buzhansky, G. Rosenman and E. Gazit, *Nat. Nanotechnol.*, 2009, **4**, 849-854.
17. C. A. E. Hauser, S. Maurer-Stroh and I. C. Martins, *Chem Soc Rev*, 2014, **43**, 5326-5345.
18. C. Q. Yan and D. J. Pochan, *Chem. Soc. Rev.*, 2010, **39**, 3528-3540.
19. R. S. Jacob, D. Ghosh, P. K. Singh, S. K. Basu, N. N. Jha, S. Das, P. K. Sukul, S. Patil, S. Sathaye, A. Kumar, A. Chowdhury, S. Malik, S. Sen and S. K. Maji, *Biomaterials*, 2015, **54**, 97-105.
20. C. X. Li, J. Adamcik and R. Mezzenga, *Nat. Nanotechnol.*, 2012, **7**, 421-427.
21. L. E. Buchanan, J. K. Carr, A. M. Fluitt, A. J. Hoganson, S. D. Moran, J. J. de Pablo, J. L. Skinner and M. T. Zanni, *Proc. Natl. Acad. Sci. U.S.A.*, 2014, **111**, 5796-5801.
22. R. S. Jacob, E. George, P. K. Singh, S. Salot, A. Anoop, N. N. Jha, S. Sen and S. K. Maji, *J. Biol. Chem.*, 2016, **291**, 5278-5298.
23. J. Ryu, S. W. Kim, K. Kang and C. B. Park, *Adv. Mater.*, 2010, **22**, 5537-5541.
24. R. Tycko and R. B. Wickner, *Acc. Chem. Res.*, 2013, **46**, 1487-1496.
25. I. W. Hamley, *Angew. Chem. Int. Ed.*, 2007, **46**, 8128-8147.
26. J. W. Kelly, *Curr. Opin. Struct. Biol.*, 1998, **8**, 101-106.
27. E. van der Linden and P. Venema, *Curr. Opin. Colloid Interface Sci.*, 2007, **12**, 158-165.
28. X. H. Yan, P. L. Zhu and J. B. Li, *Chem. Soc. Rev.*, 2010, **39**, 1877-1890.
29. C. Lara, S. Handschin and R. Mezzenga, *Nanoscale*, 2013, **5**, 7197-7201.
30. R. V. Ulijn and A. M. Smith, *Chem. Soc. Rev.*, 2008, **37**, 664-675.
31. A. Dehsorkhi, V. Castelletto and I. W. Hamley, *J. Pept. Sci.*, 2014, **20**, 453-467.
32. T. P. J. Knowles and M. J. Buehler, *Nat. Nanotechnol.*, 2011, **6**, 469-479.
33. T. P. J. Knowles and R. Mezzenga, *Adv. Mater.*, 2016, **28**, 6546-6561.
34. R. J. Ellis and F. U. Hartl, *Curr. Opin. Struct. Biol.*, 1999, **9**, 102-110.
35. C. Anfinsen and H. Scheraga, *Adv. Protein Chem.*, 1975, **29**, 205-300.
36. K. P. Murphy, P. L. Privalov and S. J. Gill, *Science*, 1990, **247**, 559.
37. F. Chiti and C. M. Dobson, *Annu. Rev. Biochem.*, 2006, **75**, 333-366.
38. V. N. Uversky, J. R. Gillespie and A. L. Fink, *Proteins: Struct. Funct. Bioinform.*, 2000, **41**, 415-427.
39. V. N. Uversky, *Protein Sci.*, 2002, **11**, 739-756.
40. H. J. Dyson and P. E. Wright, *Nat. Rev. Mol. Cell Bio.*, 2005, **6**, 197-208.
41. N. J. Greenfield, *Nat. Protocols*, 2006, **1**, 2527-2535.
42. R. L. Croke, C. O. Sallum, E. Watson, E. D. Watt and A. T. Alexandrescu, *Protein Sci.*, 2008, **17**, 1434-1445.
43. D. N. Hebert and M. Molinari, *Physiol. Rev.*, 2007, **87**, 1377-1408.

This journal is © The Royal Society of Chemistry 20xx

44. E. Gazit and R. T. Sauer, *J. Biol. Chem.*, 1999, **274**, 2652-2657.
45. A. Matouschek, *Curr. Opin. Struct. Biol.*, 2003, **13**, 98-109.
46. F. U. Hartl and M. Hayer-Hartl, *Nat. Struct. Mol. Biol.*, 2009, **16**, 574-581.
47. M. Stefani and C. M. Dobson, *J. Mol. Med.*, 2003, **81**, 678-699.
48. E. L. Opie, *J. Exper. Med.*, 1901, **5**, 527.
49. J. M. M. Lage, *J. Alzheimer's Dis.*, 2006, **9**, 15-26.
50. H. LeVine, *Amyloid, Prions, and Other Protein Aggregates*, 1999, **309**, 274-284.
51. C. Reichhardt, A. N. Jacobson, M. C. Maher, J. Uang, O. A. McCrate, M. Eckart and L. Cegelski, *Plos One*, 2015, **10**.
52. J. I. Guijarro, M. Sunde, J. A. Jones, I. D. Campbell and C. M. Dobson, *Proc. Natl. Acad. Sci. U.S.A.*, 1998, **95**, 4224-4228.
53. E. Gazit, *Angew. Chem. Int. Ed.*, 2002, **41**, 257-259.
54. A. J. Baldwin, T. P. J. Knowles, G. G. Tartaglia, A. W. Fitzpatrick, G. L. Devlin, S. L. Shammas, C. A. Waudby, M. F. Mossuto, S. Meehan, S. L. Gras, J. Christodoulou, S. J. Anthony-Cahill, P. D. Barker, M. Vendruscolo and C. M. Dobson, *J. Am. Chem. Soc.*, 2011, **133**, 14160-14163.
55. L. Khemtemourian, E. Gazit and A. Miranker, *J. Diabetes Res.*, 2016.
56. K. Tenidis, M. Waldner, J. Bernhagen, W. Fischle, M. Bergmann, M. Weber, M.-L. Merkle, W. Voelter, H. Brunner and A. Kapurniotu, *J. Mol. Biol.*, 2000, **295**, 1055-1071.
57. M. Reches, Y. Porat and E. Gazit, *J. Biol. Chem.*, 2002, **277**, 35475-35480.
58. V. Castelletto, P. Ryumin, R. Cramer, I. W. Hamley, M. Taylor, D. Allsop, M. Reza, J. Ruokolainen, T. Arnold, D. Hermida-Merino, C. I. Garcia, M. C. Leal and E. Castaño, *Sci. Rep.*, 2017, **in press**.
59. M. Reches and E. Gazit, *Science*, 2003, **300**, 625-627.
60. M. Reches and E. Gazit, *Isr. J. Chem.*, 2005, **45**, 363-371.
61. V. Nguyen, R. Zhu, K. Jenkins and R. Yang, *Nat. Commun.*, 2016, **7**, 13566.
62. P. W. Frederix, G. G. Scott, Y. M. Abul-Haija, D. Kalafatovic, C. G. Pappas, N. Javid, N. T. Hunt, R. V. Ulijn and T. Tuttle, *Nat. Chem.*, 2015, **7**, 30-37.
63. L. Adler-Abramovich, L. Vaks, O. Carny, D. Trudler, A. Magno, A. Caflisch, D. Frenkel and E. Gazit, *Nat. Chem. Biol.*, 2012, **8**, 701-706.
64. S. Shaham-Niv, L. Adler-Abramovich, L. Schnaider and E. Gazit, *Sci. Adv.*, 2015, **1**, e1500137.
65. P. Singh, S. K. Brar, M. Bajaj, N. Narang, V. S. Mithu, O. P. Katare, N. Wangoo and R. K. Sharma, *Mater. Sci. Eng., C*, 2017, **72**, 590-600.
66. G. Fichman, L. Adler-Abramovich, S. Manohar, I. Mironi-Harpaz, T. Guterman, D. Seliktar, P. B. Messersmith and E. Gazit, *ACS Nano*, 2014, **8**, 7220-7228.
67. G. Fichman and E. Gazit, *Acta Biomater.*, 2014, **10**, 1671-1682.
68. B. A. Chromy, R. J. Nowak, M. P. Lambert, K. L. Viola, L. Chang, P. T. Velasco, B. W. Jones, S. J. Fernandez, P. N. Lacor, P. Horowitz, C. E. Finch, G. A. Krafft and W. L. Klein, *Biochemistry*, 2003, **42**, 12749-12760.
69. M. L. de la Paz, K. Goldie, J. Zurdo, E. Lacroix, C. M. Dobson, A. Hoenger and L. Serrano, *Proc. Natl. Acad. Sci. U.S.A.*, 2002, **99**, 16052-16057.
70. S. Jha, J. M. Snell, S. R. Sheftic, S. M. Patil, S. B. Daniels, F. W. Kolling and A. T. Alexandrescu, *Biochemistry*, 2014, **53**, 300-310.
71. S. Kobayashi, Y. Tanaka, M. Kiyono, M. Chino, T. Chikuma, K. Hoshi and H. Ikeshima, *J. Mol. Struct.*, 2015, **1094**, 109-117.
72. I. W. Hamley, *Soft Matter*, 2011, **7**, 4122-4138.
73. K. L. Niece, J. D. Hartgerink, J. J. J. M. Donners and S. I. Stupp, *J. Am. Chem. Soc.*, 2003, **125**, 7146-7147.
74. J. D. Hartgerink, E. Beniash and S. I. Stupp, *Science*, 2001, **294**, 1684-1688.
75. J. D. Hartgerink, E. Beniash and S. I. Stupp, *Proc. Natl. Acad. Sci. U.S.A.*, 2002, **99**, 5133-5138.
76. A. Dehsorkhi, V. Castelletto, I. W. Hamley, J. Adamcik and R. Mezzenga, *Soft Matter*, 2013, **9**, 6033-6036.
77. W. Hoyer, T. Antony, D. Cherny, G. Heim, T. M. Jovin and V. Subramaniam, *J. Mol. Biol.*, 2002, **322**, 383-393.
78. B. Raman, E. Chatani, M. Kihara, T. Ban, M. Sakai, K. Hasegawa, H. Naiki, C. M. Rao and Y. Goto, *Biochemistry*, 2005, **44**, 1288-1299.
79. L. N. Arnaudov and R. de Vries, *Biomacromolecules*, 2006, **7**, 3490-3498.
80. P. J. Marek, V. Patsalo, D. F. Green and D. P. Raleigh, *Biochemistry*, 2012, **51**, 8478-8490.
81. A. Abelein, J. Jarvet, A. Barth, A. Graslund and J. Danielsson, *J. Am. Chem. Soc.*, 2016, **138**, 6893-6902.
82. M. Owczarz, T. Casalini, A. C. Motta, M. Morbidelli and P. Arosio, *Biomacromolecules*, 2015, **16**, 3792-3801.
83. R. Parker, T. E. Noel, G. J. Brownsey, K. Laos and S. G. Ring, *Biophys. J.*, 2005, **89**, 1227-1236.
84. E. H. C. Bromley, M. R. H. Krebs and A. M. Donald, *Eur. Phys. J. E*, 2006, **21**, 1-8.
85. R. Mishra and R. Winter, *Angew. Chem. Int. Ed.*, 2008, **47**, 6518-6521.
86. M. van den Heuvel, D. Lowik and J. C. M. van Hest, *Biomacromolecules*, 2008, **9**, 2727-2734.
87. J. F. Miravet, B. Escuder, M. D. Segarra-Maset, M. Tena-Solsona, I. W. Hamley, A. Dehsorkhi and V. Castelletto, *Soft Matter*, 2013, **9**, 3558-3564.
88. D. W. P. M. Löwik, E. H. P. Leunissen, M. van den Heuvel, M. B. Hansen and J. C. M. van Hest, *Chem. Soc. Rev.*, 2010, **39**, 3394-3412.
89. C. Lara, S. Gourdin-Bertin, J. Adamcik, S. Bolisetty and R. Mezzenga, *Biomacromolecules*, 2012, **13**, 4213-4221.
90. J. Kardos, A. Micsonai, H. Pal-Gabor, E. Petrik, L. Graf, J. Kovacs, Y. H. Lee, H. Naiki and Y. Goto, *Biochemistry*, 2011, **50**, 3211-3220.
91. T. Ikenoue, Y. H. Lee, J. Kardos, M. Saiki, H. Yagi, Y. Kawata and Y. Goto, *Angew. Chem. Int. Ed.*, 2014, **53**, 7799-7804.
92. A. Arora, C. Ha and C. B. Park, *Protein Sci.*, 2004, **13**, 2429-2436.
93. N. J. Cobb, A. C. Apetri and W. K. Surewicz, *J. Biol. Chem.*, 2008, **283**, 34704-34711.
94. G. Wei, T. F. Keller, J. T. Zhang and K. D. Jandt, *Soft Matter*, 2011, **7**, 2011-2018.
95. G. Wei, J. Reichert, J. Bossert and K. D. Jandt, *Biomacromolecules*, 2008, **9**, 3258-3267.
96. J. H. Viles, *Coord. Chem. Rev.*, 2012, **256**, 2271-2284.
97. A. I. Bush, *Curr. Opin. Chem. Biol.*, 2000, **4**, 184-191.
98. P. Zatta, ed., *Metal ions and neurodegenerative disorders*, World Scientific, Singapore, 2003.
99. P. A. Adlard and A. I. Bush, *J. Alzheimers Dis.*, 2006, **10**, 145-163.
100. A. C. Miu and O. Benga, *J. Alzheimers Dis.*, 2006, **10**, 179-201.
101. D. R. Brown, *Dalton Trans.*, 2009, **21**, 4069-4076.
102. M. A. Smith, P. L. R. Harris, L. M. Sayre and G. Perry, *Proc. Natl. Acad. Sci. U.S.A.*, 1997, **94**, 9866-9868.
103. L. M. Sayre, G. Perry and M. A. Smith, *Curr. Opin. Chem. Biol.*, 1999, **3**, 220-225.
104. L. M. Sayre, G. Perry, P. L. R. Harris, Y. H. Liu, K. A. Schubert and M. A. Smith, *J. Neurochem.*, 2000, **74**, 270-279.
105. M. A. Lovell, J. D. Robertson, W. J. Teesdale, J. L. Campbell and W. R. Markesbery, *J. Neurol. Sci.*, 1998, **158**, 47-52.
106. S. W. Suh, K. B. Jensen, M. S. Jensen, D. S. Silva, P. J. Kesslak, G. Danscher and C. J. Frederickson, *Brain Res.*, 2000, **852**, 274-278.
107. A. I. Bush, W. H. Pettingell, G. Multhaup, M. D. Paradis, J. P. Vonsattel, J. F. Gusella, K. Beyreuther, C. L. Masters and R. E. Tanzi, *Science*, 1994, **265**, 1464-1467.
108. A. I. Bush, W. H. Pettingell, M. D. Paradis and R. E. Tanzi, *J. Biol. Chem.*, 1994, **269**, 12152-12158.
109. C. S. Atwood, R. D. Moir, X. D. Huang, R. C. Scarpa, N. M. E. Bacarra, D. M. Romano, M. K. Hartshorn, R. E. Tanzi and A. I. Bush, *J. Biol. Chem.*, 1998, **273**, 12817-12826.
110. R. A. Cherny, J. T. Legg, C. A. McLean, D. P. Fairlie, X. D. Huang, C. S. Atwood, K. Beyreuther, R. E. Tanzi, C. L. Masters and A. I. Bush, *J. Biol. Chem.*, 1999, **274**, 23223-23228.
111. B. Raman, T. Ban, K. Yamaguchi, M. Sakai, T. Kawai, H. Naiki and Y. Goto, *J. Biol. Chem.*, 2005, **280**, 16157-16162.
112. T. Hamaguchi, K. Ono and M. Yamada, *Cell. Mol. Life Sci.*, 2006, **63**, 1538-1552.
113. C. A. Hawkes, V. Ng and J. McLaurin, *Drug Dev. Res.*, 2009, **70**, 111-124.
114. I. W. Hamley, *Chem. Rev.*, 2012, **112**, 5147-5192.
115. M. Innocenti, E. Salvietti, M. Guidotti, A. Casini, S. Bellandi, M. L. Foresti, C. Gabbiani, A. Pozzi, P. Zatta and L. Messori, *J. Alzheimers Dis.*, 2010, **19**, 1323-1329.

116. V. Pradines, A. J. Stroia and P. Faller, *New J. Chem.*, 2008, **32**, 1189-1194.
117. A. L. Fink, *Acc. Chem. Res.*, 2006, **39**, 628-634.
118. S. Bolisetty and R. Mezzenga, *Nat. Nanotechnol.*, 2016, **11**, 365-371.
119. R. Zou, Q. Wang, J. Wu, J. Wu, C. Schmuck and H. Tian, *Chem. Soc. Rev.*, 2015, **44**, 5200-5219.
120. A. D. Snow, H. Mar, D. Nochlin, K. Kimata, M. Kato, S. Suzuki, J. Hassell and T. N. Wight, *Am. J. Pathol.*, 1988, **133**, 456-463.
121. J. McLaurin, T. Franklin, X. Q. Zhang, J. P. Deng and P. E. Fraser, *Eur. J. Biochem.*, 1999, **266**, 1101-1110.
122. J. McLaurin, D. S. Yang, C. M. Yip and P. E. Fraser, *J. Struct. Biol.*, 2000, **130**, 259-270.
123. J. J. Valle-Delgado, M. Alfonso-Prieto, N. S. de Groot, S. Ventura, J. Samitier, C. Rovira and X. Fernandez-Busquets, *FASEB J.*, 2010, **24**, 4250-4261.
124. P. E. Fraser, J. T. Nguyen, D. T. Chin and D. A. Kirschner, *J. Neurochem.*, 1992, **59**, 1531-1540.
125. G. Panza, J. Stohr, E. Birkmann, D. Riesner, D. Willbold, O. Baba, T. Terashima and C. Dumpitak, *Rejuv. Res.*, 2008, **11**, 365-369.
126. O. G. Jones, J. Adamcik, S. Handschin, S. Bolisetty and R. Mezzenga, *Langmuir*, 2010, **26**, 17449-17458.
127. A. Assarsson, S. Linse and C. Cabaleiro-Lago, *Langmuir*, 2014, **30**, 8812-8818.
128. E. R. da Silva, G. Cooney, I. W. Hamley, W. A. Alves, S. Lee, B. F. O'Connor, M. Reza, J. Ruokolainen and D. Walls, *Soft Matter*, 2016, **12**, 9158-9169.
129. A. Udomprasert, M. N. Bongiovanni, R. J. Sha, W. B. Sherman, T. Wang, P. S. Arora, J. W. Canary, S. L. Gras and N. C. Seeman, *Nat. Nanotechnol.*, 2014, **9**, 537-541.
130. C. Cabaleiro-Lago, O. Szczepankiewicz and S. Linse, *Langmuir*, 2012, **28**, 1852-1857.
131. E. P. O'Brien, J. E. Straub, B. R. Brooks and D. Thirumalai, *J. Phys. Chem. Lett.*, 2011, **2**, 1171-1177.
132. T. Cedervall, I. Lynch, M. Foy, T. Berggad, S. C. Donnelly, G. Cagney, S. Linse and K. A. Dawson, *Angew. Chem. Int. Ed.*, 2007, **46**, 5754-5756.
133. C. Cabaleiro-Lago, I. Lynch, K. A. Dawson and S. Linse, *Langmuir*, 2009, **26**, 3453-3461.
134. C. Cabaleiro-Lago, F. Quinlan-Pluck, I. Lynch, S. Lindman, A. M. Minogue, E. Thulin, D. M. Walsh, K. A. Dawson and S. Linse, *J. Am. Chem. Soc.*, 2008, **130**, 15437-15443.
135. C. Cabaleiro-Lago, F. Quinlan-Pluck, I. Lynch, K. A. Dawson and S. Linse, *ACS Chem. Neurosci.*, 2010, **1**, 279-287.
136. S. I. Yoo, M. Yang, J. R. Brender, V. Subramanian, K. Sun, N. E. Joo, S. H. Jeong, A. Ramamoorthy and N. A. Kotov, *Angew. Chem. Int. Ed.*, 2011, **50**, 5110-5115.
137. W. H. Wu, X. Sun, Y. P. Yu, J. Hu, L. Zhao, Q. Liu, Y. F. Zhao and Y. M. Li, *Biochem. Biophys. Res. Commun.*, 2008, **373**, 315-318.
138. J. Geng, M. Li, J. S. Ren, E. B. Wang and X. G. Qu, *Angew. Chem. Int. Ed.*, 2011, **50**, 4184-4188.
139. F. Barandeh, P.-L. Nguyen, R. Kumar, G. J. Iacobucci, M. L. Kuznicki, A. Kosterman, E. J. Bergey, P. N. Prasad and S. Gunawardena, *Plos One*, 2012, **7**, e29424.
140. L. Di, E. H. Kerns, K. Fan, O. J. McConnell and G. T. Carter, *Eur. J. Med. Chem.*, 2003, **38**, 223-232.
141. J. S. Choi, J. J. Braymer, R. P. R. Nanga, A. Ramamoorthy and M. H. Lim, *Proc. Natl. Acad. Sci. U.S.A.*, 2010, **107**, 21990-21995.
142. S. Linse, C. Cabaleiro-Lago, W. F. Xue, I. Lynch, S. Lindman, E. Thulin, S. E. Radford and K. A. Dawson, *Proc. Natl. Acad. Sci. U.S.A.*, 2007, **104**, 8691-8696.
143. C. Fernández, G. González-Rubio, J. Langer, G. Tardajos, L. M. Liz-Marzán, R. Giraldo and G.-M. A., *Angew. Chem. Int. Ed.*, 2016, **55**, 11237-11241.
144. A. Gladytz, M. Wagner, T. Haupl, C. Elsner and B. Abel, *Part. Part. Syst. Charact.*, 2015, **32**, 573-582.
145. A. Gladytz, B. Abel and H. J. Risselada, *Angew. Chem. Int. Ed.*, 2016, **55**, 11242-11246.
146. T. P. J. Knowles, C. A. Waudby, G. L. Devlin, S. I. A. Cohen, A. Aguzzi, M. Vendruscolo, E. M. Terentjev, M. E. Welland and C. M. Dobson, *Science*, 2009, **326**, 1533-1537.
147. E. Chatani, Y. H. Lee, H. Yagi, Y. Yoshimura, H. Naiki and Y. Goto, *Proc. Natl. Acad. Sci. U.S.A.*, 2009, **106**, 11119-11124.
148. J. M. Jung, G. Savin, M. Pouzot, C. Schmitt and R. Mezzenga, *Biomacromolecules*, 2008, **9**, 2477-2486.
149. D. E. Dunstan, P. Hamilton-Brown, P. Asimakis, W. Ducker and J. Bertolini, *Soft Matter*, 2009, **5**, 5020-5028.
150. E. K. Hill, B. Krebs, D. G. Goodall, G. J. Howlett and D. E. Dunstan, *Biomacromolecules*, 2006, **7**, 10-13.
151. I. B. Bekard, P. Asimakis, C. L. Teoh, T. Ryan, G. J. Howlett, J. Bertolini and D. E. Dunstan, *Soft Matter*, 2012, **8**, 385-389.
152. F. Macchi, S. V. Hoffmann, M. Carlsen, B. Vad, A. Imparato, C. Rischel and D. E. Otzen, *Langmuir*, 2011, **27**, 12539-12549.
153. A. F. Dexter, *Langmuir*, 2010, **26**, 17997-18007.
154. R. Mezzenga and P. Fischer, *Rep Prog Phys*, 2013, **76**, 046601.
155. S. Campioni, G. Carret, S. Jordens, L. Nicoud, R. Mezzenga and R. Riek, *J. Am. Chem. Soc.*, 2014, **136**, 2866-2875.
156. M. Hoernke, J. A. Falenski, C. Schwieger, B. Koksch and G. Brezesinski, *Langmuir*, 2011, **27**, 14218-14231.
157. J. Pronchik, X. He, J. T. Giurleo and D. S. Talaga, *J. Am. Chem. Soc.*, 2010, **132**, 9797-9803.
158. I. W. Hamley, *Nat. Chem.*, 2010, **2**, 707-708.
159. A. T. Petkova, R. D. Leapman, Z. H. Guo, W. M. Yau, M. P. Mattson and R. Tycko, *Science*, 2005, **307**, 262-265.
160. C. Galvagnion, A. K. Buell, G. Meisl, T. C. T. Michaels, M. Vendruscolo, T. P. J. Knowles and C. M. Dobson, *Nat. Chem. Biol.*, 2015, **11**, 229-234.
161. G. Fusco, A. De Simone, T. Gopinath, V. Vostrikov, M. Vendruscolo, C. M. Dobson and G. Veglia, *Nat. Commun.*, 2014, **5**, 3827.
162. M. Michikawa, *J. Neurosci. Res.*, 2003, **72**, 141-146.
163. M. Michikawa, *Mol. Neurobiol.*, 2003, **27**, 1-12.
164. G. P. Gorbenko and P. K. J. Kinnunen, *Chem. Phys. Lipids*, 2006, **141**, 72-82.
165. T. Kawarabayashi, M. Shoji, L. H. Younkin, W. L. Lin, D. W. Dickson, T. Murakami, E. Matsubara, K. Abe, K. H. Ashe and S. G. Younkin, *J. Neurosci.*, 2004, **24**, 3801-3809.
166. S. I. Kim, J. S. Yi and Y. G. Ko, *J. Cell. Biochem.*, 2006, **99**, 878-889.
167. T. Okada, K. Ikeda, M. Wakabayashi, M. Ogawa and K. Matsuzaki, *J. Mol. Biol.*, 2008, **382**, 1066-1074.
168. P. K. Mandal and J. W. Pettegrew, *Neurochem. Res.*, 2004, **29**, 2267-2272.
169. M. Morita, T. Hamada, Y. Tendo, t. Hata, M. C. Vestergaard and M. Takagi, *Soft Matter*, 2012, **8**, 2816-2819.
170. N. P. Reynolds, A. Soragni, M. Rabe, D. Verdes, E. Liverani, S. Handschin, R. Riek and S. Seeger, *J. Am. Chem. Soc.*, 2011, **133**, 19366-19375.
171. Z. Jiang, M. de Messieres and J. C. Lee, *J. Am. Chem. Soc.*, 2013, **135**, 15970-15973.
172. C. M. Pfefferkorn, F. Heinrich, A. J. Sodt, A. S. Maltsev, R. W. Pastor and J. C. Lee, *Biophys. J.*, 2012, **102**, 613-621.
173. G. Comellas, L. R. Lemkau, D. H. H. Zhou, J. M. George and C. M. Rienstra, *J. Am. Chem. Soc.*, 2012, **134**, 5090-5099.
174. J. Seeliger, F. Evers, C. Jeworrek, S. Kapoor, K. Weise, E. Andreetto, M. Tolan, A. Kapurniotu and R. Winter, *Angew. Chem. Int. Ed.*, 2012, **51**, 679-683.
175. S. I. A. Cohen, M. Vendruscolo, C. M. Dobson and T. P. J. Knowles, *J. Mol. Biol.*, 2012, **421**, 160-171.
176. S. I. A. Cohen, M. Vendruscolo, M. E. Welland, C. M. Dobson, E. M. Terentjev and T. P. J. Knowles, *J. Chem. Phys.*, 2011, **135**, 065105.
177. S. W. Chen, S. Drakulic, E. Deas, M. Ouberai, F. A. Aprile, R. Arranz, S. Ness, C. Roodveldt, T. Guilliams, E. J. De-Genst, D. Klenerman, N. W. Wood, T. P. J. Knowles, C. Alfonso, G. Rivas, A. Y. Abramov, J. M. Valpuesta, C. M. Dobson and N. Cremades, *Proc. Natl. Acad. Sci. U.S.A.*, 2015, **112**, E1994-E2003.
178. N. Cremades, S. I. A. Cohen, E. Deas, A. Y. Abramov, A. Y. Chen, A. Orte, M. Sandal, R. W. Clarke, P. Dunne, F. A. Aprile, C. W. Bertoncini, N. W. Wood, T. P. J. Knowles, C. M. Dobson and D. Klenerman, *Cell*, 2012, **149**, 1048-1059.
179. N. Lorenzen, S. B. Nielsen, A. K. Buell, J. D. Kaspersen, P. Arosio, B. S. Vad, W. Paslawski, G. Christiansen, Z. Valnickova-Hansen, M. Andreasen, J. J. Enghild, J. S. Pedersen, C. M. Dobson, T. P. J. Knowles and D. E. Otzen, *J. Am. Chem. Soc.*, 2014, **136**, 3859-3868.

 This journal is © The Royal Society of Chemistry 20xx

180. A. K. Buell, A. Dhulesia, D. A. White, T. P. J. Knowles, C. M. Dobson and M. E. Welland, *Angew. Chem. Int. Ed.*, 2012, **51**, 5247-5251.
181. M. Owczarz, A. C. Motta, M. Morbidelli and P. Arosio, *Langmuir*, 2015, **31**, 7590-7600.
182. M. Tanaka, S. R. Collins, B. H. Toyama and J. S. Weissman, *Nature*, 2006, **442**, 585-589.
183. F. A. Ferrone, J. Hofrichter and W. A. Eaton, *J. Mol. Biol.*, 1985, **183**, 611-631.
184. A. Saric, Y. C. Chebaro, T. P. J. Knowles and D. Frenkel, *Proc. Natl. Acad. Sci. U.S.A.*, 2014, **111**, 17869-17874.
185. S. I. A. Cohen, S. Linse, L. M. Luheshi, E. Hellstrand, D. A. White, L. Rajah, D. E. Otzen, M. Vendruscolo, C. M. Dobson and T. P. J. Knowles, *Proc. Natl. Acad. Sci. U.S.A.*, 2013, **110**, 9758-9763.
186. V. Fodera, F. Librizzi, M. Groenning, M. van de Weert and M. Leone, *J. Phys. Chem. B*, 2008, **112**, 3853-3858.
187. A. M. Ruschak and A. D. Miranker, *Proc. Natl. Acad. Sci. U.S.A.*, 2007, **104**, 12341-12346.
188. A. K. Buell, C. Galvagnion, R. Gaspar, E. Sparr, M. Vendruscolo, T. P. J. Knowles, S. Linse and C. M. Dobson, *Proc. Natl. Acad. Sci. U.S.A.*, 2014, **111**, 7671-7676.
189. J. Habchi, P. Arosio, M. Perni, A. R. Costa, M. Yagi-Utsumi, P. Joshi, S. Chia, S. I. A. Cohen, M. B. D. Muller, S. Linse, E. A. A. Nollen, C. M. Dobson, T. P. J. Knowles and M. Vendruscolo, *Sci. Adv.*, 2016, **2**, e1501244.
190. L. Lang, P. Zetterstrom, T. Brannstrom, S. L. Marklund, J. Danielsson and M. Oliveberg, *Proc. Natl. Acad. Sci. U.S.A.*, 2015, **112**, 9878-9883.
191. R. V. Pappu, X. Wang, A. Vitalis and S. L. Crick, *Arch. Biochem. Biophys.*, 2008, **469**, 132-141.
192. J. M. Andrews and C. J. Roberts, *J. Phys. Chem. B*, 2007, **111**, 7897-7913.
193. C. J. Roberts, *Biotechnol. Bioeng.*, 2007, **98**, 927-938.
194. L. Nicoud, P. Arosio, M. Sozo, A. Yates, E. Norrant and M. Morbidelli, *J. Phys. Chem. B*, 2014, **118**, 10595-10606.
195. A. Ahmad, I. S. Millett, S. Doniach, V. N. Uversky and A. L. Fink, *Biochemistry*, 2003, **42**, 11404-11416.
196. L. Nielsen, R. Khurana, A. Coats, S. Frokjaer, J. Brange, S. Vyas, V. N. Uversky and A. L. Fink, *Biochemistry*, 2001, **40**, 6036-6046.
197. C. C. Lee, A. Nayak, A. Sethuraman, G. Belfort and G. J. McRae, *Biophys. J.*, 2007, **92**, 3448-3458.
198. M. Manno, E. F. Craparo, V. Martorana, D. Bulone and P. L. San Biagio, *Biophys. J.*, 2006, **90**, 4585-4591.
199. A. K. Buell, A. Dhulesia, M. F. Mossuto, N. Cremades, J. R. Kumita, M. Dumoulin, M. E. Welland, T. P. J. Knowles, X. Salvatella and C. M. Dobson, *J. Am. Chem. Soc.*, 2011, **133**, 7737-7743.
200. S. Raccosta, V. Martorana and M. Manno, *J. Phys. Chem. B*, 2012, **116**, 12078-12087.
201. F. Chiti, E. De Lorenzi, S. Grossi, P. Mangione, S. Giorgetti, G. Caccialanza, C. M. Dobson, G. Merlini, G. Ramponi and V. Bellotti, *J. Biol. Chem.*, 2001, **276**, 46714-46721.
202. V. J. McParland, N. M. Kad, A. P. Kalverda, A. Brown, P. Kirwin-Jones, M. G. Hunter, M. Sunde and S. E. Radford, *Biochemistry*, 2000, **39**, 8735-8746.
203. A. Nordlund, L. Leinartaite, K. Saraboji, C. Aisenbrey, G. Grobner, P. Zetterstrom, J. Danielsson, D. T. Logan and M. Oliveberg, *Proc. Natl. Acad. Sci. U.S.A.*, 2009, **106**, 9667-9672.
204. R. Khurana, J. R. Gillespie, A. Talapatra, L. J. Minert, C. Ionescu-Zanetti, I. Millett and A. L. Fink, *Biochemistry*, 2001, **40**, 3525-3535.
205. G. Esposito, R. Michelutti, G. Verdone, P. Viglino, H. Hernandez, C. V. Robinson, A. Amoresano, F. Dal Piaz, M. Monti, P. Pucci, P. Mangione, M. Stoppini, G. Merlini, G. Ferri and V. Bellotti, *Protein Sci.*, 2000, **9**, 831-845.
206. C. Lara, J. Adamcik, S. Jordens and R. Mezzenga, *Biomacromolecules*, 2011, **12**, 1868-1875.
207. R. Mishra, K. Sorgjerd, S. Nystrom, A. Nordigarden, Y. C. Yu and P. Hammarstrom, *J. Mol. Biol.*, 2007, **366**, 1029-1044.
208. C. Akkermans, P. Venema, A. J. van der Goot, H. Gruppen, E. J. Bakx, R. M. Boom and E. van der Linden, *Biomacromolecules*, 2008, **9**, 1474-1479.
209. P. Arosio, M. Beeg, L. Nicoud and M. Morbidelli, *Chem. Eng. Sci.*, 2012, **78**, 21-32.
210. P. Arosio, S. Rima, M. Lattuada and M. Morbidelli, *J. Phys. Chem. B*, 2012, **116**, 7066-7075.
211. E. Sahin, A. O. Grillo, M. D. Perkins and C. J. Roberts, *J. Pharm. Sci.*, 2010, **99**, 4830-4848.
212. C. B. Andersen, M. Manno, C. Rischel, M. Thorolfsson and V. Martorana, *Protein Sci.*, 2010, **19**, 279-290.
213. J. M. Jung and R. Mezzenga, *Langmuir*, 2010, **26**, 504-514.
214. M. Owczarz, S. Bolisetty, R. Mezzenga and P. Arosio, *J. Colloid Interface Sci.*, 2015, **437**, 244-251.
215. M. Manno, D. Giacomazza, J. Newman, V. Martorana and P. L. San Biagio, *Langmuir*, 2010, **26**, 1424-1426.
216. A. Nayak, A. K. Dutta and G. Belfort, *Biochem. Biophys. Res. Commun.*, 2008, **369**, 303-307.
217. S. L. Shammas, G. A. Garcia, S. Kumar, M. Kjaergaard, M. H. Horrocks, N. Shivji, E. Mandelkow, T. P. J. Knowles, E. Mandelkow and D. Klenerman, *Nat. Commun.*, 2015, **6**, 7025.
218. F. Ferrone, *Amyloid, Prions, and Other Protein Aggregates*, 1999, **309**, 256-274.
219. G. Meisl, J. B. Kirkegaard, P. Arosio, T. C. T. Michaels, M. Vendruscolo, C. M. Dobson, S. Linse and T. P. J. Knowles, *Nat. Protocols*, 2016, **11**, 252-272.
220. H. LeVine, *Protein Sci.*, 1993, **2**, 404-410.
221. M. Biancalana and S. Koide, *Bba-Protein Proteomics*, 2010, **1804**, 1405-1412.
222. P. Arosio, R. Cukalevski, B. Frohm, T. P. J. Knowles and S. Linse, *J. Am. Chem. Soc.*, 2014, **136**, 219-225.
223. P. Arosio, T. P. J. Knowles and S. Linse, *Phys. Chem. Chem. Phys.*, 2015, **17**, 7606-7618.
224. E. Hellstrand, B. Boland, D. M. Walsh and S. Linse, *ACS Chem. Neurosci.*, 2010, **1**, 13-18.
225. S. I. A. Cohen, P. Arosio, J. Presto, F. R. Kurudenkandy, H. Biverstal, L. Dolfe, C. Dunning, X. T. Yang, B. Frohm, M. Vendruscolo, J. Johansson, C. M. Dobson, A. Fisahn, T. P. J. Knowles and S. Linse, *Nat. Struct. Mol. Biol.*, 2015, **22**, 207-213.
226. G. Meisl, X. T. Yang, B. Frohm, T. P. J. Knowles and S. Linse, *Sci. Rep.*, 2016, **6**, 18728.
227. G. Meisl, X. T. Yang, E. Hellstrand, B. Frohm, J. B. Kirkegaard, S. I. A. Cohen, C. M. Dobson, S. Linse and T. P. J. Knowles, *Proc. Natl. Acad. Sci. U.S.A.*, 2014, **111**, 9384-9389.
228. P. Arosio, M. Vendruscolo, C. M. Dobson and T. P. J. Knowles, *Trends Pharmacol. Sci.*, 2014, **35**, 127-135.
229. P. Arosio, T. C. T. Michaels, S. Linse, C. Mansson, C. Emanuelsson, J. Presto, J. Johansson, M. Vendruscolo, C. M. Dobson and T. P. J. Knowles, *Nat. Commun.*, 2016, **7**, 10948.
230. M. H. Horrocks, L. Tosatto, A. J. Dear, G. A. Garcia, M. Iljina, N. Cremades, M. D. Serra, T. P. J. Knowles, C. M. Dobson and D. Klenerman, *Anal. Chem.*, 2015, **87**, 8818-8826.
231. M. Iljina, G. A. Garcia, M. H. Horrocks, L. Tosatto, M. L. Choi, K. A. Ganzinger, A. Y. Abramov, S. Gandhi, N. W. Wood, N. Cremades, C. M. Dobson, T. P. J. Knowles and D. Klenerman, *Proc. Natl. Acad. Sci. U.S.A.*, 2016, **113**, E1206-E1215.
232. W. F. Xue, A. L. Hellewell, W. S. Gosal, S. W. Homans, E. W. Hewitt and S. E. Radford, *J. Biol. Chem.*, 2009, **284**, 34272-34282.
233. J. Adamcik, J. M. Jung, J. Flakowski, P. De Los Rios, G. Dietler and R. Mezzenga, *Nat Nanotechnol*, 2010, **5**, 423-428.
234. J. Adamcik and R. Mezzenga, *Soft Matter*, 2011, **7**, 5437-5443.
235. J. Adamcik and R. Mezzenga, *Curr. Opin. Colloid Interface Sci.*, 2012, **17**, 369-376.
236. W. F. Xue, S. W. Homans and S. E. Radford, *Protein Eng. Des. Sel.*, 2009, **22**, 489-496.
237. W. F. Xue and S. E. Radford, *Biophys. J.*, 2013, **105**, 2811-2819.
238. D. Pinotsi, A. K. Buell, C. M. Dobson, G. S. K. Schierle and C. F. Kaminski, *ChemBioChem*, 2013, **14**, 846-850.
239. D. Pinotsi, A. K. Buell, C. Galvagnion, C. M. Dobson, G. S. K. Schierle and C. F. Kaminski, *Nano Lett.*, 2014, **14**, 339-345.
240. S. Bolisetty, J. Adamcik and R. Mezzenga, *Soft Matter*, 2011, **7**, 493-499.
241. S. S. Rogers, P. Venema, J. P. M. Van der Ploeg, E. Van der Linden, L. M. C. Sagis and A. M. Donald, *Biopolymers*, 2006, **82**, 241-252.
242. A. J. Baldwin, S. J. Anthony-Cahill, T. P. J. Knowles, G. Lippens, J.

Christodoulou, P. D. Barker and C. M. Dobson, *Angew. Chem. Int. Ed.*, 2008, **47**, 3385-3387.
243. P. Schuck, *Biophys. J.*, 2000, **78**, 1606-1619.
244. P. Schuck, *Anal. Biochem.*, 2003, **320**, 104-124.
245. P. Schuck, M. A. Perugini, N. R. Gonzales, G. J. Howlett and D. Schubert, *Biophys. J.*, 2002, **82**, 1096-1111.
246. G. J. Howlett, A. P. Minton and G. Rivas, *Curr. Opin. Chem. Biol.*, 2006, **10**, 430-436.
247. P. Arosio, T. Cedervall, T. P. J. Knowles and S. Linse, *Anal. Biochem.*, 2016, **504**, 7-13.
248. T. C. T. Michaels, H. W. Lazell, P. Arosio and T. P. J. Knowles, *J. Chem. Phys.*, 2015, **143**, 054901.
249. T. C. T. Michaels, P. Yde, J. C. W. Willis, M. H. Jensen, D. Otzen, C. M. Dobson, A. K. Buell and T. P. J. Knowles, *J. Chem. Phys.*, 2015, **143**, 164901.
250. Q. Luo, C. X. Hou, Y. S. Bai, R. B. Wang and J. Q. Liu, *Chem. Rev.*, 2016, **116**, 13571-13632.
251. C. Haass and D. J. Selkoe, *Nat. Rev. Mol. Cell Bio.*, 2007, **8**, 101-112.
252. M. Sakono, T. Zako, H. Ueda, M. Yohda and M. Maeda, *FEBS J.*, 2008, **275**, 5982-5993.
253. K. A. Conway, J. D. Harper and P. T. Lansbury, *Biochemistry*, 2000, **39**, 2552-2563.
254. C. Liu, M. R. Sawaya, P. N. Cheng, J. Zheng, J. S. Nowick and D. Eisenberg, *J. Am. Chem. Soc.*, 2011, **133**, 6736-6744.
255. C. G. Glabe, *J. Biol. Chem.*, 2008, **283**, 29639-29643.
256. M. Fandrich, *J. Mol. Biol.*, 2012, **421**, 427-440.
257. M. Mulaj, J. Foley and M. Muschol, *J. Am. Chem. Soc.*, 2014, **136**, 8947-8956.
258. N. P. Harte, I. Klyubin, E. K. McCarthy, S. Min, S. A. Garrahy, Y. J. Xie, G. P. Davey, J. J. Boland, M. J. Rowan and K. H. Mok, *J. Biol. Chem.*, 2015, **290**, 28343-28352.
259. E. Cerf, R. Sarroukh, S. Tamamizu-Kato, L. Breydo, S. Derclaye, Y. F. Dufrene, V. Narayanaswami, E. Goormaghtigh, J. M. Ruysschaert and V. Raussens, *Biochem. J*, 2009, **421**, 415-423.
260. M. Ahmed, J. Davis, D. Aucoin, T. Sato, S. Ahuja, S. Aimoto, J. I. Elliott, W. E. Van Nostrand and S. O. Smith, *Nat. Struct. Mol. Biol.*, 2010, **17**, 561-U556.
261. M. Renner, P. N. Lacor, P. T. Velasco, J. A. Xu, A. Contractor, W. L. Klein and A. Triller, *Neuron*, 2010, **66**, 739-754.
262. A. Laganowsky, C. Liu, M. R. Sawaya, J. P. Whitelegge, J. Park, M. L. Zhao, A. Pensalfini, A. B. Soriaga, M. Landau, P. K. Teng, D. Cascio, C. Glabe and D. Eisenberg, *Science*, 2012, **335**, 1228-1231.
263. K. Domanska, S. Vanderhaegen, V. Srinivasan, E. Pardon, F. Dupeux, J. A. Marquez, S. Giorgetti, M. Stoppini, L. Wyns, V. Bellotti and J. Steyaert, *Proc. Natl. Acad. Sci. U.S.A.*, 2011, **108**, 1314-1319.
264. M. Maresca, A. Derghal, C. Carravagna, S. Dudin and J. Fantini, *Phys. Chem. Chem. Phys.*, 2008, **10**, 2792-2800.
265. J. R. Silveira, G. J. Raymond, A. G. Hughson, R. E. Race, V. L. Sim, S. F. Hayes and B. Caughey, *Nature*, 2005, **437**, 257-261.
266. D. El Moustaine, V. Perrier, L. Smeller, R. Lange and J. Torrent, *FEBS J.*, 2008, **275**, 2021-2031.
267. G. Habicht, C. Haupt, R. P. Friedrich, P. Hortschansky, C. Sachse, J. Meinhardt, K. Wieligmann, G. P. Gellermann, M. Brodhun, J. Gotz, K. J. Halbhuber, C. Rocken, U. Horn and M. Fandrich, *Proc. Natl. Acad. Sci. U.S.A.*, 2007, **104**, 19232-19237.
268. S. T. Kumar, J. Meinhardt, A. K. Fuchs, T. Aumuller, J. Leppert, B. Buchele, U. Knupfer, R. Ramachandran, J. K. Yadav, E. Prell, I. Morgado, O. Ohlenschlager, U. Horn, T. Simmet, M. Gorlach and M. Fandrich, *Acs Nano*, 2014, **8**, 11042-11052.
269. C. Guo, Y. Luo, R. H. Zhou and G. H. Wei, *Nanoscale*, 2014, **6**, 2800-2811.
270. T. Matsubara, K. Iijima, N. Yamamoto, K. Yanagisawa and T. Sato, *Langmuir*, 2013, **29**, 2258-2264.
271. K. A. Conway, S. J. Lee, J. C. Rochet, T. T. Ding, R. E. Williamson and P. T. Lansbury, *Proc. Natl. Acad. Sci. U.S.A.*, 2000, **97**, 571-576.
272. D. M. Hatters, C. E. MacPhee, L. J. Lawrence, W. H. Sawyer and G. J. Howlett, *Biochemistry*, 2000, **39**, 8276-8283.
273. D. M. Hatters, C. A. MacRaild, R. Daniels, W. S. Gosal, N. H. Thomson, J. A. Jones, J. J. Davis, C. E. MacPhee, C. M. Dobson and G. J. Howlett, *Biophys. J.*, 2003, **85**, 3979-3990.
274. J. J. Dong, R. P. Apkarian and D. G. Lynn, *Biorg. Med. Chem.*, 2005, **13**, 5213-5217.
275. Y. Q. Wong, K. J. Binger, G. J. Howlett and M. D. W. Griffin, *Proc. Natl. Acad. Sci. U.S.A.*, 2010, **107**, 1977-1982.
276. M. de Messieres, R. K. Huang, Y. He and J. C. Lee, *Biochemistry*, 2014, **53**, 3261-3263.
277. C. L. Teoh, M. D. W. Griffin and G. J. Howlett, *Protein Cell*, 2011, **2**, 116-127.
278. B. L. Kagan, Y. Hirakura, R. Azimov, R. Azimova and M. C. Lin, *Peptides*, 2002, **23**, 1311-1315.
279. T. T. Ding, S. J. Lee, J. C. Rochet and P. T. Lansbury, *Biochemistry*, 2002, **41**, 10209-10217.
280. M. Zhu, J. Li and A. L. Fink, *J. Biol. Chem.*, 2003, **278**, 40186-40197.
281. R. Srinivasan, R. E. Marchant and M. G. Zagorski, *Amyloid*, 2004, **11**, 10-13.
282. C. A. Lasagna-Reeves, C. G. Glabe and R. Kayed, *J. Biol. Chem.*, 2011, **286**, 22122-22130.
283. R. Kayed, A. Pensalfini, L. Margol, Y. Sokolov, F. Sarsoza, E. Head, J. Hall and C. Glabe, *J. Biol. Chem.*, 2009, **284**, 4230-4237.
284. S. Dante, T. Hauss, A. Brandt and N. A. Dencher, *J. Mol. Biol.*, 2008, **376**, 393-404.
285. A. P. Pandey, F. Haque, J. C. Rochet and J. S. Hovis, *J. Phys. Chem. B*, 2011, **115**, 5886-5893.
286. J. Varkey, J. M. Isas, N. Mizuno, M. B. Jensen, V. K. Bhatia, C. C. Jao, J. Petrlova, J. C. Voss, D. G. Stamou, A. C. Steven and R. Langen, *J. Biol. Chem.*, 2010, **285**, 32486-32493.
287. E. Hellstrand, A. Nowacka, D. Topgaard, S. Linse and E. Sparr, *Plos One*, 2013, **8**, e77235.
288. S. Gilead and E. Gazit, *Supramol. Chem.*, 2005, **17**, 87-92.
289. I. Usov, J. Adamcik and R. Mezzenga, *ACS Nano*, 2013, **7**, 10465-10474.
290. J. C. Stroud, C. Liu, P. K. Teng and D. Eisenberg, *Proc. Natl. Acad. Sci. U.S.A.*, 2012, **109**, 7717-7722.
291. A. D. Dearborn, J. S. Wall, N. Q. Cheng, J. B. Heymann, A. V. Kajava, J. Varkey, R. Langen and A. C. Steven, *J. Biol. Chem.*, 2016, **291**, 2310-2318.
292. J. Adamcik and R. Mezzenga, *Macromolecules*, 2012, **45**, 1137-1150.
293. J. Adamcik, V. Castelletto, S. Bolisetty, I. W. Hamley and R. Mezzenga, *Angew. Chem. Int. Ed.*, 2011, **50**, 5495-5498.
294. A. W. P. Fitzpatrick, G. T. Debelouchina, M. J. Bayro, D. K. Clare, M. A. Caporini, V. S. Bajaj, C. P. Jaroniec, L. C. Wang, V. Ladizhansky, S. A. Muller, C. E. MacPhee, C. A. Waudby, H. R. Mott, A. De Simone, T. P. J. Knowles, H. R. Saibil, M. Vendruscolo, E. V. Orlova, R. G. Griffin and C. M. Dobson, *Proc. Natl. Acad. Sci. U.S.A.*, 2013, **110**, 5468-5473.
295. S. Assenza, J. Adamcik, R. Mezzenga and P. De Los Rios, *Phys. Rev. Lett.*, 2014, **113**.
296. A. Uesaka, M. Ueda, A. Makino, T. Imai, J. Sugiyama and S. Kimura, *Langmuir*, 2014, **30**, 1022-1028.
297. C. Lara, N. P. Reynolds, J. T. Berryman, A. Q. Xu, A. F. Zhang and R. Mezzenga, *J. Am. Chem. Soc.*, 2014, **136**, 4732-4739.
298. V. Castelletto, I. W. Hamley, R. A. Hule and D. Pochan, *Angew. Chem. Int. Ed.*, 2009, **48**, 2317-2320.
299. R. J. Swanekamp, J. T. M. DiMaio, C. J. Bowerman and B. L. Nilsson, *J. Am. Chem. Soc.*, 2012, **134**, 5556-5559.
300. H. A. Lashuel, S. R. LaBrenz, L. Woo, L. C. Serpell and J. W. Kelly, *J. Am. Chem. Soc.*, 2000, **122**, 5262-5277.
301. J. Adamcik, A. Sanchez-Ferrer, N. Ait-Bouziad, N. P. Reynolds, H. A. Lashuel and R. Mezzenga, *Angew. Chem. Int. Ed.*, 2016, **55**, 618-622.
302. M. Perez, J. M. Valpuesta, M. Medina, E. M. deGarcini and J. Avila, *J. Neurochem.*, 1996, **67**, 1183-1190.
303. S. Zhang, M. Andreasen, J. T. Nielsen, L. Liu, E. H. Nielsen, J. Song, G. Ji, F. Sun, T. Skrydstrup, F. Besenbacher, N. C. Nielsen, D. E. Otzen and M. D. Dong, *Proc. Natl. Acad. Sci. U.S.A.*, 2013, **110**, 2798-2803.
304. O. M. Martinez-Avila, S. P. Wu, Y. F. Cheng, R. Lee, F. Khan and S. Habelitz, *Eur. J. Oral Sci.*, 2011, **119**, 75-82.
305. K. M. M. Carneiro, H. L. Zhai, L. Zhu, J. A. Horst, M. Sitlin, M. Nguyen, M. Wagner, C. Simpliciano, M. Milder, C. L. Chen, P. Ashby, J. Bonde, W. Li and S. Habelitz, *Sci. Rep.*, 2016, **6**, 23105.
306. X. D. He, S. P. Wu, O. Martinez-Avila, Y. F. Cheng and S. Habelitz, *J. Struct. Biol.*, 2011, **174**, 203-212.

 This journal is © The Royal Society of Chemistry 20xx

307. M. N. Bongiovanni, D. B. Scanlon and S. L. Gras, *Biomaterials*, 2011, **32**, 6099-6110.
308. S. L. Gras, A. K. Tickler, A. M. Squires, G. L. Devlin, M. A. Horton, C. M. Dobson and C. E. MacPhee, *Biomaterials*, 2008, **29**, 1553-1562.
309. I. W. Hamley, *Angew. Chem. Int. Ed.*, 2014, **53**, 6866-6881.
310. R. C. Elgersma, L. M. J. Kroon-Batenburg, G. Posthuma, J. D. Meeldijk, D. T. S. Rijkers and R. M. J. Liskamp, *Eur. J. Med. Chem.*, 2014, **88**, 55-65.
311. Y. R. Zhao, L. Deng, J. Q. Wang, H. Xu and J. R. Lu, *Langmuir*, 2015, **31**, 12975-12983.
312. J. D. Brodin, S. J. Smith, J. R. Carr and F. A. Tezcan, *J. Am. Chem. Soc.*, 2015, **137**, 10468-10471.
313. L. Adler-Abramovich, P. Marco, Z. A. Amon, R. C. G. Creasey, T. C. T. Michaels, A. Levin, D. J. Scurr, C. J. Roberts, T. P. J. Knowles, S. J. B. Tendler and E. Gazit, *ACS Nano*, 2016, **10**, 7436-7442.
314. Y. A. Lin, A. G. Cheetham, P. C. Zhang, Y. C. Ou, Y. G. Li, G. S. Liu, D. Hermida-Merino, I. W. Hamley and H. G. Cui, *ACS Nano*, 2014, **8**, 12690-12700.
315. T. P. J. Knowles, T. W. Oppenheim, A. K. Buell, D. Y. Chirgadze and M. E. Welland, *Nat. Nanotechnol.*, 2010, **5**, 204-207.
316. S. Bolisetty, M. Arcari, J. Adamcik and R. Mezzenga, *Langmuir*, 2015, **31**, 13867-13873.
317. S. Jordens, K. Schwenke, I. Usov, E. Del Gado and R. Mezzenga, *Soft Matter*, 2016, **12**, 1830-1835.
318. S. Jordens, L. Isa, I. Usov and R. Mezzenga, *Nat. Commun.*, 2013, **4**, 1917.
319. J. M. Jung, D. Z. Gunes and R. Mezzenga, *Langmuir*, 2010, **26**, 15366-15375.
320. S. Jordens, P. A. Ruhs, C. Sieber, L. Isa, P. Fischer and R. Mezzenga, *Langmuir*, 2014, **30**, 10090-10097.
321. D. H. Wang, Y. Ha, J. Gu, Q. Li, L. L. Zhang and P. Yang, *Adv. Mater.*, 2016, **28**, 7414-7423.
322. S. G. Zhang, T. Holmes, C. Lockshin and A. Rich, *Proc. Natl. Acad. Sci. U.S.A.*, 1993, **90**, 3334-3338.
323. B. Dai, D. Li, W. Xi, F. Luo, X. Zhang, M. Zou, M. Cao, J. Hu, W. Y. Wang, G. H. Wei, Y. Zhang and C. Liu, *Proc. Natl. Acad. Sci. U.S.A.*, 2015, **112**, 2996-3001.
324. I. W. Hamley, A. Dehsorkhi and V. Castelletto, *Chem. Commun.*, 2013, **49**, 1850-1852.
325. Y. X. Pan, C. J. Liu, S. Zhang, Y. Yu and M. D. Dong, *Chem. Eur. J.*, 2012, **18**, 14614-14617.
326. Y. X. Pan, H. P. Cong, Y. L. Men, S. Xin, Z. Q. Sun, C. J. Liu and S. H. Yu, *ACS Nano*, 2015, **9**, 11258-11265.
327. M. Staderini, M. A. Martin, M. L. Bolognesi and J. C. Menendez, *Chem. Soc. Rev.*, 2015, **44**, 1807-1819.
328. K. K. Cheng, P. S. Chan, S. J. Fan, S. M. Kwan, K. L. Yeung, Y. X. J. Wang, A. H. L. Chow, E. X. Wu and L. Baum, *Biomaterials*, 2015, **44**, 155-172.
329. H. Watanabe, M. Ono, S. Iikuni, M. Yoshimura, K. Matsumura, H. Kimura and H. Saji, *Bioorg. Med. Chem. Lett.*, 2014, **24**, 4834-4837.
330. M. Hintersteiner, A. Enz, P. Frey, A. L. Jaton, W. Kinzy, R. Kneuer, U. Neumann, M. Rudin, M. Staufenbiel, M. Stoeckli, K. H. Wiederhold and H. U. Gremlich, *Nat. Biotechnol.*, 2005, **23**, 577-583.
331. N. Benseny-Cases, O. Klementieva, M. Cotte, I. Ferrer and J. Cladera, *Anal. Chem.*, 2014, **86**, 12047-12054.
332. S. Y. Qin, Y. Pei, X. J. Liu, R. X. Zhuo and X. Z. Zhang, *J. Mater. Chem. B*, 2013, **1**, 668-675.
333. D. Peer, J. M. Karp, S. Hong, O. C. FaroKHzad, R. Margalit and R. Langer, *Nat. Nanotechnol.*, 2007, **2**, 751-760.
334. U. Shimanovich, I. Efimov, T. O. Mason, P. Flagmeier, A. K. Buell, A. Gedanken, S. Linse, K. S. Akerfeldt, C. M. Dobson, D. A. Weitz and T. P. J. Knowles, *ACS Nano*, 2015, **9**, 43-51.
335. D. J. Selkoe, D. S. Bell, M. B. Podlisny, D. L. Price and L. C. Cork, *Science*, 1987, **235**, 873-877.
336. D. M. Fowler, A. V. Koulov, W. E. Balch and J. W. Kelly, *Trends Biochem. Sci*, 2007, **32**, 217-224.
337. P. B. Jordal, M. S. Dueholm, P. Larsen, S. V. Petersen, J. J. Enghild, G. Christiansen, P. Hojrup, P. H. Nielsen and D. E. Otzen, *Appl. Environ. Microbiol.*, 2009, **75**, 4101-4110.
338. A. Villar-Pique, R. Sabate, O. Lopera, J. Gibert, J. M. Torne, M. Santos and S. Ventura, *Plos One*, 2010, **5**, e13625.
339. L. P. Blanco, M. L. Evans, D. R. Smith, M. P. Badtke and M. R. Chapman, *Trends Microbiol.*, 2012, **20**, 66-73.
340. A. Taglialegna, I. Lasa and J. Valle, *J. Bacteriol.*, 2016, **198**, 2579-2588.
341. P. Larsen, J. L. Nielsen, M. S. Dueholm, R. Wetzel, D. Otzen and P. H. Nielsen, *Environ. Microbiol.*, 2007, **9**, 3077-3090.
342. A. Ostrowski, A. Mehert, A. Prescott, T. B. Kiley and N. R. Stanley-Wall, *J. Bacteriol.*, 2011, **193**, 4821-4831.
343. M. C. Garcia, J. T. Lee, C. B. Ramsook, D. Alsteens, Y. F. Dufrene and P. N. Lipke, *Plos One*, 2011, **6**, e17632.
344. F. A. Herbst, M. T. Sondergaard, H. Kjeldal, A. Stensballe, P. H. Nielsen and M. S. Dueholm, *J. Proteome Res.*, 2015, **14**, 72-81.
345. P. M. Gallo, G. J. Rapsinski, R. P. Wilson, G. O. Oppong, U. Sriram, M. Goulian, B. Buttaro, R. Caricchio, S. Gallucci and C. Tukel, *Immunity*, 2015, **42**, 1171-1184.
346. C. Wu, J. Y. Lim, G. G. Fuller and L. Cegelski, *Biophys. J.*, 2012, **103**, 464-471.
347. J. Y. Lim, J. M. May and L. Cegelski, *Appl. Environ. Microbiol.*, 2012, **78**, 3369-3378.
348. A. Taglialegna, S. Navarro, S. Ventura, J. A. Garnett, S. Matthews, J. R. Penades, I. Lasa and J. Valle, *PLoS Path.*, 2016, **12**, e1005711.
349. A. M. Jonker, D. W. P. M. Lowik and J. C. M. van Hest, *Chem. Mater.*, 2012, **24**, 759-773.
350. E. F. Banwell, E. S. Abelardo, D. J. Adams, M. A. Birchall, A. Corrigan, A. M. Donald, M. Kirkland, L. C. Serpell, M. F. Butler and D. N. Woolfson, *Nat. Mater.*, 2009, **8**, 596-600.
351. R. Flamia, A. M. Salvi, L. D'Alessio, J. E. Castle and A. M. Tamburro, *Biomacromolecules*, 2007, **8**, 128-138.
352. G. Bhak, S. Lee, J. W. Park, S. Cho and S. R. Paik, *Biomaterials*, 2010, **31**, 5986-5995.
353. H. Yan, A. Saiani, J. E. Gough and A. F. Miller, *Biomacromolecules*, 2006, **7**, 2776-2782.
354. J. Mains, D. A. Lamprou, L. McIntosh, I. D. H. Oswald and A. J. Urquhart, *Chem. Commun.*, 2013, **49**, 5082-5084.
355. C. X. Li and R. Mezzenga, *Langmuir*, 2012, **28**, 10142-10146.
356. W. S. Gosal, A. H. Clark and S. B. Ross-Murphy, *Biomacromolecules*, 2004, **5**, 2420-2429.
357. S. Bolisetty, L. Harnau, J. M. Jung and R. Mezzenga, *Biomacromolecules*, 2012, **13**, 3241-3252.
358. H. Shao and J. R. Parquette, *Chem. Commun.*, 2010, **46**, 4285-4287.
359. M. Tena-Solsona, J. F. Miravet and B. Escuder, *Chem. Eur. J.*, 2014, **20**, 1023-1031.
360. M. Tena-Solsona, S. Alonso-de Castro, J. F. Miravet and B. Escuder, *J. Mater. Chem. B*, 2014, **2**, 6192-6197.
361. M. J. Krysmann, V. Castelletto, A. Kelarakis, I. W. Hamley, R. A. Hule and D. J. Pochan, *Biochemistry*, 2008, **47**, 4597-4605.
362. G. Nystrom, M. P. Fernandez-Ronco, S. Bolisetty, M. Mazzotti and R. Mezzenga, *Adv. Mater.*, 2016, **28**, 472-478.
363. A. Majzik, L. Fulop, E. Csapo, F. Bogar, T. Martinek, B. Penke, G. Biro and I. Dekany, *Colloids Surf. B*, 2010, **81**, 235-241.
364. B. G. Anand, K. Dubey, D. S. Shekhawat and K. Kar, *Biochemistry*, 2016, **55**, 3345-3348.
365. D. J. Hayne, S. Lim and P. S. Donnelly, *Chem. Soc. Rev.*, 2014, **43**, 6701-6715.
366. S. Bolisetty, J. J. Vallooran, J. Adamcik and R. Mezzenga, *ACS Nano*, 2013, **7**, 6146-6155.
367. Y. H. Liao, Y. J. Chang, Y. Yoshiike, Y. C. Chang and Y. R. Chen, *Small*, 2012, **8**, 3631-3639.
368. D. Brambilla, R. Verpillot, B. Le Droumaguet, J. Nicolas, M. Taverna, J. Kona, B. Lettiero, S. H. Hashemi, L. De Kimpe, M. Canovi, M. Gobbi, V. Nicolas, W. Scheper, S. M. Moghimi, I. Tvaroska, P. Couvreur and K. Andrieux, *ACS Nano*, 2012, **6**, 5897-5908.
369. G. Wei, J. Reichert and K. D. Jandt, *Chem. Commun.*, 2008, 3903-3905.
370. S. Bolisetty, C. S. Boddupalli, S. Handschin, K. Chaitanya, J. Adamcik, Y. Saito, M. G. Manz and R. Mezzenga, *Biomacromolecules*, 2014, **15**, 2793-2799.
371. I. W. Hamley, S. Kirkham, A. Dehsorkhi, V. Castelletto, J. Adamcik, R. Mezzenga, J. Ruokolainen, C. Mazzuca, E. Gatto, M. Venanzi, E. Placidi, P. Bilalis and H. Iatrou, *Biomacromolecules*, 2014, **15**, 3412-3420.
372. E. Pazos, E. Sleep, C. M. R. Perez, S. S. Lee, F. Tantakitti and S. I. Stupp,

J. Am. Chem. Soc., 2016, **138**, 5507-5510.
373. L. H. Xiao, D. Zhao, W. H. Chan, M. M. F. Choi and H. W. Li, *Biomaterials*, 2010, **31**, 91-98.
374. O. T. W. Ng, Y. Wong, H. M. Chan, J. Cheng, X. Qi, W. H. Chan, K. K. L. Yung and H. W. Li, *Biomater. Sci.*, 2013, **1**, 577-580.
375. Y. B. Liu, L. P. Xu, W. H. Dai, H. F. Dong, Y. Q. Wen and X. J. Zhang, *Nanoscale*, 2015, **7**, 19060-19065.
376. M. J. Roberti, M. Morgan, G. Menendez, L. I. Pietrasanta, T. M. Jovin and E. A. Jares-Erijman, *J. Am. Chem. Soc.*, 2009, **131**, 8102-8107.
377. L. Quan, J. X. Wu, L. A. Lane, J. Q. Wang, Q. Lu, Z. Gu and Y. Q. Wang, *Bioconjugate Chem.*, 2016, **27**, 809-814.
378. Z. Q. Su, H. Y. Shen, H. X. Wang, J. H. Wang, J. F. Li, G. U. Nienhaus, L. Shang and G. Wei, *Adv. Funct. Mater.*, 2015, **25**, 5472-5478.
379. Y. Li, W. Zhang, L. Zhang, J. Li, Z. Su and G. Wei, *Adv. Mater. Interfaces*, 2017, **4**, 1600895.
380. C. J. Newcomb, R. Bitton, Y. S. Velichko, M. L. Snead and S. I. Stupp, *Small*, 2012, **8**, 2195-2202.
381. J. H. Wang, H. X. Wang, Y. Z. Wang, J. F. Li, Z. Q. Su and G. Wei, *J Mater Chem B*, 2014, **2**, 7360-7368.
382. J. H. Wang, Z. F. Ouyang, Z. W. Ren, J. F. Li, P. P. Zhang, G. Wei and Z. Q. Su, *Carbon*, 2015, **89**, 20-30.
383. C. X. Li, A. K. Born, T. Schweizer, M. Zenobi-Wong, M. Cerruti and R. Mezzenga, *Adv. Mater.*, 2014, **26**, 3207-3212.
384. C. X. Li and R. Mezzenga, *Nanoscale*, 2013, **5**, 6207-6218.
385. D. Khatayevich, T. Page, C. Gresswell, Y. Hayamizu, W. Grady and M. Sarikaya, *Small*, 2014, **10**, 1505-1513.
386. J. H. Luo, S. K. T. S. Warmlander, C. H. Yu, K. Muhammad, A. Graslund and J. P. Abrahams, *Nanoscale*, 2014, **6**, 6720-6726.
387. J. Wang, Y. P. Cao, Q. Li, L. Liu and M. D. Dong, *Chem. Eur. J.*, 2015, **21**, 9632-9637.
388. X. Wu, M. Li, Z. Li, L. Lv, Y. Zhang and C. Li, *J. Colloid Interface Sci.*, 2017, **490**, 336-342.
389. M. Mahmoudi, O. Akhavan, M. Ghavami, F. Rezaee and S. M. A. Ghiasi, *Nanoscale*, 2012, **4**, 7322-7325.
390. Z. X. Yang, C. C. Ge, J. J. Liu, Y. Chong, Z. L. Gu, C. A. Jimenez-Cruz, Z. F. Chai and R. H. Zhou, *Nanoscale*, 2015, **7**, 18725-18737.
391. V. Castelletto, A. Kaur, I. W. Hamley , R. H. Barnes, K. A. Karatzas, D. Hermida-Merino, S. Swioklo, C. J. Connon, J. Stasiak, M. Reza and J. Ruokolainen, *RSC Adv.*, 2017, **7**, 8366-8375.
392. R. Yoshida, *Curr. Org. Chem.*, 2005, **9**, 1617-1641.
393. Z. H. Dai, Y. L. Wang, L. Q. Liu, X. L. Liu, P. H. Tan, Z. P. Xu, J. Kuang, Q. Liu, J. Lou and Z. Zhang, *Adv. Funct. Mater.*, 2016, **26**, 7003-7010.
394. C. Zhong, T. Gurry, A. A. Cheng, J. Downey, Z. T. Deng, C. M. Stultz and T. K. Lu, *Nat. Nanotechnol.*, 2014, **9**, 858-866.
395. K. Dubey, B. G. Anand, M. K. Temgire and K. Kar, *Biochemistry*, 2014, **53**, 8001-8004.
396. M. Z. Zhang, J. Zhao and J. Zheng, *Soft Matter*, 2014, **10**, 7425-7451.
397. M. P. Nikiforov, G. L. Thompson, V. V. Reukov, S. Jesse, S. Guo, B. J. Rodriguez, K. Seal, A. A. Vertegel and S. V. Kalinin, *ACS Nano*, 2010, **4**, 689-698.
398. S. J. Ling, C. X. Li, J. Adamcik, Z. Z. Shao, X. Chen and R. Mezzenga, *Adv. Mater.*, 2014, **26**, 4569-4574.
399. J. M. Goncalves, L. R. Lima, M. L. Moraes and S. J. L. Ribeiro, *Mat Sci Eng C-Mater*, 2016, **68**, 338-342.
400. J. M. Yan, Y. X. Pan, A. G. Cheetham, Y. A. Lin, W. Wang, H. G. Cui and C. J. Liu, *Langmuir*, 2013, **29**, 16051-16057.
401. P. Q. Nguyen, Z. Botyanszki, P. K. R. Tay and N. S. Joshi, *Nat. Commun.*, 2014, **5**, 4945.
402. C. M. R. Perez, N. Stephanopoulos, S. Sur, S. S. Lee, C. Newcomb and S. I. Stupp, *Ann. Biomed. Eng.*, 2015, **43**, 501-514.
403. O. Guillame-Gentil, O. Semenov, A. S. Roca, T. Groth, R. Zahn, J. Voros and M. Zenobi-Wong, *Adv. Mater.*, 2010, **22**, 5443-5462.
404. C. X. Li, S. Bolisetty and R. Mezzenga, *Adv. Mater.*, 2013, **25**, 3694-3700.
405. B. Adhikari and A. Banerjee, *Soft Matter*, 2011, **7**, 9259-9266.
406. J. H. Kim, D. H. Nam, Y. W. Lee, Y. S. Nam and C. B. Park, *Small*, 2014, **10**, 1272-1277.
407. R. Riek and D. S. Eisenberg, *Nature*, 2016, **539**, 227-235.
408. A. G. Cheetham, P. C. Zhang, Y. A. Lin, L. L. Lock and H. G. Cui, *J. Am. Chem. Soc.*, 2013, **135**, 2907-2910.
409. H. Choi, M. T. Jeena, L. Palanikumar, Y. Jeong, S. Park, E. Lee and J. H. Ryu, *Chem. Commun.*, 2016, **52**, 5637-5640.
410. T. Waku, Y. Kitagawa, K. Kawabata, S. Nishigaki, S. Kunugi and N. Tanaka, *Chem. Lett.*, 2013, **42**, 1441-1443.
411. T. Waku and N. Tanaka, *Polym. Int.*, 2017, **66**, 277-288.
412. L. L. Lock, Y. G. LI, X. P. Mao, H. W. Chen, V. Staedtke, R. Bai, W. Ma, Y. Lin, G. S. Liu and H. G. Cui, *ACS Nano*, 2017, **11**, 797-805.
413. C. C. Capule, C. Brown, J. S. Olsen, S. Dewhurst and J. Yang, *J. Am. Chem. Soc.*, 2012, **134**, 905-908.
414. M. Yolamanova, C. Meier, A. K. Shaytan, V. Vas, C. W. Bertoncini, F. Arnold, O. Zirafi, S. M. Usmani, J. A. Muller, D. Sauter, C. Goffinet, D. Palesch, P. Walther, N. R. Roan, H. Geiger, O. Lunov, T. Simmet, J. Bohne, H. Schrezenmeier, K. Schwarz, L. Standker, W. G. Forssmann, X. Salvatella, P. G. Khalatur, A. R. Khokhlov, T. P. J. Knowles, T. Weil, F. Kirchhoff and J. Munch, *Nat. Nanotechnol.*, 2013, **8**, 130-136.
415. G. A. Silva, C. Czeisler, K. L. Niece, E. Beniash, D. A. Harrington, J. A. Kessler and S. I. Stupp, *Science*, 2004, **303**, 1352-1355.
416. M. N. Bongiovanni and S. L. Gras, *Biomaterials*, 2015, **46**, 105-116.
417. N. P. Reynolds, M. Charnley, M. N. Bongiovanni, P. G. Hartley and S. L. Gras, *Biomacromolecules*, 2015, **16**, 1556-1565.
418. R. M. Gouveia, V. Castelletto, S. G. Alcock, I. W. Hamley and C. J. Connon, *J. Mater. Chem. B*, 2013, **1**, 6157-6169.
419. R. M. Gouveia, V. Castelletto, C. J. Connon and I. W. Hamley, *Tissue Eng. A*, 2015, **21**, 1772-1784.
420. M. Zhou, A. M. Smith, A. K. Das, N. W. Hodson, R. F. Collins, R. V. Ulijn and J. E. Gough, *Biomaterials*, 2009, **30**, 2523-2530.
421. G. Cheng, V. Castelletto, C. M. Moulton, G. E. Newby and I. W. Hamley *Langmuir*, 2010, **26**, 4990-4998.
422. S. Das, K. Zhou, D. Ghosh, N. N. Jha, P. K. Singh, R. S. Jacob, C. C. Bernard, D. I. Finkelstein, J. S. Forsythe and S. K. Maji, *NPG Asia Mater.*, 2016, **8**, e304.
423. J. Healy, K. Wong, E. B. Sawyer, C. Roux, L. Domigan, S. L. Gras, M. Sunde, N. G. Larsen, J. Gerrard and M. Vasudevamurthy, *Biopolymers*, 2012, **97**, 595-606.
424. M. Kaur, J. Healy, M. Vasudevamurthy, M. Lasse, L. Puskar, M. J. Tobin, C. Valery, J. A. Gerrard and L. Sasso, *Nanoscale*, 2014, **6**, 13169-13178.
425. N. P. Reynolds, K. E. Styan, C. D. Easton, Y. L. Li, L. Waddington, C. Lara, J. S. Forsythe, R. Mezzenga, P. G. Hartley and B. W. Muir, *Biomacromolecules*, 2013, **14**, 2305-2316.
426. N. P. Reynolds, M. Charnley, R. Mezzenga and P. G. Hartley, *Biomacromolecules*, 2014, **15**, 599-608.
427. C. X. Li, M. M. Alam, S. Bolisetty, J. Adamcik and R. Mezzenga, *Chem. Commun.*, 2011, **47**, 2913-2915.
428. P. Hanczyc, M. Samoc and B. Norden, *Nat. Photonics*, 2013, **7**, 969-972.
429. K. J. Channon, G. L. Devlin and C. E. MacPhee, *J. Am. Chem. Soc.*, 2009, **131**, 12520-12521.
430. J. Ryu, S. W. Kim, K. Kang and C. B. Park, *ACS Nano*, 2010, **4**, 159-164.
431. S. Barrau, F. Zhang, A. Herland, W. Mammo, M. R. Andersson and O. Inganas, *Appl. Phys. Lett.*, 2008, **93**, 023307.
432. S. Bolisetty, J. Adamcik, J. Heier and R. Mezzenga, *Adv. Funct. Mater.*, 2012, **22**, 3424-3428.
433. S. Chaves, L. M. Pera, C. L. Avila, C. M. Romero, M. Baigori, F. E. M. Vieyra, C. D. Borsarelli and R. N. Chehin, *RSC Adv.*, 2016, **6**, 8528-8538.
434. J. H. Kim, M. Lee, J. S. Lee and C. B. Park, *Angew. Chem. Int. Ed.*, 2012, **51**, 517-520.
435. H. Acar, R. Garifullin, L. E. Aygun, A. K. Okyay and M. O. Guler, *J. Mater. Chem. A*, 2013, **1**, 10979-10984.
436. G. Scott, S. Roy, Y. M. Abul-Haija, S. Fleming, S. Bai and R. V. Ulijn, *Langmuir*, 2013, **29**, 14321-14327.
437. W. H. Leung, W. H. Lo and P. H. Chan, *RSC Adv.*, 2016, **6**, 58363-58364.
438. D. Li, H. Furukawa, H. X. Deng, C. Liu, O. M. Yaghi and D. S. Eisenberg, *Proc. Natl. Acad. Sci. U.S.A.*, 2014, **111**, 191-196.
439. D. Li, E. M. Jones, M. R. Sawaya, H. Furukawa, F. Luo, M. Ivanova, S. A. Sievers, W. Y. Wang, O. M. Yaghi, C. Liu and D. S. Eisenberg, *J. Am. Chem. Soc.*, 2014, **136**, 18044-18051.
440. T. Scheibel, R. Parthasarathy, G. Sawicki, X. M. Lin, H. Jaeger and S. L. Lindquist, *Proc. Natl. Acad. Sci. U.S.A.*, 2003, **100**, 4527-4532.
441. Q. L. Zou, K. Liu, M. Abbas and X. H. Yan, *Adv. Mater.*, 2016, **28**, 1031-

 This journal is © The Royal Society of Chemistry 20xx

1043.
442. O. Carny, D. E. Shalev and E. Gazit, *Nano Lett.*, 2006, **6**, 1594-1597.
443. V. Dinca, E. Kasotakis, A. Mourka, A. Ranella, M. Farsari, A. Mitraki and C. Fotakis, *Phys. Status Solidi C*, 2008, **5**, 3576-3579.
444. V. Dinca, E. Kasotakis, J. Catherine, A. Mourka, A. Ranella, A. Ovsianikov, B. N. Chichkov, M. Farsari, A. Mitraki and C. Fotakis, *Nano Lett.*, 2008, **8**, 538-543.
445. M. Amit, S. Appel, R. Cohen, G. Cheng, I. W. Hamley and N. Ashkenasy, *Adv. Funct. Mater.*, 2014, **24**, 5873-5880.
446. M. Hamedi, A. Herland, R. H. Karlsson and O. Inganas, *Nano Lett.*, 2008, **8**, 1736-1740.
447. C. Meier, I. Lifincev and M. E. Welland, *Biomacromolecules*, 2015, **16**, 558-563.
448. D. Y. Tu, D. Nilsson and R. Forchheimer, *J. Disp. Technol.*, 2013, **9**, 755-759.
449. A. Herland, P. Bjork, K. P. R. Nilsson, J. D. M. Olsson, P. Asberg, P. Konradsson, P. Hammarstrom and O. Inganas, *Adv. Mater.*, 2005, **17**, 1466-1471.
450. H. Tanaka, A. Herland, L. J. Lindgren, T. Tsutsui, M. R. Andersson and O. Inganas, *Nano Lett.*, 2008, **8**, 2858-2861.
451. A. Rizzo, O. Inganas and N. Solin, *Chem. Eur. J.*, 2010, **16**, 4190-4195.
452. A. Rizzo, N. Solin, L. J. Lindgren, M. R. Andersson and O. Inganas, *Nano Lett.*, 2010, **10**, 2225-2230.
453. N. Solin and O. Inganas, *Isr. J. Chem.*, 2012, **52**, 529-539.
454. A. K. Buell, E. K. Esbjorner, P. J. Riss, D. A. White, F. I. Aigbirhio, G. Toth, M. E. Welland, C. M. Dobson and T. P. J. Knowles, *Phys. Chem. Chem. Phys.*, 2011, **13**, 20044-20052.
455. M. Yemini, M. Reches, J. Rishpon and E. Gazit, *Nano Lett.*, 2005, **5**, 183-186.
456. M. Yemini, M. Reches, E. Gazit and J. Rishpon, *Anal. Chem.*, 2005, **77**, 5155-5159.
457. S. Kim, J. H. Kim, J. S. Lee and C. B. Park, *Small*, 2015, **11**, 3623-3640.
458. L. Sasso, S. Suei, L. Domigan, J. Healy, V. Nock, M. A. K. Williams and J. A. Gerrard, *Nanoscale*, 2014, **6**, 1629-1634.
459. D. Men, Z. P. Zhang, Y. C. Guo, D. H. Zhu, L. J. Bi, J. Y. Deng, Z. Q. Cui, H. P. Wei and X. E. Zhang, *Biosens. Bioelectron.*, 2010, **26**, 1137-1141.
460. Y. Leng, H. P. Wei, Z. P. Zhang, Y. F. Zhou, J. Y. Deng, Z. Q. Cui, D. Men, X. Y. You, Z. N. Yu, M. Luo and X. E. Zhang, *Angew. Chem. Int. Ed.*, 2010, **49**, 7243-7246.
461. I. W. Hamley, *Soft Matter*, 2010, **6**, 1863-1871.
462. A. M. Corrigan, C. Muller and M. R. H. Krebs, *J. Am. Chem. Soc.*, 2006, **128**, 14740-14741.
463. J. G. Zhao, S. Bolisetty, J. Adamcik, J. Han, M. P. Fernandez-Ronco and R. Mezzenga, *Langmuir*, 2016, **32**, 2492-2499.
464. T. H. Han, J. Kim, J. S. Park, C. B. Park, H. Ihee and S. O. Kim, *Adv. Mater.*, 2007, **19**, 3924-3927.
465. M. J. Krysmann, V. Castelletto, J. E. McKendrick, L. A. Clifton, I. W. Hamley, P. J. F. Harris and S. A. King, *Langmuir*, 2008, **24**, 8158-8162.
466. J. Ryu, S. Y. Lim and C. B. Park, *Adv. Mater.*, 2009, **21**, 1577-1581.
467. X. H. Yan, Y. Su, J. B. Li, J. Fruh and H. Mohwald, *Angew. Chem. Int. Ed.*, 2011, **50**, 11186-11191.
468. X. H. Yan, J. B. Li and H. Mowald, *Adv. Mater.*, 2011, **23**, 2796-2801.
469. Y. Shen, L. Posavec, S. Bolisetty, F. M. Hilty, G. Nystrom, J. Kohlbrecher, M. Hilbe, A. Rossi, J. Baumgartner, M. B. Zimmermann and R. Mezzenga, *Nat. Nanotechnol.*, 2017, DOI: 10.1038/nnano.2017.1058.

Gang Wei received his Ph.D from Changchun Institute of Applied Chemistry, Chinese Academy of Sciences, China, in 2007. Following the doctoral studies, he worked as the Alexander-von-Humboldt (2007) and Carl-Zeiss (2009) Postdoctoral Fellow at the Friedrich-Schiller-University of Jena, Germany. Since 2012, he worked as a senior researcher and group leader in Hybrid Materials Interfaces Group at University of Bremen, Germany. His research interests include carbon-based nanomaterials, supramolecular self-assembly, sensors and biosensors, as well as single molecule force spectroscopy.

Zhiqiang Su was born in 1975 and completed his Ph.D. studies in 2005 at the Institute of Chemistry, Chinese Academy of Sciences. After a postdoctoral stay at the Tsinghua University, he joined the Beijing University of Chemical Technology in 2007 and was appointed as Full Professor in 2012. In 2011 he studied at Friedrich-Schiller-University Jena, Germany as an experienced research fellow of Alexander von Humboldt Foundation. His research interests include nanohybrids, biomedical materials, biosensors, and bioelectronics. So far, he has published more than 80 papers in international peer reviewed journals.

Ian W. Hamley is Diamond Professor of Physical Chemistry at the University of Reading. He has more than 20 years' experience of research on different types of soft materials, including peptides, polymers, liquid crystals and surfactants. He obtained his PhD from the University of Southampton in 1991 and then undertook postdoctoral research at AMOLF, Amsterdam, and the University of Minnesota. In 1993, he returned to a lectureship at the University of Durham, UK, and moved to the University of Leeds in 1995 where he was promoted to a professorship in 2004. He relocated to the University of Reading in 2005. He received a Royal Society-Wolfson Research Merit Award in 2011, the RSC Peter Day Award for Materials Chemistry (2016) and the MacroGroup UK Medal (2017). His research programme and peptide and peptide-conjugate based materials focuses on their self-assembly behaviour and its relationship to bioactivity. He has supervised more than forty postdoctoral and postgraduate researchers. He has published over 350 journal publications (h-index 59) and several edited and authored books.

Raffaele Mezzenga finished his PhD at EPFL Lausanne (2001) and a postdoc at UCSB Santa Barbara, before joining in 2003 the Nestlé Research Center in Lausanne. In 2005 he was hired as Associate Professor in Physics at the University of Fribourg, and he then joined ETH Zurich on 2009 as Full Professor. His research focuses on the fundamental understanding of self-assembly processes in soft condensed matter. His work has been internationally recognized by several prestigious distinctions such as the Biomacromolecules/Macromolecules Young Investigator Award (2013, American Chemical Society), the Dillon Medal (2011, American Physical Society), and the Young Scientist Research Award (2011, American Oil Chemist Society).

This journal is © The Royal Society of Chemistry 20xx